Structures and Solvation in Deep Eutectic Solvents

Bathke, Elly Kim

2024

Document Version:
Publisher's PDF, also known as Version of record

Structures and Solvation in Deep Eutectic Solvents

Structures and Solvation in Deep Eutectic Solvents

Elly K. Bathke

LUND
UNIVERSITY

Coverphoto by Elly K. Bathke

Faculty LTH
Department Chemistry

ISBN (Printed) 978-91-8096-048-9
ISBN (digitak) 978-91-8096-049-6

Printed in Sweden by Media-Tryck, Lund University
Lund 2024

To anyone out there.

Table of Contents

1.1 Acknowledgements

Completing a PhD is a lengthy process, that requires help at many steps along the way. Sometimes it's practical things like helping out with experiments at a research facility, just by moving something into the fridge for you once it's done, so you can run off to do other things or showing you the trick how to format something better in a document. Communicating with others and bouncing off ideas is also so very important, so I would like to thank everyone I have met along the way.

First and foremost, I would like to thank my supervisor *Karen*, for all the support, inspiration and feedback throughout the years. With COVID-19 and the move to a different country you were still able to find time for regular meetings. I was also always impressed how you could catch the countless spelling mistakes in my drafts, and your enthusiasm for joining in on beamtimes is very appreciated. Thank you for your guidance and ensuring that my output is up to standard!

I would also like to thank my co-supervisor *Daniel*. Similarly, I am grateful that you were able to join the regular group meetings. It was always pleasant to have a chat with you, online or in person, and your expertise and engagement with my project was very reassuring, especially when there were problems.

For their essential support at the beamline and after, I thank the beamline scientists *Diego*, *Fátima*, *Luke* and *Olga*, as well as *Ann, Oliver, Sophia, Terri-Louise* and *Tristan*. Especially *Sylain* and *Tom* must not have had a fun time running some of my samples remotely, due to their high viscosity, so I am especially thankful.

And of course, I would like to tons of thanks everyone I met in the Edler groups, *Brad*, *George*, *Iva*, *Laura*, *Maggie*, *Marcello*, *Matheus*, *Niamh*, *Phillip*, *Ronak, Saffron, Subrame* and *Zakir* (alphabetical order haha)! Meetings were always fun, and everyone is delightfully helpful as well. It is a pity that due to COVID-19 related things, it was quite difficult to meet up in person for a long time, but also thank you for being my in real life connection to the human world during that time. Keeping each other sane during every day operations is a job not to be underestimated at the best of times. Moving countries was also not the easiest job, and it was good that a group us were able to move together, so no one was stranded alone in a foreign country. Thanks to the group members I met here in Sweden as well, I was happy that we could all learn to indulge in the Swedish fika tradition in a good atmosphere with plenty of snacks! Also, an especial shout out to everyone who joined in during the long hours of synchrotron and neutron beam times. It can be stressful and long hours, but that doesn't mean we can't have fun either!

I was lucky to have great administrative support along the way! For my time in Bath I received a lot of help from the CSCT, and I would like to thank *Aida*, *Amanda* and *Francesca* for all they did, and also all the events and socials they organized!

Here at CAS I also received so much help, coming here as the first from my group, not knowing how anything works here. Thanks to *Maria* and *Sara* for their crucial help, without which thing could not be running! I was always a good time chatting

to you during fika! Also thank you *Kornelje*, your reliable proactive help with instruments, or any problem really, is very appreciated. Also thanks to everyone at KC purchase that I paid almost daily visits to at the beginning of my time at Lund, especially *Katarina*, *Fatima,* and *Ulf* for sorting anything IT related!

Finally I would like to thank my family and friends, who, although scattered over various countries, provided me with the essential support and motivation to keep going. Especially not being able to leave the country during COVID-19 times was hard, but in the end we were able to move on and I even got to celebrate the start of the year of 2021 twice, as I communicated over zoom with the future. Thank you for everything.

1.2 Popular Science Summary

In order to produce everyday items from shoes to phones to toothpaste, many chemical processes are involved to make its ingredients, plastics and other components. Many of these processes take place in “solvents”, liquids that facilitate the formation of these components in the right type and form to be useful. There are many of these solvents in use and they have a variety of properties in order to be able to produce the plethora of materials required in modern items.

But many of these solvents can be harmful for humans and the environment, evaporate easily or are flammable, posing risks that need to be carefully managed when using them. They are also commonly sourced from fossil fuels and can contribute negatively to climate change. It is one goal in science to find better and less harmful ways to produce things, and over the years some of the most harmful solvents have been retired and substituted.

In this thesis we investigate a group of new modern solvents, called “Deep eutectic solvents” (from here DES). They can be made by simply mixing two or more common ingredients at room temperature or under moderate heating. One of their strong points is that these ingredients can be things like sugars and other materials already produced on a large scale for from bio-sources, making them potentially more sustainable and less environmentally harmful. Another pro is that due to the many components available, and the change in solvent properties with components, component ratios and additives, they have a good potential as “designer solvents” with tailorable properties due for specific applications. There have been a range of applications found for them, but as they still have limits in predictable interactions and relatively high viscosity, research in this field is very active.

One of the main concepts behind DES is the eutectic – a property describing the phenomenon of a reduced melting point when mixing two components, relative to the melting points of each component. A famous example of this in DES is the mixture of urea and choline chloride, both molecules that can be found in the body, which in their pure form are solids, looking similar to sugar, but turn into a liquid upon mixing at a specific ratio even without heating. These liquids can then be used as solvents at room temperatures.

These DES have been found to have many unique properties, which help them be able to dissolve, assemble or react materials in them in interesting ways. Here we looked at the structure and interactions of some of these DES systems. Knowing how the molecules and even their atoms interact in these liquids can help understand how these DES form and interact with other molecules. This can help both the basic understanding, and hopefully future predictions, as well as laying the foundation for further application tests.

1.3 List of Papers

1.3.1.1 Paper I

Elly K. Bathke, Daniel Bowron, Iva Manasi, Karen J. Edler (2024) The influence of chirality on the structure of a tartaric acid-choline chloride deep eutectic solvent

Accepted manuscript by the Journal of Molecular Liquids

1.3.1.2 Paper II

Elly K. Bathke, Daniel Bowron, Tom F. Headen, Laura Deeming, George M. Neville, Karen J. Edler (2024) Iron Nitrate solvation in betaine-glycerol deep eutectic solvent

Submitted to Green Chemistry

1.3.1.3 Paper III

Elly K. Bathke, Sylvain Prévost, Fátima Herranz, Laura Deeming, Ronak Kakadiya, Maggie Koon, Daniel Bowron, Karen J. Edler (2024) Cationic and Non-ionic Surfactant Micelles in a Halogen-Free Carboxylic Acid-Based Deep Eutectic Solvent

Manuscript

1.4 Author's contribution to the papers

1.4.1.1 Paper I

I planned and performed most of the experimental work and data analysis. For the neutron scattering experiment, I was helped by Daniel B., Iva M. and Karen E.. I wrote the paper with feedback from the other authors.

1.4.1.2 Paper II

I planned and performed most of the experimental work and data analysis. For the neutron scattering experiment, I was helped by Daniel B., Tom H., Laura D., George N. and Karen E.. I wrote the paper with feedback from the other authors.

1.4.1.3 Paper III

I planned and performed most of the experimental work and data analysis. The small angle neutron scattering experiments were performed remotely by Sylvain P. from samples I prepared and sent to the facility. For the small angle X-ray scattering experiment, I was helped by Fátima H., Ronak K., Maggie K., Laura D. and Karen E.. I wrote the paper with feedback from the other authors.

1.5 List of Papers not included in this thesis

1.5.1.1 Paper I

Saffron J. Bryant, Elly K. Bathke, Karen J. Edler (2021) Bottom-up cubosome synthesis without organic solvents

Journal of Colloid and Interface Science, 601 (2021) 98–105

1.5.1.2 Paper II

Philip B. Yang, Matthew G. Davidson, Karen J. Edler, Niamh Leaman, Elly K. Bathke, Strachan N. McCormick, Olga Matsarskaia, Steven Brown (2022) Comparison of Cyclic and Linear Poly(lactide)s Using Small-Angle Neutron Scattering

Macromolecules 2022, 55, 24, 11051–11058

1.5.1.3 Paper III

Oliver S. Hammond, Elly K. Bathke, Daniel T. Bowron, Karen J. Edler (2024) Trace Water Changes Metal Ion Speciation in Deep Eutectic Solvents: Ce^{3+} Solvation and Nanoscale Water Clustering in Choline Chloride–Urea–Water Mixtures

Inorganic Chemistry 2023, 62, 44, 18069–18078

1.6 Abbreviations

$C_{12}EO_6$ – Dodecyl hexaoxyethylene glycol monoether
C_{12}TAB – Dodecyltrimethylammonium bromide
C_{16}TAB – Cetyltrimethylammonium bromide
CA – Citric acid
CeNO – Cerium nitrate hexahydrate
ChCl – Choline chloride
CMC – Critical micelle concentration
DES – Deep eutectic solvent
DSC – Differential scanning calorimetry
EAN – Ethylammonium nitrate
EG – Ethylene glycol
EPSR – Empirical potential structure refinement
FeNO – Iron nitrate nonahydrate
Gly – Glycerol
MA – Malic acid
Mal – Malonic acid
HBA – Hydrogen bond acceptor
HBD – Hydrogen bond donor
IL – Ionic liquid
SAS – Small angle scattering
SDS – Sodium dodecyl sulfate
SLD – Scattering length density
TA – Tartaric acid
U – Urea

2 Fundamentals

In this section the main concepts and motivations behind the use of the emerging solvent class of Deep Eutectic Solvents, as well as amphiphile self-assembly will be explained.

2.1 Deep Eutectic Solvents

Deep eutectic systems (DES) are an emerging class of modern solvents with unique properties, that are highly regarded for their potential as "green" solvents. They are low transition temperature mixtures [4], formed by mixing two or more components, in order to form a liquid around room temperature. These systems can be formed by mixing a variety of organic or inorganic molecules, such as sugars, metal salts, carboxylic acids, amino acids and alcohols [5-10]. Hydrophobic DES based on e.g. phenol or menthol have also found various uses [11, 12], but this thesis work is only focused on hydrophilic DES.

In these mixtures the components can act as hydrogen bond donor (HBD), e.g. urea (U), with a hydrogen bond acceptor (HBA), e.g. choline chloride (ChCl), which then form a hydrogen bonded liquid. These mixtures often form a liquid over a range of molar ratios. They are eutectics, where the melting temperature of the mixture is below that of the individual components. Often the eutectic ratio, the composition where the melting point of the mixture is at a minimum, is used since the liquid state is most favored at this point (**Figure 1**) [13-15].

Due to many DES being formed from "green" precursors like urea, they are of particular interest in research for green solvent alternatives. For DES made from naturally occurring materials the term Natural Deep Eutectic Solvents (NADES) [16], has been coined. The wide range of possible constituents leads to solvents with tuneable properties, where factors such as component choice, molar ratio, additives and even temperature can lead to significant changes in properties like hydrophobicity [17, 18], conductivity [19-21], biocompatibility [22-24] and their ability so solubilize other components [25-27]. This also makes it possible to focus on safer and “greener” solvent combinations and use conditions, producing solvents that are low in toxicity, flammability and volatility, as well as exhibit good biodegradability and can be sourced sustainably [28-32]. It has been found that their use can also allow for the use of less harsh chemicals, milder temperature or pressure

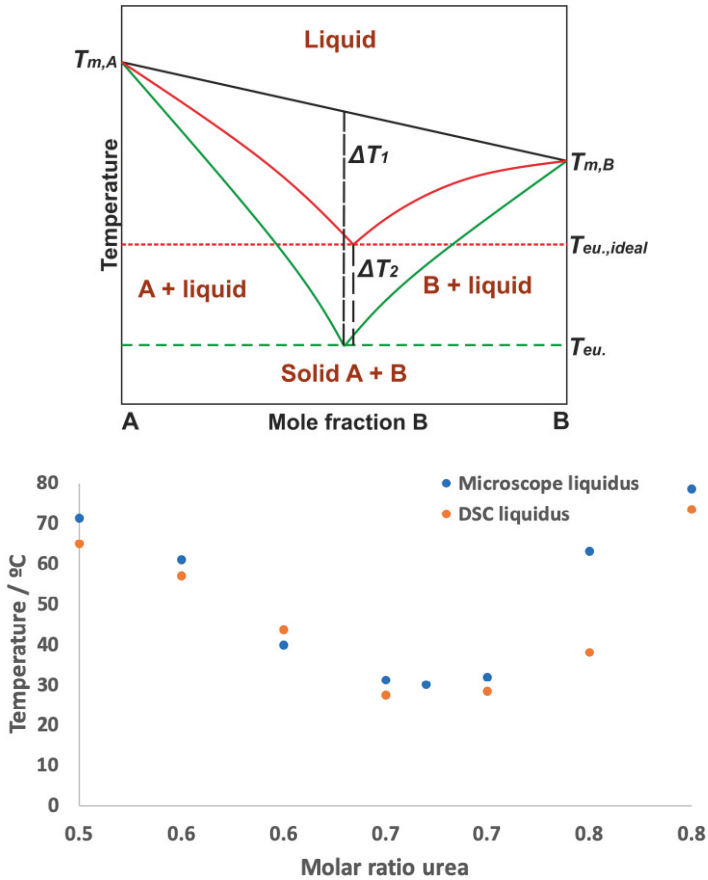

Figure 1: Schematic phase diagram of a DES for mole fraction of component B in A and temperature (top). The bottom graph shows experimental liquidus temperatures over mole fraction of urea for 1:2 ChCl:U from microscopic (blue dots) and DSC (red dots) measurements. Data replotted from reference [2].

requirements, or more straightforward synthesis and extraction routes, leading to applications in fields like organic and materials synthesis [33-37], extraction [38-40], electrochemistry [41, 42] and pharmaceutical applications [43, 44], among many others. Especially their ability to dissolve a wide range of metal components [27, 45-48] and surfactants, as well as allowing for surfactant self-assembly [49-52], and how they can be manipulated through parameters such as component choice, molar ratio, water content and salt addition, will be explored and discussed in this thesis.

DES were first reported in their modern understanding by Abbott et al. in 2001, with their work on DES formed by $ZnCl_2$ and choline chloride at a 2:1 molar ratio [6]. The term DES was then coined by the same group in 2003 in their seminal work

Table 1: Composition and transition temperature at the eutectic point of some common DES.

DES	Components	Transition temperature
1:2 Choline chloride : Urea (ChCl:U)	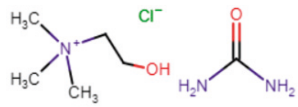	25°C [2]
1:2 Choline chloride : Glycerol (ChCl:Gly)	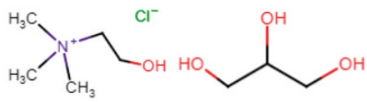	-40°C [54]
1:2 Choline chloride : Ethylene glycol (ChCl:EG)	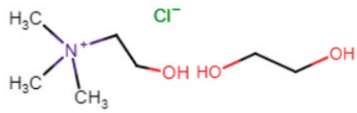	-66°C [55]
1:1 Choline chloride : Malonic acid (ChCl:Mal)	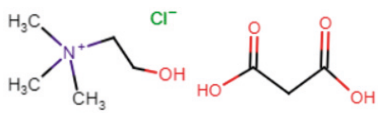	10°C [5]
1:3.5 Cerium nitrate hexahydrate : Urea (CeNO:U)	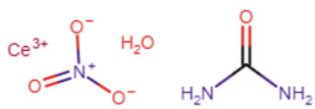	-60°C [8]

studying the mixtures of a range of quaternary ammonium salts with urea [53]. Among them was ChCl:U at a 1:2 molar ratio, which is now one of the most widely studied DES. The eutectic ratio was found by mixing the two components at different molar ratios and measuring the melting point. Abbott et al. reported a melting point of 12 °C for the eutectic, forming a stable liquid at room temperature, while pure choline chloride has a melting point of 302 °C and urea of 133 °C. This melting temperature for the eutectic mixture was later found to be influenced by water absorbed into the highly hygroscopic liquid, with the melting point of the dry mixture being closer to 25 °C [2]. In their current understanding DES usually refer to eutectic mixtures with a eutectic melting temperature T_{eu} below the expected ideal melting temperature $T_{eu;ideal}$ as can be seen in **Figure 1** [56]. Since their initial discovery interest and research into DES have increased significantly and steadily.

DES are typically created by mixing the precursors at ambient or moderately elevated temperatures, until a clear liquid is formed. In rarer cases the precursors are dissolved in a solvent such as water, mixed, and the water is subsequently removed [57]. Typical molar ratios for DES formation are 1:1, 1:2 and 1:3, but also

1:2.5 and wider ratios like 1:10. The components and transition temperatures at the eutectic point composition of some common DES can be seen in **Table.1**.

DES have sometimes been categorized as a subgroup of ionic liquids (IL), but have been shown to exhibit a range of differing properties and behaviors from these, and are now mostly regarded separately. Ionic liquids are generally described as a group of salts with low melting points close to room temperature, with one type of discrete anion and cation, such as ethylammonium nitrate (EAN) [58]. DES are of interest as they show distinct solubilization and reaction behaviors in comparison to traditional organic solvents, ILs or water. They can also be easier to procure and form, cheaper, more environmentally benign, easier to sustainably source and biodegrade than most ILs. Similar to ionic liquids, properties such as a wide liquid window, low volatility and the sheer range of possible DES mixtures make them attractive as "designer" solvents, where the solvent properties can be modified to the specific needs of the application. As they are a relatively new class of solvents, the potential of DES is still far from reached, and in this thesis, we hope to help shine a light into some of the yet unexplored corners of this field.

2.1.1 DES structure

As mentioned in the section above, the solvent-solvent interactions in DES are dominated by hydrogen bonding between the components. The liquid structure of some of DES has been reported, investigated through both simulation [59-62] and experimental means [8, 63, 64], revealing a range of complex hydrogen bonding networks within these solvents. Studies of the common DES 1:2 ChCl:U for example show strong interactions between chloride and both the hydroxyl hydrogen of the choline ion and the hydrogen atoms on the urea [59, 63]. But between different DES the structure and prominent interactions can vary significantly. This can lead to more or less structured hydrogen bond networks, depending on factors such as size, shape and polarity of the components, as well as rigidity and number of hydrogen bonding groups per molecule [59, 61, 62, 65, 66]. The influence of specific components on the DES structure, and through this the solvent properties, is still an active field of research, and will be delved into further in this thesis.

It is well established that the properties of some DES can be modified through the addition of water, leading e.g. to a significant decrease in viscosity even for small added amounts [67, 68]. The effect of water on the solvent structure has been studied through methods such as modeling [62, 69], ^{1}H NMR [65, 67, 70] and neutron scattering [64, 71, 72]. These investigations show that the DES structure is relatively stable for additions of up to 50 wt% water in these DES. At very low concentrations, water can even contribute to the hydrogen bonding network and strengthen HBD-HBA interactions [67], with the water molecules increasingly separating the DES domains at higher concentrations. At high enough concentrations, the DES structure starts to break down, forming an aqueous solution. The exact point at which these changes occur is dependent on the

interactions between the DES components [71]. Besides water, additives such as small organic molecules or salts also influence the solvent structure and overall DES behavior [73-76]. Understanding the underlying interactions taking place in a solvent can then be used to explain and predict processes like solubilization or aggregation.

2.1.2 DES Types

For general understanding, DES are often categorized into five types based on their components [14, 15, 77], as shown in **Table 1**.

While the introduction of water going from Type I to Type II might not always be desirable, the use of metal salt hydrates opens up a wider variety of metal precursors, as well as decreasing the water sensitivity of the DES. As it has been found that the addition of small amounts of water also lowers the melting point of many DES [2], this can also aid liquid formation at ambient temperatures. Type III DES include many of the most common DES, such as 1:2 ChCl:U and 1:2 ChCl:Gly, as they are composed of relatively cheap, non-toxic components that are already produced on an industrial scale, and exhibit many useful properties such as the ability to promote formation of surfactant aggregates or solubilize metal salts, as mentioned in the previous sections.

Table 1: DES types and their components.

Type of DES	**Components**
Type I	Quaternary ammonium salts + metal salts, e.g. ChCl + $ZnCl_2$ [78]
Type II	Quaternary ammonium salts + metal salt hydrates, e.g. ChCl + $CrCl_3 \cdot 6\ H_2O$ [79]
Type III	Quaternary ammonium salts + HBD, including many small, organic molecules like carboxylic acids and alcohols, e.g. ChCl + U [53], ChCl + EG [80] and ChCl + carboxylic acids [57]
Type IV	Metal salt + HBD, e.g. $ZnCL_2$ + U [81] and $Ce(NO_3)_3 \cdot 6\ H_2O$ + U [8]
Type V	Non-ionic HBA + non-ionic HBD, e.g. thymol + menthol [77]

2.1.3 DES Properties

As mentioned in the first section, DES can have a wide range of properties, with the possibility of tuneability, and can be cheap, safe and formed from sustainable materials. But they can be limited in other regards. Many of the components, such as sugars, are not very thermally stable, and reactivity between DES components also must be kept in mind when the use requires elevated temperatures, e.g. esterification reactions are common between choline chloride and carboxylic acids [57, 82]. This influences factors such as the reusability of the solvent, or can be desirable when the DES components are also used to facilitate a synthesis, such as the breakdown of urea to produce metal oxide nanomaterials [33, 34]. Monitoring degradation through e.g. the use of ^{1}H-NMR should therefore be a standard procedure. DES also tend to have significantly lower vapor pressures than water and many organic solvents, but they often have higher and more variable vapor pressures than ILs [83].

Although most DES are liquid at and around room temperature, one of the most common practical limitations is their high viscosity. Viscosity and other DES properties can be modified through simple means like adding small amounts of small molecules such as methanol [84] or water [67], without greatly changing the underlying DES structure and properties. Dai et al. [67, 85] e.g. found that for a variety of NADES a significant decrease in viscosity can be achieved, e.g. from 397 to 7.2mm^{2}s^{-1}, for 2:5 glucose : ChCl at 25% water added (v/v). The conductivity was also increased, density decreased, water activity increased, and the polarity modified in the direction of water polarity levels. This could be achieved while still maintaining the characteristic strong hydrogen bonding within the DES, as measured by FT-IR and ^{1}H-NMR. This change in properties has to be kept in mind when handling the highly hygroscopic DES especially, as exposure to the moisture in the air can significantly influence behavior. Measuring the water content through e.g. Karl Fischer titration should therefore be a standard procedure.

The molar ratio between the components of a DES can also be changed within a certain liquid forming window, which thereby alters their properties. Rodriguez et al. e.g. found that DES formed by *p*-toluenesulfonic acid and ChCl at molar ratios of 2:1, 1:1 and 1:2 differ significantly in their ability to solubilize various transition metal oxides [27]. Atri at al. also found that the self-assembly behavior of surfactants could be significantly modified through a change in molar ratio of components within a ternary DES comprised of ChCl:Gly:U [49].

2.1.4 Melting Points, Eutectic Points and Glass Transitions

To describe and compare materials, numerous parameters or definitions could be used. For DES especially the phase behaviour is of general interest. For a material the melting point (T_m) can be defined as the temperature at which liquid and solid phases coexist at an equilibrium. It marks the phase transition between the solid and

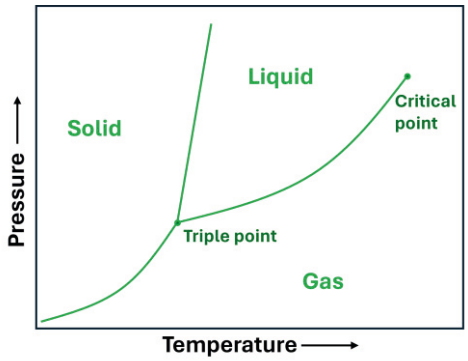

Figure 2: General pressure-temperature phase diagram of a one-component system.

the liquid state, which is governed by temperature, and weakly by pressure. Considered as fundamental phases are gas, liquid and solid, with some materials also forming more unusual phases or not forming certain phases at some temperatures or pressures. Besides transitions between these phases, it is also possible for some materials to have transitions within one of these fundamental phases. A typical simple phase diagram can be seen in **Figure 2**. [86]

One type of these unusual phases are the supercooled liquids, which many DES are capable of forming. These form when cooling a material below their melting point, but no crystallization into the solid phase occurs. One example of this is typical window glass, which forms an amorphous, solid-like phase upon cooling down. This formation and the structure of the formed material can strongly depend on the thermal history and cooling rate. Formation of this phase is often done by cooling a material faster than what is needed for crystal formation, effectively "freezing" the molecules into place in their liquid position. To describe a glass, the glass transition temperature (T_g) can be used. While the properties of a material can vastly differ above and below this temperature, it is not considered a phase transition in the terms of e.g. T_m, as it represents a non-equilibrium state. Furthermore, T_g depends on the measurement method and conditions, resulting in there being no exact value for it between samples of similar materials, and reports of T_g are governed by convention. Differential thermal analysis and differential scanning calorimetry (DSC) are among the commonly used methods of finding T_m and T_g, and DSC will be used in this thesis. [87-89]

Mixing multiple components can change phase behavior of a material, due to a change in molecular interactions. An interesting example of this can be seen in eutectic mixtures, for which the melting or glass transition temperatures decrease drastically in comparison to the components, and, as mentioned in the in previous sections, a hydrogen bond network forms between its components. Here, the eutectic point corresponds to the molar ratio at which the liquid phase can coexist with solid phases of *A* and *B*, with the corresponding eutectic temperature T_E (**Figure 1**). Over time the term "Deep Eutectic" has found different uses, one being

that it is simply an eutectic mixture with a significant eutectic depression and a liquid operating window (molar ratios x_1 to x_2 at the operating temperature $T_{operating}$) around room temperature [15]. Others have used the term to describe mixtures which exhibit a behavior that derivates strongly from the eutectic depression that could be described by ideal mixture models [56]. The first definition is more widely used, where the eutectic depression is described as the temperature difference T_1 between the linear combination of the melting points of the pure components and T_E, while T_2 from the second definition would describe the difference between eutectic temperature $T_{E,ideal}$ and T_E. While the second, more theoretically based definition is gaining popularity especially for theoretical discussions, in this thesis the more general definition of a deep eutectic without its relation to an ideal mixture will be used, especially since a change of molar ratio regardless of the exact eutectic composition is a useful tool for modifying solvent properties.

2.2 Amphiphile Self-Assembly

2.2.1 Surfactants

Surfactants, or surface active agents, are a group of amphiphilic molecules that consist of one or multiple distinctly hydrophilic and hydrophobic parts. They are of great commercial interest as e.g. detergents, emulsifiers and foaming agents in everyday and industrial settings. They can also be used more specific applications such as in biotechnology for unfolding proteins or lysing cells or other in fields to e.g. template nanomaterials [90-93].

In a typical surfactant the hydrophilic part is often referred to as the "head" group, and contains heteroatoms such as oxygen, sulphur or nitrogen within a functional group such as an alcohol, sulphate or amide. The hydrophobic "tail" group usually consists of one or more long hydrocarbon chains. The surfactants will have a tendency to accumulate at boundaries, e.g. at air-water or water-oil interfaces, and lower the interfacial or "surface" tension. Depending on their composition and dissociation behaviour in a solvent, they can be separated into non-ionic and ionic surfactants, where ionic surfactants are further separated into anionic, cationic and zwitterionic surfactants (**Figure 3**). [94, 95]

One of the most common surfactants that can be found in many shampoos and detergents is the anionic sodium dodecyl sulfate (SDS, **Figure 3**). It has a hydrophilic sulfate headgroup, a hydrophobic hydrocarbon tail with a 12 carbons

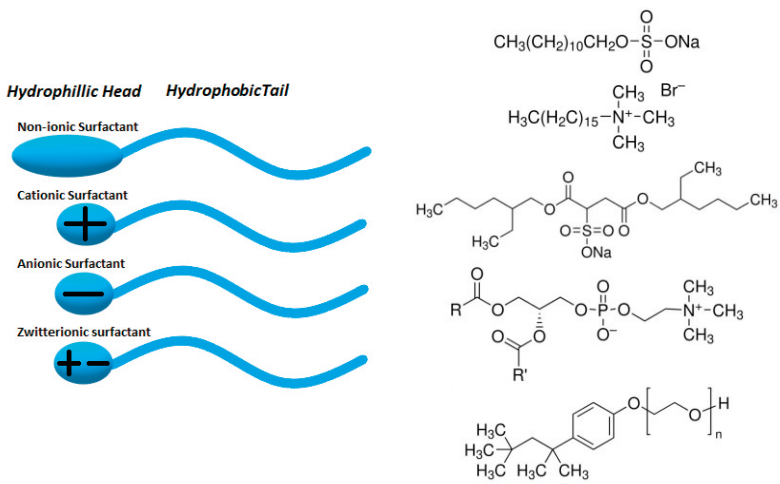

Figure 3: Schematic representation of different surfactant types (left). Examples of different types of surfactants are shown on the left, going top to bottom: Sodium dodecyl sulfate (SDS), hexadecyltrimethylammonium bromide (C_{16}TAB), dioctyl sulfosuccinate sodium salt, L-α-Phosphatidylcholine, Triton™ X-100.

containing backbone, as well as a positively charged sodium counter ion. Other simple anionic surfactants with differing properties can be produced by exchanging the sulfate headgroup for other headgroups such as carboxylates or phosphates, varying the length of the tailgroup and changing the counter ion. [94, 95]

Cationic surfactants have a similar structure, but with a cationic headgroup such as a quaternary ammonium group, and an anionic counter ion, often a halide ion. A common example of this is cetyltrimethylammonium bromide (C_{16}TAB, **Figure 3**), used widely in antiseptics, hair conditioners and in nanoparticle synthesis among other things. [94, 95]

Zwitterionic surfactants are less commonly used in comparison to cationic or anionic ones. They contain positive and negative charges in their headgroup, a commercial representative being myristamine oxide, used as a mild surfactant in e.g. children's shampoos. The charge of zwitterionic surfactants can be dependent on the pH of the surrounding medium. They exhibit both positively and negatively charged groups at a certain pH, acquiring a predominantly positive charge in more acidic pH and a more negative charge in alkaline solutions. [94, 95]

In non-ionic surfactants the head group is hydrophilic, but does not dissociate into ions. The most common types are based on ethylene oxide, such as dodecyl hexaoxyethylene glycol monoether ($C_{12}EO_6$) with six repetitions of the hydrophilic ethylene oxide group (EO) in a chain and hydrophobic 12 carbon containing tail. [94, 96]

In **Figure 3** schematic representations of the different surfactant types are shown alongside examples. As can be seen, it is also possible for surfactants to be more complex, branching and containing other structures like aromatic units. [94]

2.2.2 Surfactant self-assembly

At low concentrations surfactants can be found free in solution or at interfaces. Aggregates called micelles start forming past a specific concentration, called the Critical Micelle Concentration (CMC). Depending on solvent polarity, either the hydrophilic or hydrophobic part of the surfactant will be in contact with the solvent, while the other parts stay in contact with each other, thereby minimizing unfavourable interactions. These micelles can vary in shape depending on surfactant and solvent properties, with examples being spherical, rod-like or lamellar as shown in **Figure 4**, or can be more complex for example in the case of bilayer vesicles. [94, 96, 97]

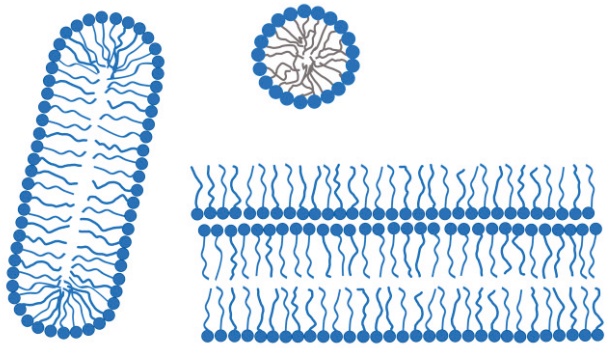

Figure 4: Schematic representation of examples of surfactant self assembly: rod-like micelle (left), spherical micelle (right, top), lamellar phase (right, bottom). To illustrate both headgroup and tail group behavious, these represent the cross section of the three dimensional structures.

As the physico-chemical behaviour of surfactant systems above and below the CMC differ greatly, it is an important parameter for surfactant characterization and application. Due to a range of property changes taking place at the CMC, it can be measured using different methods. These include surface tensiometry, light scattering techniques, fluorescence, calorimetry and more. The CMC mainly depends on the surfactant and the solvent properties, as well as additives, e.g. polar additives such as alcohols or urea can decrease or increase the CMC. For ionic surfactants the addition of salt can strongly affect the CMC as well. [94, 98-100]

The influence of pressure and temperature on the other hand are comparatively weak. Rather than influence the CMC directly, the temperature can play a bigger role in regard to surfactant solubility (**Figure 5**). Ionic surfactants show a strong increase in solubility above a specific temperature, the so-called "Krafft

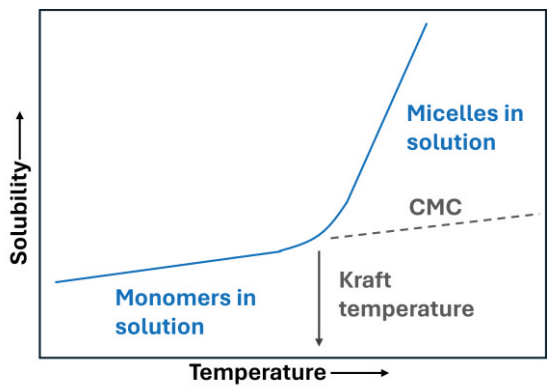

Figure 5: The influence of temperature on ionic surfactant solubility, CMC and Kraft temperature.

temperature". Here the solubility is equal to the CMC, leading to a steep increase in solubility due to the formation of highly soluble micelles. Non-ionic surfactants do not exhibit a Krafft point, and e.g. ethylene oxide based non-ionics decrease in solubility with increasing temperature. In water, their CMC tends to be around two orders of magnitude below that of ionic surfactants as well. At increasing temperature, above the so called "cloud point", they tend to separate into a surfactant rich phase and a surfactant poor phase. [94, 95]

2.2.3 Surfactant self-assembly in DES

Surfactants can form self-assembled structures in a range of solvents such as water, various oils and ILs. As mentioned above, the type of surfactant that is soluble and how they self-assemble depends on the systems. DES have also been found to support the formation of a range of structures [101, 102]. It is an active field of research and applications such as templating nanomaterials [103, 104], in electrodeposition [105, 106] and for medical applications have been investigated [101, 107, 108].

Self-assembly of anionic [49, 109-111], cationic [49, 52, 112-114], zwitterionic [50, 115, 116] and non-ionic [110] surfactants has been reported. In many DES surfactant solubility and aggregation behaviour has a strong dependence on the components, with only either cationic or anionic surfactants being soluble in many DES, while non-ionic surfactants like hexaethylene glycol mono-n-dodecyl ether are not soluble in most of the common choline chloride+HBD or betaine+HBD based DES. Atri et al. have shown that what types of surfactants can be dissolved and how they aggregate can be modulated through a change in molar ratio of the H-bond donors in a ternary DES based on ChCl:Gly:U [49], and Hammond et al. showed differences in aggregation behaviour in different ChCh:Diol based DES [117]. Differences in counter ions have also shown to have a slight effect in some DES [110, 118, 119], as well as the presence of additives such as salts [120].

3 Methods

In this section the basics behind the methods used in the thesis will be explained.

3.1 Scattering

Trying to understand structures, interactions and processes of things on the scales from single atoms to macroscopic particles and beyond has long been an essential part of chemistry. To achieve this a variety of methods have been developed over the years. These include X-ray and neutron diffraction, which will be an essential part of this thesis, but also various microscopic and spectroscopic methods among others, that can be used to probe different properties of a material to elucidate the structure. Combining these with modern computer modeling techniques enables the reconstruction of the sizes and shapes of particles and molecules, and also individual bonds and atomic interactions. The general background of the employed methods will be presented below.

3.1.1 X-ray Scattering

X-rays are electro-magnetic waves with a wavelength (λ) in the Ångstrom range. They were first described by Wilhelm Röntgen in 1895. In 1912 Max von Laue showed that when passing X-ray radiation through a crystal, a characteristic diffraction pattern will be created, which can be used to gain information about the crystal structure and material. Since then, many methods have been developed based on the interactions between X-rays and matter. Classical light microscopy is often restricted by a limited wavelength range, making it not straight forward to use it to investigate smaller, molecular and atomic dimensions. With X-rays on the other hand, it is easy to generate waves with a wavelength around the scale of typical inter-atomic distances. This makes X-rays an useful tool for material characterization and imaging, alongside element sensitivity and the possibility of non-destructive measurements. [121, 122]

When X-rays interact with a material, they cause the electrons in atoms to start oscillating. Depending on the conditions, this can be either through elastic or inelastic, coherent or incoherent processes. In elastic processes the energy carried

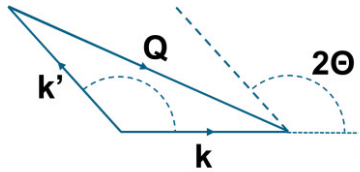

Figure 6: Schematic representation of the wavevector transfer Q.

by the X-ray is conserved after the interaction, and only the propagation direction might change. Inelastic scattering involves the loss of energy, e.g. through transfer of parts of it to the electron, as is the case with Compton scattering. Compton scattering is also an incoherent process, where, unlike with coherent scattering, a phase shift occurs, and the scattered waves cannot interfere constructively. For use of X-rays generally elastic, coherent scattering is preferred, as this carries the most information, and inelastic, incoherent signals are minimized in an experiment, or their influence later removed from the data when possible. Besides electrons, X-rays can also interact with the atom nucleus. But due to its much higher mass the resulting oscillation is weaker, and the interaction can generally be neglected. [121, 122]

In a basic approach for describing diffraction, electrons can be seen as point scatterers for X-rays. The incident wave can be described using the wave vector k, defined as $k = 2\pi/\lambda_i$, and the scattered wave k', which in the case of elastic scattering has the same wavelength as the incident wave. They can be connected using the scattering vector, also called wavevector transfer, Q given in $Å^{-1}$ (**Figure 6**). It is defined as [121]

$$Q = \mathrm{k} - \mathrm{k}' \tag{1}$$

One way to describe the scattering behaviour in an experiment is by using the fundamental quality of the differential scattering cross section ($d\sigma/d\Omega$), defined as [121]

$$\frac{d\sigma}{d\Omega} = \frac{I_{sc}}{\Phi_0 \Delta\Omega} \tag{2}$$

Here I_{sc} is the number of photons recorded per second on a detector, Φ_0 is the flux of the incident beam describing the number of photons passing through unit area per second and $\Delta\Omega$ is the solid angle that the detector spans when at a distance R from the scattering object. The differential scattering cross section describes the photons scattered in a certain direction Q onto a detector area and is proportional to the square of the amplitude of the scattered waves. [123]

For a real material it has to be considered that the electrons are not completely free as assumed above, but can be described as an electron density distribution $\rho(r)$ over a volume. The amplitude of the scattered wave is then given by the Fourier transform of the electron density, the so called atomic form factor f [121]

$$f^0(Q) = \int \rho(r) e^{iQ \cdot r} d \quad (3)$$

This form factor is characteristic for every atom type and increases with the number of electrons, while at the same time decreasing with increasing Q. To get the Q-dependent scattering amplitude for a material and not only individual atoms, the sum over all atomic form factors can be taken according to [121]

$$F(Q) = \Sigma_v f(Q)_v e^{i(Q \cdot r_v)} \quad (4)$$

with the Q dependent atomic form factor $f(Q)_v$ of each atom v and it's position r_v. In an experiment only the intensity $\Psi(Q)^2$, but not the amplitude of a wave can be measured. In principle, if $(\Psi(Q))^2$, the scattering intensity, can be determined through experiments for a sufficient number of Q values, then the location r_v of the atom in the material can be determined. In practice the signal of e.g. one molecule is not strong enough to be measurable and therefore a sample of higher mass is needed. For this purpose, crystalline materials are especially suitable, as they can be described by a unit cell consisting of a small amount of atoms in comparison to the overall number of atoms, and exhibit translational symmetry elements. Some crystals can be even further simplified, and represented by an even smaller number of atoms in the asymmetric unit along with crystallographic symmetry elements. For these crystals scattering can also be described by Bragg's law [121]

$$m\lambda = 2dsin(\theta) \quad (5)$$

A schematic figure of a common scattering experiment setup, such as would be used in powder diffraction or small angle scattering is shown in **Figure 7**.

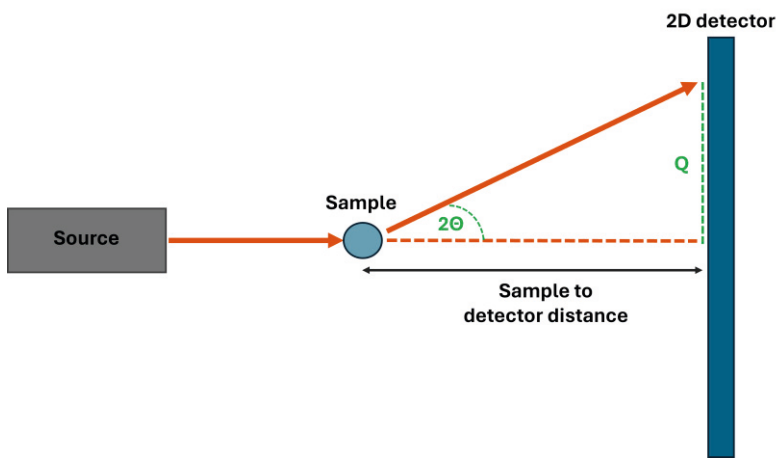

Figure 7: Schematic representation of a common scattering experiment setup.

3.1.2 Neutron Scattering

The principles of neutron scattering are like to those for X-ray scattering, and similar calculations can be used. Both share similar common experimental setups, with the use of neutrons or X-rays having different strengths and weaknesses. Unlike X-rays, neutrons are subatomic particles with a mass equivalent to 1839 electrons, $1.674928 \cdot 10^{-27}$ kg, and a spin of 1/2 [124]. They do not have a charge, and in a scattering experiment their main interaction with a sample is with the atomic nuclei via nuclear forces. Neutrons also have a magnetic moment and can interact with unpaired electrons in magnetic materials, but for the materials and methods used in this thesis, primarily the nuclear interactions are relevant and will be discussed here. [125]

As described by quantum mechanics neutrons are particles which can exhibit a wave character, and the wavelength of a neutron is inversely proportional to its speed. In scattering experiments wavelengths between 0.1 and 1 nm are most commonly used. [126]

Analogous to X-rays with electrons, the basis of interactions between neutrons and nuclei can be described as the scattering of a neutron beam with the atomic nuclei, represented by the wave function [125]

$$\Psi_i = e^{ikz} \tag{6}$$

with the distance z between neutron and nucleus, and the wave number k. The individual interactions are very short range, with the interaction potential $V(r)$ falling to zero within 10^{-15}m [124]. This leads to a significantly lower probability of interaction in comparison to X-rays with the more diffuse electron distribution, allowing for thicker samples and containers to be used for measuring. In the case of elastic scattering from a single nucleus the scattered wave is isotropic and can be described as[125]

$$\Psi_f = -\frac{b}{r} e^{ikr} \tag{7}$$

were b is the scattering length, the neutron scattering equivalent of the atomic form factor f for X-rays. Unlike the atomic form factor, the scattering length can vary strongly from one element to the next in the periodic table, as well as between isotopes of the same element as can be seen in **Figure 8**. For most materials besides strong neutron absorbers such as Cd, Gd and B, b can be treated as a constant. This makes neutrons especially suitable for studying light materials that do not scatter X-rays strongly. It also opens the door to isotopic-substitution experiments, where specific parts of the sample can be substituted with a different isotope of the same element. For example, hydrogen and deuterium are widely used, as their coherent b differ significantly with 1H at $-3.74 \cdot 10^{-5}$Å and 2H at $6.67 \cdot 10^{-5}$Å [116]. Analogous

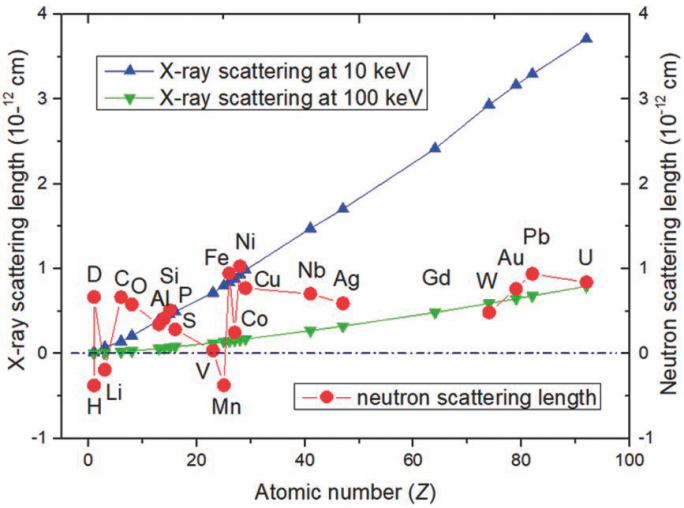

Figure 8: Neutron scattering lengths (red dots) and X-ray scattering lengths/atomic form factors (blue and green triangles) for some elements from Ren and Zuo 2018, CC-BY [3].

to X-rays a scattering cross section can be defined to relate the scattering to the signal measured on the detectors. [124-126]

3.1.3 X-ray sources

Since the first discovery of X-rays from a Geisler discharge tube by W. Röntgen, different methods of generating X-rays have been developed. Nowadays the most common methods used to generate them is by either using in-house X-ray tubes or through synchrotron facilities. [121]

On in-house sources, X-rays can be generated by accelerating electrons onto a metal target. The accelerated electrons interact with electrons in the electron shells of the atoms of the target material and can remove them. This in turn causes electrons from an energetically higher shell to fall into the more energetically favorable vacancy. Each of these transitions has a fixed energy, specific for each material, and the generated radiation is named depending on which shell the electron comes from and falls into. In for example K radiation, a 1s-electron, an electron from the innermost shell, is removed and a 2p-electron falls into its position. This process releases energy in the form of X-ray radiation (**Figure 9**). As this energy is specific to the target material, it creates a characteristic X-ray spectrum. A non-characteristic continuous X-ray spectrum, the so-called Bremsstrahlung, is

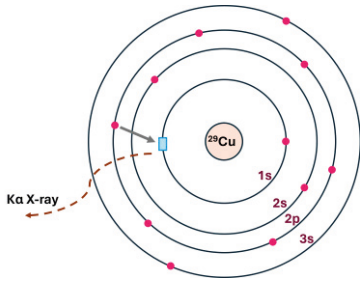

Figure 9: Schematic representation of Kα X-ray generation from a copper source, representing the electron transition between the shells, where a 2p-electron falls into the vacancy left by an 1s-electron.

generated as well. These X-rays are created through the deceleration of the initial electrons in the beam as they hit the target material. The energies for this depend on how individual electrons are decelerated. [121]

For most in-house measurements the X-ray beam should be monochromatic, which means that the beam consists of ideally one, or practically a narrow distribution of X-ray wavelengths. Monochromaticity can be achieved by directing the beam through a filter or monochromator. In order to get a parallel beam with a small spot size, the beam can be collimated. Common target materials used for X-ray generation are e.g. copper (Kα 1.54 Å) and silver (Kα 0.56 Å). [121]

Another, more powerful tool for generating X-rays is by using synchrotron sources such as at Diamond in Didcot, UK, or MAX IV in Lund, Sweden. In these dedicated facilities, X-rays are generated through bending the path of extremely fast electron circulating inside a storage ring, due to quantum mechanical processes. They can provide extremely high fluxes and a range of wavelength among other properties conducive for X-ray experiments. [121]

3.1.4 Neutron sources

The use of neutrons for scientific studies goes back to the early 1940s, not too long after their first discovery by James Chadwick in 1932. While it is common to have X-ray scattering equipment in-house at research institutes, this is not the case with neutron scatting instruments. Safely generating neutron radiation with sufficient flux for scattering experiments can be a lot more challenging, and experiments are primarily conducted at dedicated facilities. [127]

Modern neutron facilities can be divided into two categories based on their neutron source. The first type are fission reactor based sources. These were the first neutron reactors, with the first being built in 1942. This reactor type continuously generates neutrons with a wide range of wavelengths through a process called fission. To achieve this, nuclear fuels are used, such as enriched uranium with a high content of ^{235}U. This fuel becomes unstable upon the absorption of a neutron and

breaks into lighter nuclei, generating more neutrons and other subatomic particles in the process. Neutron sources based on this type of source include the Institut Laue-Langevin in Grenoble, France, and the High Flux Isotope Reactor in Tennessee, USA. [123, 125, 127]

The other type are non-continuous, accelerator driven spallation sources. In these, protons are accelerated to high energies around 1 GeV in a particle accelerator and made to hit a heavy metal target like tungsten, mercury or uranium. Then, through a process called spallation, fast neutrons with energies up to several MeV are generated from the nucleus. The resulting neutron signal can be pulsed at several pulses per second, as it is possible to control the timing of the protons hitting the target. Each pulse contains a distribution of neutrons with different energies. Examples of this type of neutron sources include ISIS Pulsed Neutron and Muon Facility in Didcot, UK, and the European Spallation Source in Lund, Sweden. There can be advantages in a non-continuous neutron stream, and a mechanical chopper can also be used at a reactor source. [123, 125]

To be of use for most experiments, the high energy neutrons generated by fission or spallation sources need to be slowed down. This can be done with the help of "moderators", usually hydrogenated materials. Through inelastic collisions, they slow these neutrons down to thermal energies, or wavelengths of around 1 Å. These slower neutrons are also called "thermal neutrons". This wavelength and energy range generally corresponds to the scale of interatomic spacings and to molecular, magnetic and crystal vibrations, and can therefore be used to probe them. Depending on the application it is also possible to generate neutrons with higher or lower energies through a change in moderation. The generated neutrons can escape out of the moderator towards the scattering instruments through holes in its reflective casing. [123, 125]

Because the neutrons are generated isotropically, multiple instruments can be attached to one reactor or target station. Measurements can be run simultaneously, but only a fraction of the neutrons released can be harnessed for individual experiments. This remains a limiting factor, as low neutron flux can lead to long counting times in order to get good statistics for experiments. The instruments can be situated either directly at the source, or neutrons can be directed to the instrument by use of gently curved neutron guides, which reflect neutrons within a certain incident angle through total reflection. [123, 125]

After collimation of the beam, the neutron spectrum is controlled through monochromation at continuous sources, losing up to 99% of them in the process. At spallation sources, and sometimes at reactor sources as well, the so called "Time of flight" (TOF) method is used, where neutrons with a range of wavelengths are utilized by measuring the time it takes for each neutron to travel from the moderator, through the sample and to the detector. Knowing the distance from the source to the detector makes it possible to determine their velocity and thereby energy. [123, 128]

3.1.5 Small angle scattering

Both X-rays and neutrons can be used for Small Angle Scattering (SAXS and SANS, or SAS in general). SAS makes use of the signals measured in scattering experiments in a similar fashion to other common methods like powder diffraction, but utilizes measurements in the low Q range, at small scattering angles. Practically, this is often achieved by moving the detector further away, with the sample to detector distance determining the Q range that can be adjusted to the expected length scales within the sample (**Figure 7**). Depending on the sample, the scattered intensity at small angles can be very low in comparison to the incident intensity, requiring either long measurement times or high flux available at e.g. synchrotron sources. [121, 128]

Due to the broad range of samples that can be measured, including crystalline and non-crystalline, as well as liquid or solid samples, simple sample preparation, relatively fast measurements, SAS is an important and widely used method. While the access to SANS instruments is mostly limited to dedicated neutron facilities, commercial SAXS instruments are available for in-house use. Using SAS, structures in the 1 to 100s or more nm length scale, such as biomolecules, crystalline domains, nanoparticles and surfactant micelles, can be investigated (**Figure 10**), and information on properties like size, shape and interactions can be gained. SANS in particular offers the unique ability to highlight specific domains of the structures of interest through the use of isotropic substitution, especially using ^{1}H hydrogen and ^{2}H deuterium. [121, 128]

For a SAS measurement to be sensible, the sample must exhibit structural inhomogeneities, meaning differences in scattering properties, on the right length scale, such as between nanoparticles and a solvent. Here the particles and solvent can be described by each having a scattering length density (SLD_P and SLD_N) [123]:

$$SLD^{Neut.} = \frac{\sum_{i=1}^{n} b_{c_i}}{V_m} \tag{8}$$

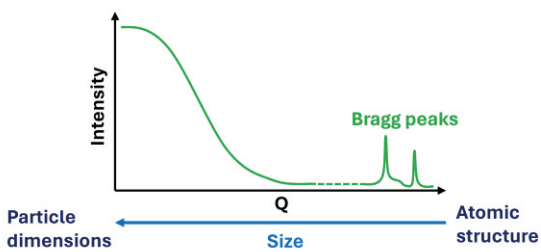

Figure 10: Schematic scattering curve as intensity over Q, with the relation to the corresponding distances in the sample.

Figure 11: The effect of contrast variation on distinguishable structures in a neutron scattering experiment.

for neutron scattering, with the bound coherent scattering length b_{ci} of the i-th of n atoms in a molecule and the molecular volume V_m, and analog [123]

$$SLD^{X-ray} = \frac{\sum_{i=1}^{n} Z r_e}{V_m} \tag{9}$$

for X-ray scattering, with Z as the atomic number of the i-th atom in the molecular volume V_m and the classical electron radius r_e. The overall scattering intensity is then given by [121]

$$I(Q) = (SLD_p - SLD_s)^2 N_p V_p^2 P(q) S(q) \tag{10}$$

with the number N_p and volume V_p of particles, the form factor $P(q)$ and the structure factor $S(q)$. The form factor contains a term with the distance between points in the particle itself, and thus gives information about the particle shape and size. The structure factor contains a term with the distances between the particles, the inter-particle correlation, and thus gives information about the average distance between particles in the sample, which is especially important at non-dilute concentrations. [121]

Strong, locally very specific contrast can be achieved in SANS through the use of isotope substitution as mentioned before. It allows for the highlighting of various substructures, by measuring different "contrasts". This can be seen in **Figure 11**, where the domains with different contrast are represented by different colours. Matching various parts of the structure with the SLD of the solvent can make them "appear" or "disappear" in the measurement, and detailed structural models can be built from measuring different contrast variations. [121, 128]

Different methods for analyzing SAS data have been developed, a common one is the Guinier Approximation. It describes the asymptotic behavior in the small Q region, approximating the form factor at small angles and providing the radius of gyration, a reasonably accurate particle size. This approximation can be used for

dilute systems, where any structure factor can be neglected, when good data can be measured at sufficiently small angles. In this case the measured intensity is [121]

$$I^{SAXS} \approx \Delta\rho^2 V_p^2 e^{-(Q^2 {R_g}^2/3)} \tag{11}$$

with the radius of gyration R_g, where the intensity is proportional to the exponential of $(-(Q^2R_g^2)/3)$. Plotting log $I^{SAXS}(Q)$ as a function of Q^2 should therefore produce a line with slope $-R_g^2/3$, from which the radius of gyration can be calculated. The radius of gyration R_g of a particle is defined as the root-mean-squared distance from the particle's centre of gravity. [121, 128]

This approximation can be applied to any dilute systems that contain particles of arbitrary shapes. In the case of spherical particles, the radius R_g can be directly correlated to R through $R_g^2=(3/5)R^2$. In case of non-spherical particles, factors like length or cross section need to be known to be able to calculate more dimensions from R_g. [121, 128]

Using this approximation, the scattering intensity at small angles can be used to gain information about the shape of particles with well-defined shapes, e.g. spheres, cylinders and disks (**Figure 12**). For this range they can be described using different descriptions for the intensity behaviour, e.g. a sphere can be describe by [128]:

$$\ln I(Q) \cong \ln I(0) - \frac{R_{g,sphere}^2}{3} Q^2 \tag{12}$$

Using the slope and oscillating features a characteristic shape can thereby be determined. Another way to roughly classify is by calculating the power law of the form factor at intermediate angles. Using a log-log plot, e.g. a smooth spherical particle has a slope around -4, a cylindrical particle has a slope around -1 and a disk-

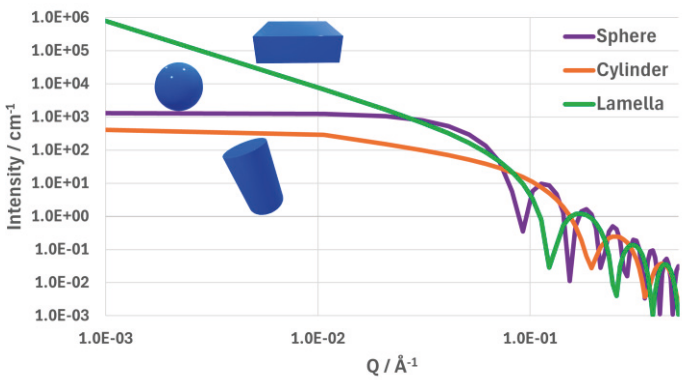

Figure 12: Schematic scattering curves of samples with differently shaped particles on a typical log-log scale: Sphere (purple), cylinder (orange) and lamella (green).

like one around -2. Slopes between -3 and -4 indicate fractal aggregates, dissolved polymers or particles with rough interfaces. [121, 128]

To further gain information from data obtained through SAS measurements, various mathematical models and software packages have been developed. In this thesis the models contained in the software SASview were used [129]. The choice of model is important, and often multiple models can be fit to a system similarly well. For fitting, it is important to keep in mind prior knowledge of the system. In the systems presented here, e.g. size and volume of the surfactant head and tail groups, requirements to form a physical micelle, such as minimal aggregation numbers, and expected behavior upon a change in concentration, inform the model choice, alongside comparisons to published, similar systems. Additionally, minimizing the number of fitted parameters by choosing a model that is as simple as is sensible, while using multiple data sets from e.g. different neutron contrasts measurements, can provide more confidence in the results. [130-132]

3.2 Disordered Materials

In comparison to just single atoms or molecules, bulk materials show an additional range of observable properties. Forces between molecules, together with temperature and pressure which relate to the kinetic energy in the system, translate into bulk phases like liquids and solids, as mentioned in a previous section. The arrangements of these atoms or molecules can be described by the structure of this bulk phase. In turn, knowing the structure of a material can yield information about prominent interactions and their conditions, which can be used to further fundamental understanding, and to plan and improve future processes and predictions. [133]

Molecules in a gas can be described as having high kinetic energy and weak intermolecular forces, where individual molecules are far apart and randomly arranged. A solid on the other hand has low kinetic energy and stronger intermolecular forces, with atoms or molecules rigidly packed together. In crystalline solids these molecules are arranged in regular patterns, that represent an energetically favorable coordination. Molecules in the liquid state exhibit both considerable kinetic energy and intermolecular forces. These molecules are densely packed, similar to a solid, but can move more freely, and the bulk liquid does not retain a definite shape. Liquids do not usually exhibit the regular long-range order of solids, but their structure is also not completely random like a gas. Their structural order is both short range and dynamic, making them harder to study then many solids. [134]

One focus of this thesis is the investigation of the DES liquid structure. This is possible though the use of modern techniques including neutron scattering experiments in combination with computer simulations.

3.2.1 Total scattering and distribution functions

The structure of crystalline materials can be modelled by analysing their pattern of Bragg peaks, but that is not possible for disordered materials. In order to gain an insight into the atomic structure of these materials, other methods have to be employed. This can be done through Total Scattering (TS), which makes use of the whole scattering signal, any Bragg peaks together with diffuse scattering. TS can be used for crystalline, non-crystalline or partially crystalline materials, and is measured using a similar experimental setup as SAS. Unlike SAS, which is measured over a small Q-range, total scattering requires a wider Q-range. Using the corrected and normalized data from such measurements, the structure of the material can be mathematically described in different ways. [135, 136]

A straightforward function describing interactions is the radial distribution function G(r) (RDF), sometimes also called the pair distribution function or pair correlation function, but other times defined slightly differently depending on the author. The RDF represents a distribution of density fluctuations as a function of distance (**Figure 13**). Using the local number density at position r in the material, it can be described as [136]

$$n(\mathbf{r}) = \sum_j \delta(\mathbf{r} - \mathbf{R_j}) \tag{13}$$

with the position R_j of a random atom j. This can be related back to the average distances between atoms in the material through the performance of an autocorrelation on the density distribution [136]

$$G(\mathbf{r}) = \frac{1}{N}\sum_{ij} \delta(\mathbf{r} + \mathbf{R_j} - \mathbf{R_j}) \tag{14}$$

with the position R_i of a random atom i. Separating terms where $j = i$ and $j \neq i$

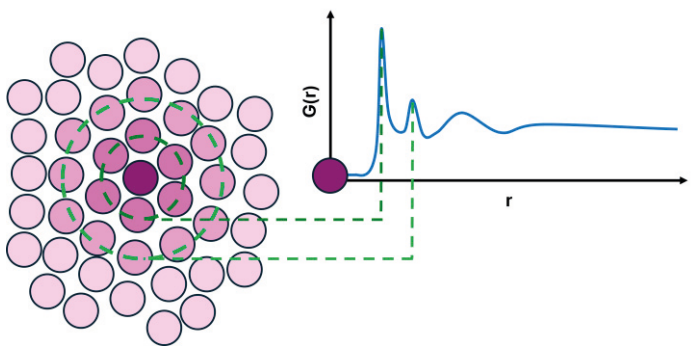

Figure 13: Schematic representation of a disordered material (left) and the corresponding RDF (right).

leads to [136]

$$G(\mathbf{r}) = \delta(\mathbf{r}) + \frac{1}{N}\sum_{i \neq j} \delta\left(\mathbf{r} + \mathbf{R_j} - \mathbf{R_j}\right) \tag{15}$$

$$G(\mathbf{r}) = \delta(\mathbf{r}) + \rho g(\mathbf{r}) \tag{16}$$

with the average atomic number density ρ. Through this, a representation of the material can be gained in a similar way as seen in **Figure 13**, a measure of the average distances from one random, but fixed, atom to all others. [136]

In the case of a multi component system it makes sense to split up G(r) into multiple terms, one for each atom type. For a system consisting of atoms of the type α and β the full autocorrelation function can be given by [136]

$$G(\mathbf{r}) = \sum_{\alpha} c_\alpha \delta(\mathbf{r}) + \rho \sum_{\alpha,\beta \geq \alpha} \left(2 - \delta_{\alpha\beta}\right) c_\alpha c_\beta g_{\alpha\beta}(\mathbf{r}) \tag{17}$$

where $c_\alpha = \rho_\alpha/\rho$ and ρ_α is the number density of atoms of type α.

3.2.2 EPSR modelling

Empirical Potential Structure Refinement (EPSR) is a computational technique and software package that can be used for modelling total scattering data. It is based on a simulation based refinement approach, to match experimental data the interatomic potentials are systematically perturbed. an atomistic reverse Monte Carlo simulation that corrects employed pair interaction potentials through comparison with diffraction data, and can be used to build atomic and molecular models of disordered systems. In order to run a good simulation, a box is first built using known properties such as atomic and molecule compositions and structures, alongside appropriate parameters. Within EPSR these molecules can perform four types of movement: whole molecule translations, whole molecule rotations, rotation of specific side groups, and individual atomic movements within the molecule. While EPSR is running, random small moves are performed, and which move is accepted is based on the change in potential energy ΔU of the system [137]

$$\Delta U = U_{after} - U_{before} \tag{18}$$

If $\Delta U > 0$, then the move is accepted. If $\Delta U < 0$, then it is accepted with a probability of $\exp[-\Delta U/kT]$, where k is the Boltzmann constant and T is the temperature. The total potential energy of the system can represented as [137]

$$U = U^{Ref} + U^{Ep} \tag{19}$$

U^{Ref} is the reference potential, and stems from the intermolecular potential of the atoms and molecules building the box, taking into consideration things like sensible geometries and charge, where parameters might be found in literature. It is usually a simple Lennard-Jones 12-6 potential plus effective Coulomb charges [138]

$$U_{ref} = \frac{1}{2}\sum_{i,j\neq i}\sum_{\alpha,\beta}\left\{4\epsilon_{\alpha\beta}\left[\left(\frac{\sigma_{\alpha\beta}}{r_{\alpha_i\beta_j}}\right)^{12} - \left(\frac{\sigma_{\alpha\beta}}{r_{\alpha_i\beta_j}}\right)^{6}\right] + \frac{q_\alpha q_\beta}{4\pi\epsilon_0 r_{\alpha_i\beta_j}}\right\} \quad (20)$$

with one half of the sum over the distinct atoms *i* and *j*, and the sum over the different atom types α and β to avoid double counting. Using the EPSR shell, the basic molecule structure can be built in the included molecule builder Jmol, and the correct parameters can be added into the resulting .mol file. The simulation box can then be built under the consideration of density, and the molecules randomly spread and oriented inside of it. U_{Ep} is the empirical potential that relates the experimental and simulated structure factors, with removal of artifacts in the data. [137, 138]

By using ESPR realistic 3D models of liquids and other disordered systems can be built and through this high degrees of structural information gained. EPSR includes a variety of sub routines that can be utilized to investigate specific aspects of the system. Some of the ones used in this thesis include COORD, used to calculate coordination numbers, CLUSTERS, used to analyze clustering of specific sides or molecules, CHAINS, used to analyze the formation of extended e.g. hydrogen bonding chains, and SDF, which can be used to visualize the three-dimensional probability spread of atoms or molecules around each other. [137, 138]

3.3 Differential Scanning Calorimetry

Differential scanning calorimetry (DSC) is a well-established method for measuring thermal effects on samples. It allows for a relatively quick and simple determination of properties like heat capacity, heat of transition, kinetic behaviour, purity and melting and glass transitions.

For a DSC experiment, the change in change in heat flow rate to a sample is measured and compared to the simultaneous measurement of a reference under temperature control. During chemical reactions or phase transitions in the sample, its temperature undergoes changes, which can be picked up by the DSC instrument. By using a thermal ramp program, thermally induced processes, such as the phase transitions relevant in this project, can be examined.

In this thesis, a heat flux type DSC with turret-type measuring system was used. Here the heat flow passes from the bottom of the furnace through jacket of two thin-walled cylinders, and the sample and reference are placed on top of each. In our case the data is saved as Heat flow (in mW) over temperature (in °C) and can be directly analysed in the internal program. A schematic representation of a measurement curve can be seen in **Figure 14**. The glass transition temperature T_g appears as a stepwise change, the crystallization temperature T_c as a peak and the melting point T_m as a minimum. Conventionally the peak values of T_c and T_m are reported, while for T_g either the onset temperature or middle temperature is used. In this thesis the middle temperature will be used for T_g. [139]

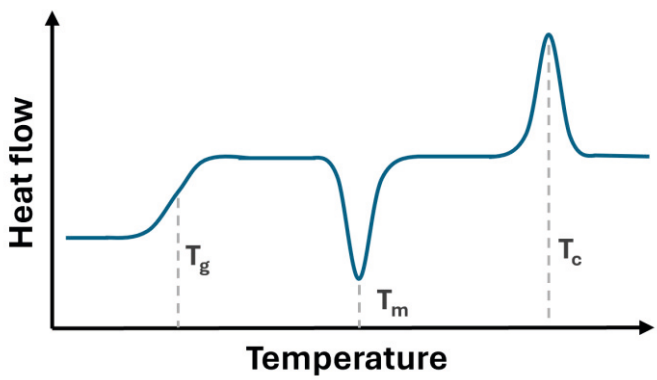

Figure 14: Representation of a typical DSC measurement of a material that has a glass transition temperature, crystallisation temperature and melting point.

3.4 NMR

Nuclear Magnetic Resonance (NMR) spectroscopy is a widely used method for investigating molecular structures. It is a non-destructive, relatively fast and simple method. Chemical reactions, dynamic processes, as well as concentrations, can be directly observed, and samples are not limited to, but are most commonly small organic molecules.

The method is based on the interaction of the characteristic nuclear spin I of an atomic nucleus with an outside magnetic field. Using atom specific radio frequency waves, characteristic transitions between nuclear energy levels are promoted. This is measured, and can be analysed to gain insight into the molecular structure. [86]

Not all atoms are NMR active. Their activity depends on the overall nuclear spin. In a nucleus, both protons and neutrons have a net spin of 1/2 each, with further interactions that can change the overall spin. In general, it can be said that when the number of protons (Z) and the number of neutrons (N) is even $I = 0$, e.g. ^{12}C and ^{16}O, and the nucleus is not NMR active. For Z even and N odd I is a half-integral, e.g. $I = 1/2$ for ^{1}H, ^{13}C and ^{19}F, and the nucleus is NMR active. This group of isotopes includes some of the most used for NMR. For Z odd and N even I is an integral, e.g. $I = 1$ for ^{2}H and ^{14}N. [86]

The nucleus has an associated magnetic moment alongside the spin, which causes it to behave similarly to a small bar magnet. When no external magnetic field is present, these bar magnets are randomly oriented. Exposure to an external magnetic field aligns them with or against this field, each of which state has a discrete energy level. This energy is relatively small and depends on the atom, it's environment and the strength of the applied magnetic field. Transition between the states can be induced through the addition of energy in the form of radio waves. [86]

The environment of each nucleus plays an important role in their signal output. The local electron density has a shielding effect, reducing the magnetic field experienced by each nucleus. Therefore, different chemical shifts can be seen through the measurement creating a unique sample pattern for each molecule. Some nuclei like ^{1}H can also experience spin-spin coupling, which can lead to a splitting of the associated signal. Quantitative measurements can be performed, as the area underneath the corresponding peaks is directly proportional to the number of the associated nuclei. [86]

With knowledge of which structures could be present in a sample, NMR can be used as a quick tool to check for their presence and calculate the relative amount of different components. In this thesis it is used to as check for reactions within the samples, as well as calculate the degree of deuteration on components used for neutron scattering.

3.5 Karl Fischer titration

Water content can have a significant impact on DES properties, and as many DES are hygroscopic, monitoring their water content is a standard procedure. One method of doing this is Karl Fischer (KF) titration.

KF titration is based on the reaction of the titrant, usually iodine, sulfur dioxide, a base (RN) and an alcohol, here the solvent consisting of methanol, with the water in the sample [140]

$$H_2O + I_2 + SO_2 + CH_3OH + 3RN = [RNH]SO_2CH_3 + 2[RNH]I \qquad (21)$$

The main types of KF titrators are based either on either coulometric or volumetric measurements. In coulometric KF titrator the reagent, here iodine, is generated in solution through application of an electrical current, while in a volumetric KF titrator the reagent is added through a burette. The endpoint of the reaction in both types is detected using an indicator electrode. [140, 141]

While being a very precise and relatively fast method for water determination under the right conditions, a significant limitation of KF titration lies within reactivity of the components. Reactions can occur either with the KF reactants, altering their behaviour, or with the solvent, where water can be formed, e.g. in an esterification reaction. Measurements especially of ketones and aldehydes, but also some acids, oxides and peroxides can be significantly off the actual initial water content, and need to be approached with caution using counter measures to reduce the effect. In this thesis work the pH of acid containing samples was neutralized using imidazole, in order to reduce water producing esterification reactions, before KF titration was used.

3.6 Fluorescence

The use of fluorescent probes to determine the CMC of a surfactant system is a well-established process. Here, the fluorescent probe changes its fluorescent behaviour depending on its environment. In comparison to aqueous systems, a fluorescent probe might work differently in a DES system and not be suitable for measuring CMCs. Pyrene (**Figure 15**) has been found to be suitable for CMC in DES, and has been used in this project.

The fluorescent signal, in particular the intensities of the first and third peak (usually expressed as I_1/I_3), of pyrene changes depending on the polarity of the surrounding environment. In a polar solvent, the ratio is bigger, with a sharp decrease observable around the CMC, as pyrene is encapsulated in the more hydrophobic environment of a micelle. The value of the CMC can then be

determined from the plot of the ratio of intensity values against the concentration. Here, the CMC is determined to be at the onset of the change.[86, 142, 143]

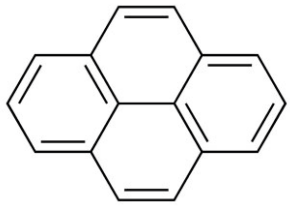

Figure 15: Chemical structure of pyrene.

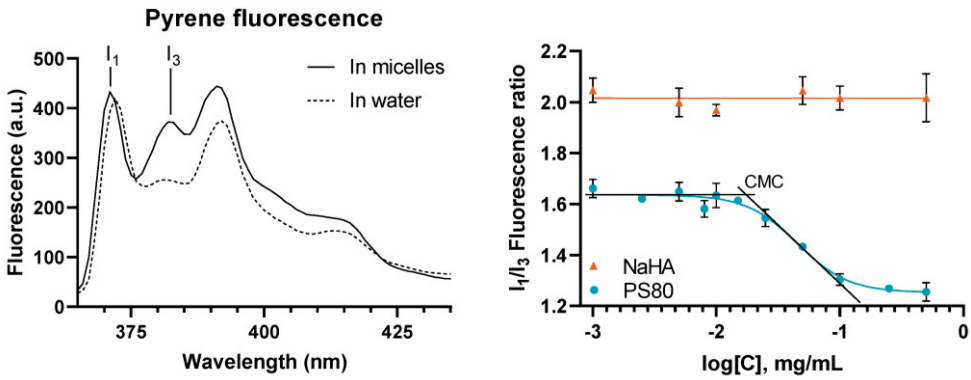

Figure 16: Left: Fluorescent emission spectrum of pyrene in water (dashed line) and with surfactants above the CMC (solid line). Right: Corresponding relative ratio I_1/I_3 of the peaks as a function of the concentration of sodium hyaluronate (orange triangles) and polysorbate 80 (blue dots), with the linear regressions to determine the CMC. Figure taken from Alviset et. Al, 2022, CC-BY [1].

4 Summary of papers

The papers in this thesis delve into the structures and formation of structures in Deep Eutectic solvents. As explained in the previous sections, Deep Eutectic Solvents are a class of solvents that have emerged in the last 20 years, gaining increasing traction in the last 10 years. Many DES are complex, mostly hydrogen bonding liquids, and their properties are greatly affected by their components, molar ratio, additives and other parameters. Here, we examine different aspects of these effects, as well as their interactions with added components, that could be useful for their application.

The first paper looks at the influence of chiral components and water on the DES structure, as well as examining the influence of size and hydrogen bonding groups on specific interactions in the solvent.

The second paper looks at the structure of the commonly used, but less structurally examined hydrophilic DES based on a zwitterionic and a molecular component, instead of the more common inclusion of at least one ionic component. Here we also examine how the addition of a metal salt influences this structure, and how this metal salt interacts with the solvent components.

The last paper looks at the formation of surfactant self-assembled structures in hydrophilic, halogen free acid-based DES. We find that the ethylene oxide-based non-ionic surfactants, which are often not soluble in the commonly used type IV DES, can be dissolved and form self-assembled structures depending on the molar ratio of the constituents used, while cationic surfactants form spherical micelles, distinct from those in other acid-containing DES.

Overall, in this thesis we fill gaps in some of the fundamental DES structure examination and solvation, through experimental methods, contributing to the foundation upon which further structural predictions and applications can be planned.

4.1 Paper 1

4.1.1 The solvent structure and what a chiral component does to it

Many biologically derived components and biologically useful molecules are chiral. These types of molecules have been shown to be useful DES components, but little research has been performed on the influence of using molecules with differing chirality on the structure of these DES. This can also impact and inform their use as chiral solvents, which are potentially important in organic syntheses and chiral extraction, by shining a light on chiral interactions within a DES.

In this paper we present the structure of 2:1 choline chloride with the chiral small carboxylic acid tartaric acid. We compare the structure of the single enantiomeric L-tartaric acid with the racemic DL-tartaric acid-based DES. We find that using L- vs DL-tartaric acid does not significantly change the overall solvent structure, but it does change the interactions present between tartaric acid molecules. The hydrogen bonding interactions that lead to a change in behaviour compared to the solid form of the acids are dominated by choline and chloride interactions, which lead to significant overall structuring of the DES, whereas tartaric acid-tartaric acid interactions are relatively weak overall.

This would suggest that for most applications DES based on the different enantiomers can be treated similarly. For use as a chiral solvent this suggests strong competitive behaviour between non-chiral DES components and chiral interactions, so to use these solvents in chirally selective syntheses, the substrate would require significantly stronger interactions with the tartaric acid than the other species present.

Overall, the interactions of the HBD-choline-chloride are similar to what has been found in other systems, with a dominance of chloride interactions, while tartaric acid and choline chloride all form system spanning percolating clusters with no sign of separation into domains or specific longer range hydrogen bonded chains.

4.1.2 Comparing choline chloride + carboxylic acid DES

Carboxylic acids are a popular DES component, and here we compare our 2:1 tartaric acid : choline chloride with systems based on malic and oxalic acid systems. Oxalic acid is a smaller carboxylic acid, while malic acid is almost identical to tartaric acid, but missing one central hydroxyl group. These systems have been studied at a 1:1 ratio with choline chloride.

Clear effects of the size of the acids can be seen in the interaction distances (oxalic < malic < tartaric acid), while the oxalic acid also has the highest coordination numbers of the molecular centres. Malic acid has slightly lower coordination

numbers than tartaric acid even though it is slightly smaller, but here the overlap in effect of the difference in molar ratio and one less hydrogen bonding site in malic acid can be seen.

4.1.3 Effect of water addition on the solvent structure

The addition of water at a 2:1:2 molar ratio of choline chloride : L-tartaric acid : water is also presented. Similar to what has been found for other DES systems, a decrease in coordination of the other components around each other can be seen as they start interacting with water. Especially choline exchanges interactions with itself and tartaric acid for those with water, leading to the biggest differences in the structure. Overall interaction distances and liquid structure remain similar, with water diffusely interacting with all components. Similar to the other components water forms small clusters, but unlike the other components it does have system spanning percolation. Adding small amounts of water could therefore be a potential method to weaken the choline-tartaric acid interactions and so enhance the interactions between a solute and the chiral tartaric acid. This would need to be tested in a selective reaction, and will still require the substrate-tartaric acid interactions to be stronger than those of either species with water.

4.2 Paper 2

4.2.1 Interaction networks in betaine + glycerol and how they differ from choline chloride based systems

Betaine is a renewably sourced zwitterionic molecule, structurally related to the common DES component choline chloride, that has been found to form a range of useful DES. Betaine forms fewer DES, which are usually more viscous and with higher melting points than choline chloride-based DES with similar HBD. In this paper we investigate the structure of the 1:3 betaine : glycerol DES, and compare it to what has been found in the 1:2 choline chloride : glycerol DES.

Between the equivalent main interactions, the coordination in betaine : glycerol is higher, which is expected as chloride also coordinates to both of these species in the choline chloride-based DES. The peak positions in their radial distribution functions, indicating the most prominent distance between the molecules is also similar.

We find that the zwitterionic betaine in this liquid forms significant chains between its positively and negatively charged termini, similar to that what has been found for betaine in aqueous solutions. This is quite different from the choline interactions in choline chloride-based DES, as choline is a cation and does not form significant chains or show other significant self-interaction. This could contribute to the often higher viscosity found in betaine containing DES.

Betaine – betaine and betaine – glycerol also form system spanning percolating clusters, but glycerol does not, and mainly interacts by forming long hydrogen bonded chains. Glycerol also forms chains in choline chloride : glycerol DES, where they are even longer.

The betaine – glycerol interactions also differ significantly with the terminal carboxylate in the betaine acting as a hydrogen acceptor to the glycerol hydroxyl group, while the terminal hydroxyl group in choline acts primarily as a hydrogen bond donor. Betaine and glycerol also form only shorter chains (23 vs 60 molecules), but similar small clusters.

The spatial density functions for the molecular centres also reveal that both betaine and glycerol compete for the glycerol hydrogen bonding sites in very similar relative positions, unlike in choline chloride glycerol, where they form more distinct, separate domains. The probability distribution around betaine on the other hand is more similar to that around choline, with more discrete domains, with them being more diffuse here than in the ChCl based systems.

4.2.2 Solvation structure of iron nitrate

For applications it is common to add solutes to the solvent system, be it as precursors, catalysts, additives or others. DES are also finding application in the selective dissolution of metal ions for recycling or ore refining. Here we look at the solvent structure upon the addition of 0.25 mol/kg^{-1} iron (III) nitrate nonahydrate, a potential precursor for formation of iron oxide nanoparticles. The iron interacts with all the hydrogen bonding oxygens in the system, and is mostly prominently solvated by glycerol and nitrate. This differs from previous work on the same salt in choline chloride:urea solvents where the chloride had a significant role in coordinating the iron ions, even though both DES show extremely high solubility of the iron salt (>20 wt%). Nitrate interacts with all hydroxyl hydrogens and the positively charged terminus of betaine, but all interactions besides with iron have low coordination numbers. Water shows various and very diffuse interactions with all hydrogen bond acceptor and hydrogen bond donator sites, but is most coordinated by iron, nitrate and water.

For betaine – glycerol and betaine – betaine no significant changes besides the expected decrease in coordination number due to the new interaction and a slight increase in distances as the small solutes intercalate can be seen. Glycerol – glycerol interactions on the other hand show a significant increase in the coordination of the terminal hydrogen bonding groups with each other and an increase in length of the overall hydrogen bonded chains in the system.

As shown both in the DES structure and interaction with dissolved iron, halide ions interact very strongly with the other components. Removing that interaction could lead to a change in how the solute can interact with other components in the system, e.g. lead to a change component reactivity or in particle morphology in a nanomaterial synthesis, or factors like “salting out” specific components in an extraction process.

4.3 Paper 3

4.3.1 Dissolving surfactants in DES

Another common solute are surfactants, amphiphilic molecules comprising of a hydrophilic "head" group and a hydrophobic "tail" group. Outside of everyday use as soap, they have varied specialized applications in solvent systems, from modifying wetting and interfacial behaviour, to lysing cells and templating nanomaterials. In this paper we investigate the solubility and self-assembly of different surfactants in citric acid and glycerol-based systems.

Here, we tested the solubility of common surfactants like the anionic SDS, the cationic C_{12}TAB, C_{16}TAB, and the non-ionic Brij L4® and L23® in 1:2 and 1:4 citric acid: glycerol (CA:Gly), as well as neat glycerol for comparison. As in many DES, not all three surfactant types were soluble in these solvents, with SDS showing insignificant solubility in all three systems. C_{12}TAB on the other hand was soluble at room temperature in all systems, and C_{16}TAB was soluble at 50 °C. Using pyrene fluorescence, we were able to find that the CMC of both surfactants is significantly higher than in water, showing very good solubility. For C_{16}TAB in 1:2 CA:Gly the CMC is an order of magnitude higher than in both water and other reported DES, based on ChCl:Gly or ChCl:maonic acid. Marked, non-linear differences in CMCs for C_{12}TAB between neat glycerol, 1:4 CA:Gly and 1:2 CA:Gly could be seen too, exhibiting a modulation of solubility.

The non-ionic surfactants on the other hand were only soluble in 1:2 CA:Gly, and insoluble in the other systems. This is interesting, as non-ionic surfactants, are less commonly soluble in typical hydrophilic DES, such as ChCl : urea or ChCl : tartaric acid, and their solubility in our system can be changed with molar ratio. The surfactants remain soluble and still self-assemble upon the addition of 10 wt% of water, while this addition does not induce better solubility in 1:4 CA:Gly or neat glycerol, which is promising for future applications, as the addition of water significantly reduces the DES viscosity, making it more practical to work with without altering the fundamental solute dissolution behaviour..

4.3.2 Cationic and non-ionic surfactants self-assembly

For future work in e.g. templating catalytic nanomaterials it is best to avoid halide counterions. In the Hofmeister series, the nitrate and bromide counterions are adjacent and are known to have very similar effects on CMC, micelle size and morphology for C_nTA surfactants. Therefore, we investigated the self-assembly of the nitrates of C_{12}TA (C_{12}TANO) and C_{16}TA (C_{16}TANO) and nonionic Brij L23® surfactants in 1:2 and 1:4 CA:Gly, in systems where homogeneous solutions were formed, using small angle scattering. For C_{12}TANO, C_{16}TANO and Brij L23® in 1:2 CA:Gly we found that they form spherical micelles. Similar spheroid micelles of

C_{12}TAB were found in water and other DES. The micelles formed by C_{16}TANO show similarities to those found in water and DES such as 1:2 ChCl:Gly as well, but are different from the elongated micelles found in 1:1 ChCl:Mal. In that system the authors hypothesized that the deprotonated acid contributes to this elongation becoming favourable, similar to what has been seen in aqueous systems. It is interesting to see that no elongation can be seen in our system, which should also contain a significantly deprotonated carboxylic acid (testing with pH paper indicates a pH of around 1).

Brij L23® can be fit using a core-shell model. It can be seen that here the micellar radius is relatively large, indicating that the surfactant tails are fully extended and the aggregation number per micelle is high. The head groups are also relatively extended, similar to what can be seen in water. This is unlike that has been shown for DES like 1:3.5 cerium nitrate : urea and IL like EAN, where the micelle shell as relatively thin, indicating either a loss of contrast or coiling in the head groups. But this shows that for 1:2 CA:Gly little coiling occurs, with the headgroups retaining high solubility in the DES.

The micellization behaviour of C_{12}TANO and C_{16}TANO in neat glycerol, 1:4 CA:Gly and 1:2 CA:Gly was also investigated through SAXS, but little difference between these can be seen. This is not unexpected, as micellar elongation is often supported by the addition of more ionic components, and not as much with molecular ones. As the solubilities of the surfactants in these solvents differs, a difference in phase behaviour at higher concentrations than those measured here can be expected.

Overall, this shows the versatility of DES systems, whereby adjusting the molar ratio or individual components, solubilities can be drastically changed. This also supports what has been seen on the structural level, where the solvent structure and primary interactions remain intact upon the addition of small amounts of water to a DES, seeing that the two non-ionic surfactants remain soluble and insoluble in the hydrated 1:2 and 1:4 CA: Gly respectively.

5 Conclusions and Outlook

In this thesis we took a close look at the DES solvent structure and the interplay between component properties and solutes. In the first paper we looked at how component chirality and addition of water can affect the DES structure and interactions, in a choline chloride : tartaric acid-based DES. In the second paper we looked at a DES that does not contain any small ions like halogens, in a betaine : glycerol-based DES, and how this DES solvates an iron nitrate salt. In the third paper we looked at the solubilization and self-assembly of surfactants in another halogen free DES, in citric acid : glycerol.

As expected of multi-component systems, the interactions and behavior of solutes are not straight forward. As can be seen in the chiral choline chloride : tartaric acid DES, preferred interactions from the solid state of L- and DL-tartaric acid do not translate into preferred interactions in the DES, as interaction sites are overtaken by other, stronger interactions with ChCl. The betaine : glycerol system with iron nitrate also shows how the presence of small ions can noticeably alter the interaction between the DES components, and how the iron is significantly solvated by non-ionic components, with the other iron salt components highly dissolved in the DES. The citric acid : glycerol system also shows both the sensitivity of surfactant solvation to a change in DES components and molar ratio, but simultaneously robustness towards hydration, where the effect each of these factors is yet hard to predict. Conducting more studies into how such factors influence solvation and self-assembly processes remains as relevant as ever, in order to lay a foundation for their behavior, as has been done previously in solvents like water and ethanol. Additionally, such experimental work can be used to refine computational and machine learning approaches, in order to be able to efficiently predict and tailor solvent properties for specific applications.

In the frame of this project, we have conducted more experiments that are not yet included in this thesis, which will be published in the future. We have found that it is possible to produce small, non-agglomerated iron oxide particles in both Bet:Gly and CA:Gly, with and without the addition of urea, at relatively low temperatures from 90 to 120 °C. This is quite promising for their application, to use them as versatile, low temperature synthesis media. We have also found that SDS forms spheroid micelles in Bet:Gly, unlike the usually significantly elongated micelles found in ChCl-based systems. We suspect that, similar to the CA:Gly system in the third paper, this could be an effect of the relatively low concentration of small ions in the DES influencing aggregation behavior. In our experiments we have also seen

how the presence of salts can significantly influence the solubility and aggregation behavior of surfactants. For the use of surfactants to be used to e.g. influence the formation and morphology during nanomaterial synthesis, these complex effects remain to be untangled.

DES are varied and complex systems, it is one of their big advantages, but it also limits how predictable they are. In this thesis we illuminated a small corner of how these systems work, in the hope that it will further the general understanding and enable better predictability and thus optimized applications from greener syntheses, to recycling and improved extractions for environmental monitoring. And, in doing so, we hope to have contributed to a more sustainable future.

6 References

1. Alviset, G., et al., *New Preservative-Free Formulation for the Enhanced Ocular Bioavailability of Prostaglandin Analogues in Glaucoma.* Pharmaceutics, 2022. **14**(2).
2. Meng, X.Q., et al., *Impact of water on the melting temperature of urea plus choline chloride deep eutectic solvent.* New Journal of Chemistry, 2016. **40**(5): p. 4492-4499.
3. Ren, Y. and X.B. Zuo, *Synchrotron X-Ray and Neutron Diffraction, Total Scattering, and Small-Angle Scattering Techniques for Rechargeable Battery Research.* Small Methods, 2018. **2**(8).
4. Francisco, M., A. van den Bruinhorst, and M.C. Kroon, *Low-Transition-Temperature Mixtures (LTTMs): A New Generation of Designer Solvents.* Angewandte Chemie-International Edition, 2013. **52**(11): p. 3074-3085.
5. Abbott, A.P., et al., *Deep eutectic solvents formed between choline chloride and carboxylic acids: Versatile alternatives to ionic liquids.* Journal of the American Chemical Society, 2004. **126**(29): p. 9142-9147.
6. Abbott, A.P., et al., *Preparation of novel, moisture-stable, Lewis-acidic ionic liquids containing quaternary ammonium salts with functional side chains.* Chemical Communications, 2001(19): p. 2010-2011.
7. Bi, W.T., M.L. Tian, and K.H. Row, *Evaluation of alcohol-based deep eutectic solvent in extraction and determination of flavonoids with response surface methodology optimization.* Journal of Chromatography A, 2013. **1285**: p. 22-30.
8. Hammond, O.S., D.T. Bowron, and K.J. Edler, *Structure and Properties of "Type IV" Lanthanide Nitrate Hydrate:Urea Deep Eutectic Solvents.* Acs Sustainable Chemistry & Engineering, 2019. **7**(5): p. 4932-4940.
9. Hayyan, A., et al., *Fruit sugar-based deep eutectic solvents and their physical properties.* Thermochimica Acta, 2012. **541**: p. 70-75.
10. Liang, Y., et al., *Novel betaine-amino acid based natural deep eutectic solvents for enhancing the enzymatic hydrolysis of corncob.* Bioresource Technology, 2020. **310**.
11. Ribeiro, B.D., et al., *Menthol-based Eutectic Mixtures: Hydrophobic Low Viscosity Solvents.* Acs Sustainable Chemistry & Engineering, 2015. **3**(10): p. 2469-2477.
12. Zainal-Abidin, M.H., M. Hayyan, and W.F. Wong, *Hydrophobic deep eutectic solvents: Current progress and future directions.* Journal of Industrial and Engineering Chemistry, 2021. **97**: p. 142-162.

13. El Achkar, T., H. Greige-Gerges, and S. Fourmentin, *Basics and properties of deep eutectic solvents: a review.* Environmental Chemistry Letters, 2021. **19**(4): p. 3397-3408.
14. Hansen, B.B., et al., *Deep Eutectic Solvents: A Review of Fundamentals and Applications.* Chemical Reviews, 2021. **121**(3): p. 1232-1285.
15. Smith, E.L., A.P. Abbott, and K.S. Ryder, *Deep Eutectic Solvents (DESs) and Their Applications.* Chemical Reviews, 2014. **114**(21): p. 11060-11082.
16. Choi, Y.H., et al., *Are Natural Deep Eutectic Solvents the Missing Link in Understanding Cellular Metabolism and Physiology?* Plant Physiology, 2011. **156**(4): p. 1701-1705.
17. Florindo, C., et al., *From Phase Change Materials to Green Solvents: Hydrophobic Low Viscous Fatty Acid Based Deep Eutectic Solvents.* Acs Sustainable Chemistry & Engineering, 2018. **6**(3): p. 3888-3895.
18. Xu, K.J., P.L. Xu, and Y.Z. Wang, *Aqueous biphasic systems formed by hydrophilic and hydrophobic deep eutectic solvents for the partitioning of dyes.* Talanta, 2020. **213**.
19. Agieienko, V. and R. Buchner, *A Comprehensive Study of Density, Viscosity, and Electrical Conductivity of (Choline Chloride plus Glycerol) Deep Eutectic Solvent and Its Mixtures with Dimethyl Sulfoxide.* Journal of Chemical and Engineering Data, 2021. **66**(1): p. 780-792.
20. Chen, Y., et al., *Effect of organic solvents on the conductivity of polyethylene glycol-based deep eutectic solvents.* Journal of Molecular Liquids, 2022. **346**.
21. Cruz, H., et al., *Alkaline Iodide-Based Deep Eutectic Solvents for Electrochemical Applications.* Acs Sustainable Chemistry & Engineering, 2020. **8**(29): p. 10653-10663.
22. Ferreira, I.J., et al., *Uncovering biodegradability and biocompatibility of betaine-based deep eutectic systems.* Environmental Science and Pollution Research, 2023.
23. Garralaga, M.P., et al., *Ecotoxicological study of bio-based deep eutectic solvents formed by glycerol derivatives in two aquatic biomodels.* Green Chemistry, 2022. **24**(13): p. 5228-5241.
24. Jung, D., et al., *Toxico-metabolomics study of a deep eutectic solvent comprising choline chloride and urea suggests in vivo toxicity involving oxidative stress and ammonia stress.* Green Chemistry, 2021. **23**(3): p. 1300-1311.
25. Palmelund, H., et al., *Tailor-made solvents for pharmaceutical use? Experimental and computational approach for determining solubility in deep eutectic solvents (DES).* International Journal of Pharmaceutics-X, 2019. **1**.
26. Pontes, P.V.D., et al., *Choline chloride-based deep eutectic solvents as potential solvent for extraction of phenolic compounds from olive leaves: Extraction optimization and solvent characterization.* Food Chemistry, 2021. **352**.

27. Rodriguez, N.R., L. Machiels, and K. Binnemans, *p-Toluenesulfonic Acid-Based Deep-Eutectic Solvents for Solubilizing Metal Oxides.* Acs Sustainable Chemistry & Engineering, 2019. **7**(4): p. 3940-3948.
28. Hayyan, M., et al., *Are deep eutectic solvents benign or toxic?* Chemosphere, 2013. **90**(7): p. 2193-2195.
29. Hayyan, M., et al., *Toxicity Profiling of Ammonium-Based Deep Eutectic Solvents.* Plos One, 2015. **10**(2).
30. Nejrotti, S., et al., *Critical Assessment of the Sustainability of Deep Eutectic Solvents: A Case Study on Six Choline Chloride-Based Mixtures.* Acs Omega, 2022. **7**(51): p. 47449-47461.
31. Perna, F.M., P. Vitale, and V. Capriati, *Deep eutectic solvents and their applications as green solvents.* Current Opinion in Green and Sustainable Chemistry, 2020. **21**: p. 27-33.
32. Zaib, Q., et al., *Are deep eutectic solvents really green?: A life-cycle perspective.* Green Chemistry, 2022. **24**(20): p. 7924-7930.
33. Hammond, O.S., et al., *Deep eutectic-solvothermal synthesis of nanostructured ceria.* Nature Communications, 2017. **8**: p. 7.
34. Hammond, O.S., et al., *Microwave-assisted deep eutectic-solvothermal preparation of iron oxide nanoparticles for photoelectrochemical solar water splitting.* Journal of Materials Chemistry A, 2017. **5**(31): p. 16189-16199.
35. Hooshmand, S.E., et al., *Deep eutectic solvents: cutting-edge applications in cross-coupling reactions.* Green Chemistry, 2020. **22**(12): p. 3668-3692.
36. Mulks, F.F., et al., *Continuous, stable, and safe organometallic reactions in flow at room temperature assisted by deep eutectic solvents.* Chem, 2022. **8**(12): p. 3382-3394.
37. Yu, D.K., Z.M. Xue, and T.C. Mu, *Deep eutectic solvents as a green toolbox for synthesis.* Cell Reports Physical Science, 2022. **3**(4).
38. Cunha, S.C. and J.O. Fernandes, *Extraction techniques with deep eutectic solvents.* Trac-Trends in Analytical Chemistry, 2018. **105**: p. 225-239.
39. Padwal, C., et al., *Deep Eutectic Solvents: Green Approach for Cathode Recycling of Li-Ion Batteries.* Advanced Energy and Sustainability Research, 2022. **3**(1).
40. Ruesgas-Ramon, M., M.C. Figueroa-Espinoza, and E. Durand, *Application of Deep Eutectic Solvents (DES) for Phenolic Compounds Extraction: Overview, Challenges, and Opportunities.* Journal of Agricultural and Food Chemistry, 2017. **65**(18): p. 3591-3601.
41. Abbott, A.P., *Deep eutectic solvents and their application in electrochemistry.* Current Opinion in Green and Sustainable Chemistry, 2022. **36**.
42. Tome, L.I.N., et al., *Deep eutectic solvents for the production and application of new materials.* Applied Materials Today, 2018. **10**: p. 30-50.

43. Emami, S. and A. Shayanfar, *Deep eutectic solvents for pharmaceutical formulation and drug delivery applications.* Pharmaceutical Development and Technology, 2020. **25**(7): p. 779-796.
44. Pedro, S.N., et al., *Deep eutectic solvents comprising active pharmaceutical ingredients in the development of drug delivery systems.* Expert Opinion on Drug Delivery, 2019. **16**(5): p. 497-506.
45. Aragón-Tobar, C.F., D. Endara, and E. de la Torre, *Dissolution of Metals (Cu, Fe, Pb, and Zn) from Different Metal-Bearing Species (Sulfides, Oxides, and Sulfates) Using Three Deep Eutectic Solvents Based on Choline Chloride.* Molecules, 2024. **29**(2).
46. Hartley, J.M., et al., *EXAFS Study into the Speciation of Metal Salts Dissolved in Ionic Liquids and Deep Eutectic Solvents.* Inorganic Chemistry, 2014. **53**(12): p. 6280-6288.
47. Richter, J. and M. Ruck, *Synthesis and Dissolution of Metal Oxides in Ionic Liquids and Deep Eutectic Solvents.* Molecules, 2020. **25**(1).
48. Soldner, A., J. Zach, and B. Konig, *Deep eutectic solvents as extraction media for metal salts and oxides exemplarily shown for phosphates from incinerated sewage sludge ash.* Green Chemistry, 2019. **21**(2): p. 321-328.
49. Atri, R.S., et al., *Morphology Modulation of Ionic Surfactant Micelles in Ternary Deep Eutectic Solvents.* Journal of Physical Chemistry B, 2020. **124**(28): p. 6004-6014.
50. Bryant, S.J., R. Atkin, and G.G. Warr, *Spontaneous vesicle formation in a deep eutectic solvent.* Soft Matter, 2016. **12**(6): p. 1645-1648.
51. Sanchez-Fernandez, A., et al., *Micelle structure in a deep eutectic solvent: a small-angle scattering study.* Physical Chemistry Chemical Physics, 2016. **18**(20): p. 14063-14073.
52. Sanchez-Fernandez, A., et al., *Surfactant-Solvent Interaction Effects on the Micellization of Cationic Surfactants in a Carboxylic Acid-Based Deep Eutectic Solvent.* Langmuir, 2017. **33**(50): p. 14304-14314.
53. Abbott, A.P., et al., *Novel solvent properties of choline chloride/urea mixtures.* Chemical Communications, 2003(1): p. 70-71.
54. Abbott, A.P., et al., *Glycerol eutectics as sustainable solvent systems.* Green Chemistry, 2011. **13**(1): p. 82-90.
55. Shahbaz, K., et al., *Using Deep Eutectic Solvents Based on Methyl Triphenyl Phosphunium Bromide for the Removal of Glycerol from Palm-Oil-Based Biodiesel.* Energy & Fuels, 2011. **25**(6): p. 2671-2678.
56. Martins, M.A.R., S.P. Pinho, and J.A.P. Coutinho, *Insights into the Nature of Eutectic and Deep Eutectic Mixtures.* Journal of Solution Chemistry, 2019. **48**(7): p. 962-982.
57. Zhang, M., et al., *Preparation strategy and stability of deep eutectic solvents: A case study based on choline chloride-carboxylic acid (vol 345, 131028, 2022).* Journal of Cleaner Production, 2022. **354**.
58. Greaves, T.L. and C.J. Drummond, *Protic ionic liquids: Properties and applications.* Chemical Reviews, 2008. **108**(1): p. 206-237.

59. Kaur, S., S. Sharma, and H.K. Kashyap, *Bulk and interfacial structures of reline deep eutectic solvent: A molecular dynamics study.* Journal of Chemical Physics, 2017. **147**(19).
60. Migliorati, V. and P. D'Angelo, *Deep eutectic solvents: A structural point of view on the role of the anion.* Chemical Physics Letters, 2021. **777**.
61. Stefanovic, R., et al., *Nanostructure, hydrogen bonding and rheology in choline chloride deep eutectic solvents as a function of the hydrogen bond donor.* Physical Chemistry Chemical Physics, 2017. **19**(4): p. 3297-3306.
62. Zhekenov, T., et al., *Formation of type III Deep Eutectic Solvents and effect of water on their intermolecular interactions.* Fluid Phase Equilibria, 2017. **441**: p. 43-48.
63. Hammond, O.S., D.T. Bowron, and K.J. Edler, *Liquid structure of the choline chloride-urea deep eutectic solvent (reline) from neutron diffraction and atomistic modelling.* Green Chemistry, 2016. **18**(9): p. 2736-2744.
64. Hammond, O.S., D.T. Bowron, and K.J. Edler, *The Effect of Water upon Deep Eutectic Solvent Nanostructure: An Unusual Transition from Ionic Mixture to Aqueous Solution.* Angewandte Chemie-International Edition, 2017. **56**(33): p. 9782-9785.
65. Gabriele, F., et al., *Effect of water addition on choline chloride/glycol deep eutectic solvents: Characterization of their structural and physicochemical properties.* Journal of Molecular Liquids, 2019. **291**.
66. Turner, A.H. and J.D. Holbrey, *Investigation of glycerol hydrogen-bonding networks in choline chloride/glycerol eutectic-forming liquids using neutron diffraction.* Physical Chemistry Chemical Physics, 2019. **21**(39): p. 21782-21789.
67. Dai, Y.T., et al., *Tailoring properties of natural deep eutectic solvents with water to facilitate their applications.* Food Chemistry, 2015. **187**: p. 14-19.
68. Ma, C.Y., et al., *The peculiar effect of water on ionic liquids and deep eutectic solvents.* Chemical Society Reviews, 2018. **47**(23): p. 8685-8720.
69. Kumari, P., et al., *Influence of Hydration on the Structure of Reline Deep Eutectic Solvent: A Molecular Dynamics Study.* Acs Omega, 2018. **3**(11): p. 15246-15255.
70. Dong, H.C., et al., *Insight into the Molecular Structure, Interaction, and Dynamics of Aqueous Reline Deep Eutectic Solvent: A Nuclear Magnetic Resonance Investigation.* Journal of Physical Chemistry B, 2023. **127**(4): p. 1013-1021.
71. Hammond, O.S., et al., *Resilience of Malic Acid Natural Deep Eutectic Solvent Nanostructure to Solidification and Hydration.* Journal of Physical Chemistry B, 2017. **121**(31): p. 7473-7483.
72. López-Salas, N., et al., *Looking at the "Water-in-Deep-Eutectic-Solvent" System: A Dilution Range for High Performance Eutectics.* Acs Sustainable Chemistry & Engineering, 2019. **7**(21): p. 17565-17573.

73. Agieienko, V. and R. Buchner, *Variation of Density, Viscosity, and Electrical Conductivity of the Deep Eutectic Solvent Reline, Composed of Choline Chloride and Urea at a Molar Ratio of 1:2, Mixed with Dimethylsulfoxide as a Cosolvent.* Journal of Chemical and Engineering Data, 2020. **65**(4): p. 1900-1910.
74. Dhingra, D., Bhawna, and S. Pandey, *Effect of lithium chloride on the density and dynamic viscosity of choline chloride/urea deep eutectic solvent in the temperature range (303.15-358.15) K.* Journal of Chemical Thermodynamics, 2019. **130**: p. 166-172.
75. Pietro, M.E.D., et al., *Lithium Salt Effects on the Liquid Structure of Choline Chloride-Urea Deep Eutectic Solvent.* Acs Sustainable Chemistry & Engineering, 2022.
76. Wang, Y.X., et al., *Thermodynamic Study of Choline Chloride-Based Deep Eutectic Solvents with Water and Methanol.* Journal of Chemical and Engineering Data, 2020. **65**(5): p. 2446-2457.
77. Abranches, D.O. and J.A.P. Coutinho, *Type V deep eutectic solvents: Design and applications.* Current Opinion in Green and Sustainable Chemistry, 2022. **35**.
78. Padvi, S.A. and D.S. Dalal, *Choline chloride-ZnCl2: Recyclable and efficient deep eutectic solvent for the 2+3 cycloaddition reaction of organic nitriles with sodium azide.* Synthetic Communications, 2017. **47**(8): p. 779-787.
79. Cao, J., et al., *Deep eutectic solvent choline chloride center dot 2CrCl(3)center dot 6H(2)O: an efficient catalyst for esterification of formic and acetic acid at room temperature.* Rsc Advances, 2016. **6**(26): p. 21612-21616.
80. Leron, R.B. and M.H. Li, *Solubility of carbon dioxide in a choline chloride-ethylene glycol based deep eutectic solvent.* Thermochimica Acta, 2013. **551**: p. 14-19.
81. Abbott, A.P., et al., *Eutectic-based ionic liquids with metal-containing anions and cations.* Chemistry-a European Journal, 2007. **13**(22): p. 6495-6501.
82. Rodriguez, N.R., et al., *Degradation of Deep-Eutectic Solvents Based on Choline Chloride and Carboxylic Acids.* Acs Sustainable Chemistry & Engineering, 2019. **7**(13): p. 11521-11528.
83. Shahbaz, K., et al., *Thermogravimetric measurement of deep eutectic solvents vapor pressure.* Journal of Molecular Liquids, 2016. **222**: p. 61-66.
84. Alcalde, R., M. Atilhan, and S. Aparicio, *On the properties of (choline chloride plus lactic acid) deep eutectic solvent with methanol mixtures.* Journal of Molecular Liquids, 2018. **272**: p. 815-820.
85. Dai, Y.T., et al., *Natural Deep Eutectic Solvents as a New Extraction Media for Phenolic Metabolites in*

L. Analytical Chemistry, 2013. **85**(13): p. 6272-6278.
86. Hofmann, A., *Physical Chemistry Essentials*. 2018, Springer International Publishing : Imprint: Springer,: Cham. p. 1 online resource (XV, 499 pages 181 illustrations, 164 illustrations in color.
87. Baur, E., *Chemical resistance of commodity thermoplastics*. Plastics design library. 2016, Amsterdam: Elsevier. xli, 1148 pages.
88. Debenedetti, P.G. and F.H. Stillinger, *Supercooled liquids and the glass transition.* Nature, 2001. **410**(6825): p. 259-67.
89. Rudin, A. and P. Choi, *The elements of polymer science and engineering*. Third edition / ed. 2013, San Diego: Elsevier/AP. xx, 563 pages.
90. Le Guenic, S., et al., *Renewable Surfactants for Biochemical Applications and Nanotechnology.* Journal of Surfactants and Detergents, 2019. **22**(1): p. 5-21.
91. Otzen, D., *Protein-surfactant interactions: A tale of many states.* Biochimica Et Biophysica Acta-Proteins and Proteomics, 2011. **1814**(5): p. 562-591.
92. Pang, Z.L., et al., *Selection of surfactants for cell lysis in chemical cytometry to study protein-DNA interactions.* Electrophoresis, 2006. **27**(8): p. 1489-1494.
93. Pérez-Page, M., et al., *Template-based syntheses for shape controlled nanostructures.* Advances in Colloid and Interface Science, 2016. **234**: p. 51-79.
94. Fainerman, V.B., D. Möbius, and R. Miller, *Surfactants : chemistry, interfacial properties, applications*. 1st ed. Studies in interface science,. 2001, Amsterdam ; New York: Elsevier Science, Ltd. xvi, 661 p.
95. Witten, T. and P.A. Pincus, *Structured fluids : polymers, colloids, surfactants*. 2004, Oxford ; New York: Oxford University Press. xiv, 216 p.
96. Shiri, M.S.Z., W. Henderson, and M.R. Mucalo, *A Review of The Lesser-Studied Microemulsion-Based Synthesis Methodologies Used for Preparing Nanoparticle Systems of The Noble Metals, Os, Re, Ir and Rh.* Materials, 2019. **12**(12).
97. Ghosh, S., A. Ray, and N. Pramanik, *Self-assembly of surfactants: An overview on general aspects of amphiphiles.* Biophysical Chemistry, 2020. **265**.
98. Belhaj, A.F., et al., *The effect of surfactant concentration, salinity, temperature, and pH on surfactant adsorption for chemical enhanced oil recovery: a review.* Journal of Petroleum Exploration and Production Technology, 2020. **10**(1): p. 125-137.
99. Chang, Z.Y., X.M. Chen, and Y.J. Peng, *The adsorption behavior of surfactants on mineral surfaces in the presence of electrolytes - A critical review.* Minerals Engineering, 2018. **121**: p. 66-76.
100. Javadian, S. and J. Kakemam, *Intermicellar interaction in surfactant solutions; a review study.* Journal of Molecular Liquids, 2017. **242**: p. 115-128.

101. Basu, M., P.A. Hassan, and S.B. Shelar, *Modulation of surfactant self-assembly in deep eutectic solvents and its relevance to drug delivery-A review.* Journal of Molecular Liquids, 2023. **375**.
102. Trivedi, S., et al., *Solvation within deep eutectic solvent-based systems: A review.* Green Sustainable Process for Chemical and Environmental Engineering and Science, 2023: p. 145-192.
103. Hu, L.H., et al., *Surfactant aggregates within deep eutectic solvent-assisted synthesis of hierarchical ZIF-8 with tunable porosity and enhanced catalytic activity.* Journal of Materials Science, 2019. **54**(16): p. 11009-11023.
104. Manasi, I., et al., *Surfactant effects on the synthesis of porous cerium oxide from a type IV deep eutectic solvent.* Journal of Materials Chemistry A, 2022. **10**(35): p. 18422-18430.
105. Hsieh, Y.T. and Y.R. Liu, *Micelle Structure in a Deep Eutectic Solvent for the Electrochemical Preparation of Nanomaterials.* Langmuir, 2018. **34**(35): p. 10270-10275.
106. Häckl, K., et al., *Potential Dependence of Surfactant Adsorption at the Graphite Electrode/Deep Eutectic Solvent Interface.* Journal of Physical Chemistry Letters, 2019. **10**(18): p. 5331-5337.
107. Li, M.H., et al., *Multifunctional Deep Eutectic Solvent-Based Microemulsion for Transdermal Delivery of Artemisinin.* Langmuir, 2024. **40**(10): p. 5098-5105.
108. Sakuragi, M., S. Tsutsumi, and K. Kusakabe, *Deep Eutectic Solvent-Induced Structural Transition of Microemulsions Explored with Small-Angle X-ray Scattering.* Langmuir, 2018. **34**(42): p. 12635-12641.
109. Arnold, T., et al., *Surfactant Behavior of Sodium Dodecylsulfate in Deep Eutectic Solvent Choline Chloride/Urea.* Langmuir, 2015. **31**(47): p. 12894-12902.
110. Manasi, I., et al., *Self-assembly of ionic and non-ionic surfactants in type IV cerium nitrate and urea based deep eutectic solvent.* Journal of Chemical Physics, 2021. **155**(8).
111. Sanchez-Fernandez, A., et al., *Micelle structure in a deep eutectic solvent: a small-angle scattering study.* Phys Chem Chem Phys, 2016. **18**(20): p. 14063-73.
112. Banjare, R.K., et al., *Micellization Behavior of Conventional Cationic Surfactants within Glycerol-Based Deep Eutectic Solvent.* Acs Omega, 2020. **5**(31): p. 19350-19362.
113. Pal, M., R.K. Singh, and S. Pandey, *Evidence of Self-Aggregation of Cationic Surfactants in a Choline Chloride plus Glycerol Deep Eutectic Solvent.* Chemphyschem, 2015. **16**(12): p. 2538-2542.
114. Sanchez-Fernandez, A., et al., *Micellization of alkyltrimethylammonium bromide surfactants in choline chloride: glycerol deep eutectic solvent.* Physical Chemistry Chemical Physics, 2016. **18**(48): p. 33240-33249.

115. Bryant, S.J., R. Atkin, and G.G. Warr, *Effect of Deep Eutectic Solvent Nanostructure on Phospholipid Bilayer Phases.* Langmuir, 2017. **33**(27): p. 6878-6884.
116. Sanchez-Fernandez, A., et al., *Self-assembly and surface behaviour of pure and mixed zwitterionic amphiphiles in a deep eutectic solvent.* Soft Matter, 2018. **14**(26): p. 5525-5536.
117. Hammond, O.S., et al., *Mix-and-Match Diols: Adjusting Self-Assembly of Micellar Phases in Choline Chloride Eutectics.* Crystals, 2022. **12**(11).
118. Sanchez-Fernandez, A., et al., *Counterion binding alters surfactant self-assembly in deep eutectic solvents.* Physical Chemistry Chemical Physics, 2018. **20**(20): p. 13952-13961.
119. Sanchez-Fernandez, A., et al., *Long-Range Electrostatic Colloidal Interactions and Specific Ion Effects in Deep Eutectic Solvents.* Journal of the American Chemical Society, 2021. **143**(35): p. 14158-14168.
120. Sanchez-Fernandez, A., et al., *Complex by design: Hydrotrope-induced micellar growth in deep eutectic solvents.* Journal of Colloid and Interface Science, 2021. **581**: p. 292-298.
121. Als-Nielsen, J. and D. McMorrow, *Elements of modern X-ray physics*. 2nd ed. 2011, Hoboken: Wiley. xii, 419 p.
122. Blow, D.M., *Outline of crystallography for biologists*. 2002, Oxford ; New York: Oxford University Press. viii, 236 p.
123. Egami, T. and S.J.L. Billinge, *Underneath the Bragg peaks : structural analysis of complex materials*. Second edition. ed. Pergamon materials series. 2012, Amsterdam: Elsevier. xxi, 481 pages.
124. Jackson, A.J., *Introduction to small-angle neutron scattering and neutron reflectometry.* NIST Center for Neutron Research, 2008: p. 1-24.
125. Kisi, E.H. and C.J. Howard, *Applications of neutron powder diffraction*. Oxford series on neutron scattering in condensed matter. 2012, Oxford: Oxford University Press. xvii, 486 pages.
126. Rinaldi, R., L. Liang, and H. Schober, *Neutron applications in earth, energy, and environmental sciences*. 2009: Springer.
127. Carlile, C., et al., *Neutron scattering facilities in Europe: present status and future perspectives.* ESFRI Report, European Landscape of Research Infrastructures-ESFRI, 2016: p. 123.
128. Fritzsche, H., D. Fruchart, and J. Huot, *Neutron Scattering and Other Nuclear Techniques for Hydrogen in Materials*, in *Neutron Scattering Applications and Techniques,*. 2016, Springer International Publishing : Imprint: Springer,: Cham. p. 1 online resource (VIII, 413 pages 225 illustrations, 112 illustrations in color.
129. *SASview software*. 2024 [cited 2024 08.04]; Available from: www.sasview.org.
130. Borsali, R. and R. Pecora, *Soft-matter characterization*. 2008: Springer Science & Business Media.

131. Goyal, P.S. and V.K. Aswal, *Combined SANS and SAXS in studies of nanoparticles with core-shell structure.* Indian Journal of Pure & Applied Physics, 2006. **44**(10): p. 724-728.
132. Jacques, D.A. and J. Trewhella, *Small-angle scattering for structural biology-Expanding the frontier while avoiding the pitfalls.* Protein Science, 2010. **19**(4): p. 642-657.
133. Ossi, P.M., *Disordered materials : an introduction*. Advanced texts in physics,. 2003, Berlin ; New York: Springer. xii, 288 p.
134. Tabor, D., *Gases, liquids, and solids : and other states of matter*. 3rd ed. 1991, Cambridge ; New York: Cambridge University Press. xxi, 418 p.
135. Dinnebier, R.E. and S.J.L. Billinge, *Powder diffraction : theory and practice*. 2008, Cambridge: Royal Society of Chemistry. xxi, 582 p.
136. Soper, A., *GudrunN and GudrunX: Programs for Correcting Raw Neutron and X-Ray Total Scattering Data to Differential Cross Section. GUDRUN Manual.* ISIS Spallation Source, 2017.
137. Soper, A.K. *Empirical Potential Structure Refinement: A User's Guide*. 2017 [cited 2024 06-04]; Available from: https://www.isis.stfc.ac.uk/Pages/Empirical-Potential-Structure-Refinement.aspx.
138. Soper, A.K., *Tests of the empirical potential structure refinement method and a new method of application to neutron diffraction data on water.* Molecular Physics, 2001. **99**(17): p. 1503-1516.
139. Höhne, G., W. Hemminger, and H.J. Flammersheim, *Differential scanning calorimetry : an introduction for practitioners*. 2nd rev. and enl. ed. 2003, Berlin ; New York: Springer. xii, 298 p.
140. De Caro, C.A., A. Aichert, and C.M. Walter, *Efficient, precise and fast water determination by the Karl Fischer titration.* Food Control, 2001. **12**(7): p. 431-436.
141. Scholz, E., *Karl Fischer titration : determination of water*. Chemical laboratory practice. 1984, Berlin ; New York: Springer. x, 138 p.
142. Ananthapadmanabhan, K.P., et al., *Fluorescence Probes for Critical Micelle Concentration.* Langmuir, 1985. **1**(3): p. 352-355.
143. Piñeiro, L., M. Novo, and W. Al-Soufi, *Fluorescence emission of pyrene in surfactant solutions.* Advances in Colloid and Interface Science, 2015. **215**: p. 1-12.

Paper I

The influence of chirality on the structure of a tartaric acid-choline chloride deep eutectic solvent

Elly K. Bathke[a], Daniel Bowron[b], Iva Manasi[c], Karen J. Edler[a]

[a]*Center for Analysis and Synthesis, Department of Chemistry, Lund University, Getingevägen 60, Lund, 22241, Scania, Sweden*
[b]*ISIS Neutron and Muon Source, Science and Technology Facilities Council, Rutherford Appleton Laboratory, Didcot, OX11 0QX, Oxfordshire, United Kingdom*
[c]*Department of Chemistry, University of Bath, Claverton Down, Bath, BA2 7AY, Somerset, United Kingdom*

Abstract

The wide range of properties, relative ease and low cost of using Deep Eutectic Solvents garners them interest in an ever expanding range of applications. Among common DES components many are naturally occurring chiral molecules. Here we present the liquid structure of either single enantiomeric or racemic tartaric acid with choline chloride with (molar ratio of 2 choline chloride to 1 tartaric acid), as well as the influence of low amounts of added water (2:1:2) from neutron scattering data with H/D isotropic substitution, refined using empirical potential structure refinement. We show that the overall structure remains the same between the different enatiomeric compositions, with small differences in interactions only occurring between the tartaric acid molecules. The overall structure is also robust towards hydration, similar to what has been found in other DES. We also compare our structures to the structures of DES comprising of similar carboxylic acids (1:1 choline chloride - malic acid, 1:1 choline chloride - oxalic acid), finding overall similar dominant interactions, with differences that may be attributable to the number of available hydrogen bonding sites and steric effects.

Keywords: deep eutectic solvents, ionic liquids, nanostructures, neutron diffraction, chiral

1. Introduction

Deep eutectic solvents (DES) are an emerging type of innovative solvents, showing unique properties and versatility in a variety of applications from electrochemistry [1, 2] and organic and materials synthesis [3, 4, 5, 6, 7] to extraction [8, 9, 10] and pharmaceutical applications [11]. They are formed by mixing at least two components to create a eutectic mixture that is dominated by hydrogen bond interactions, in which one component acts as a hydrogen bond donor (HBD) and another as a hydrogen bond acceptor (HBA). A wide range of organic and inorganic molecules, such as sugars, metal salts, carboxylic acids, amino acids and alcohols [12, 13, 14, 15, 16], can be used to make DES, leading to the formation of countless DES systems with a great range of properties. By varying factors such as the choice of HBD and HBA, the molar ratio of the components, temperature and the presence of additives solvent properties like hydrophobicity [17, 18], conductivity [19, 20, 21], chirality [22, 23], biocompatibility [24, 25, 26] and other properties such as the ability to solubilize different types of components [27, 28, 29] and the support of self assembly [30, 31, 32, 33] can be adjusted. They are potential "designer" solvents, where the solvent can adjusted to specific applications, similar to Ionic Liquids (IL). To form DES many "green" and naturally occurring precursors like urea can be used [34] and this makes them extremely relevant in the field of green solvent alternatives.

Chirality often occurs in biomolecules, as well as other materials such as polymers and metal complexes. During their synthesis stereoselectivity has to be achieved through the interaction with other chiral molecules, as other physicochemical properties of the enantiomeric forms are identical. This is often achieved through the addition of chiral selector molecules. Stereoselectivity or enhancement of the chiral selector molecules efficiency can also be achieved through use of a chiral solvent. The first successful use of chiral solvents for stereoselective synthesis has been reported in 1975 by Seebach et al. [35] using a chiral amino-ether as the solvent, achieving an enantioselectivity of 22% ee. Due to high costs and moderate selectivity results research in the field was limited for a time, until the emergence of first chiral IL [36, 37], and now chiral DES opened up the field to a wide range of affordable and tunable chiral solvents. DES in particular are of high interest for this, as they can easily take direct advantage of naturally occurring single-enantiomeric compounds such as amino acids, sugars, carboxylic acids, etc. without further need for processing [38]. Enantiomer selectivity can be used in synthesis, but also in analytical and preparative applications, and studies into the use of chiral DES in the context of e.g. asymmetric organocatalysis [23, 39], for chiral extraction [40, 41], electroanalysis [42], or as solvents to induce circularly polarized luminescence of chiral light-emitting materials [22, 43]. Knowledge of the possibilities DES can offer has spread within the last two decades, but research on chiral DES is still in its initial stages with an increasing number of papers being published within the last few years. Among these, papers on the

Email address: karen.edler@chem.lu.se (Karen J. Edler)

structural properties of these DES remain limited [44, 23, 45].
Tartaric acid (TA) is a well studied commonly occurring chiral biomolecule with two chiral centers, occurring in either a L, D or meso form. Being one of the earliest known chiral molecules [46, 47], it and it's derivatives still enjoy frequent use as an additive for different applications [48, 49, 50] or as chiral selectors [51, 52] among many other things. Similar to other small carboxylic acids it can be used to form DES, and studies on DES based on TA [53, 54, 55, 56, 57, 58, 59, 60, 61] and the effect of the addition of TA to other DES [62] have been published.
In this study we present the liquid structure of DES formed by mixing either single enantiomeric LTA or the racemic mixture of DLTA with the popular DES-forming component choline chloride (ChCl) at the eutectic molar ratio of 2:1 (ChCl:LTA, ChCl:DLTA), investigated through neutron scattering experiments in combination with EPSR analysis. Among carboxylic acids many components can form DES, and we compare our results to that of similar DES such as 1:1 choline chloride : malic acid (ChCl:Ma)[44], which contains the structurally very similar malic acid, and 1:1 choline chloride : oxalic acid (ChCl:Ox)[63], a smaller acid containing two carboxylic acid groups. Hammond et al. have previously found that the structure of ChCl:Ma is reasonably resilient towards the addition of small amounts of other molecules such as water[64, 44], while Turner et al.[65] have found only slight shifts in the partial radial distribution functions (pRDFs)and coordination numbers when comparing DES comprising of choline chloride and glycerol at the molar ratios of 1:1 and 1:2. These factors make the comparison to 1:1 ChCl:Ma and 1:1 ChCl:Ox suitable and interesting, though it is possible the effect of a change in molar ratio might affect these DES differently. Finally, we also investigate the influence of small amounts of water by looking at choline chloride : LTA : water (ChCl:LTA:W) at a molar ratio of 2:1:2 and compare it to the structure of the 1:1:2 malic acid : choline chloride : water previously reported by Hammond et al.[44].

2. Experimental

2.1. Sample preparation

Hydrogenated choline chloride (>98%), hydrogenated L- and DL-tartaric acid (>99%) and D_2O (>99%, 99.9 atom % D) were purchased from Sigma-Aldrich and used as received. Trimethyl-d9-choline chloride ($((CD_3)_3N(CH_2)_2OHCl$) (>99%, 99.6 atom % D) was purchased from ckisotopes and used as provided. Deuterated d4-L- (>99.5%, 95 atom % D) and d4-DL-tartaric acid (>95%, 95 atom % D) were produced through recrystallization of the hydrogenated compounds in D_2O followed by lyophilisation repeated three times, and the degree of deuteration was determined through ^{1}H-NMR.
Directly before use ChCl components were vacuum dried at 60°C over night to remove moisture. The DES were prepared by precisely weighting out the components and mixing them at 110°C for up to 4 hours. The formation of esters between the choline and tartaric acid was monitored via ^{1}H-NMR, and

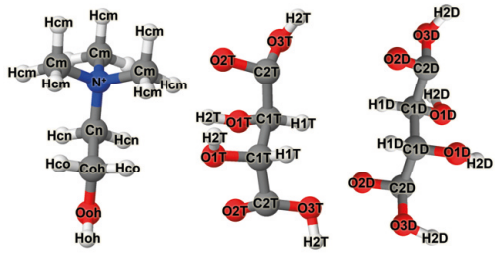

Figure 1: Schematic representations of choline (left), L-tartaric acid (middle) and D-tartaric acid (left) with their assigned atom labels used in EPSR modelling.

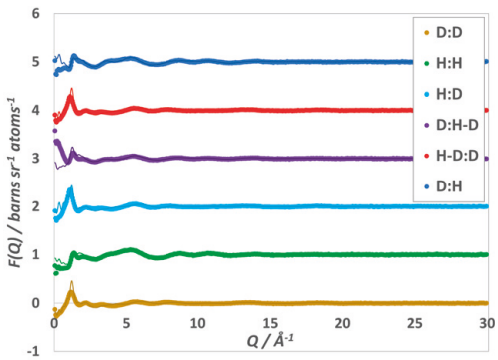

Figure 2: Structure factors F(Q) over Q of the six measured isotropic contrasts of 2:1 ChCl:LTA from neutron scattering data (dots) and their EPSR fits (solid lines). The different contrasts are offset from each other for better readability.

determined to be around 5% (see SI Table 4, Fig. 7-9). The inclusion of esters into the model was tested but did not significantly change the structures determined for these mixtures, and the following analysis does not consider the presence of esters. For the neutron experiments six different isotropic contrasts were produced for the binary L- or DLTA:ChCl: H:H, H:D, D:H, D:D, H/D:D and D:H/D, with H/D denoting the equimolar mixture of the hydrogenated and deuterated forms. Hydrated samples were produced from the recovered DES by mixing appropriate amounts of the DES with two mole equivalents of H_2O (Milli-Q, 18.2 MΩ) or D_2O to form eight contrasts: H:H:H, H:H:D, H:D:D, D:H:D, D:D:D, H/D:D:D, D:H/D:D, H/D:H/D:D.

2.2. Neutron Total Scattering Experiments

Total scattering experiments were performed on the Near and InterMediate Range Order Diffractometer (NIMROD) at Target Station 2 of the STFC ISIS Neutron and Muon Source, Rutherford Appleton Laboratory, Harwell, UK. Measurements were taken over the full available Q-range of 0.02 to 50Å^{-1}, using

time-of-flight. Null-scattering Ti0.68Zr0.32 (TiZr) alloy flat-plate cells with internal dimensions of 1 × 35 × 35 mm and 1 mm thickness were filled to the top with approximately 1.5 g of sample and sealed using PTFE vacuum seals. Additionally, the empty instrument, a 3 mm thick vanadium standard and each empty TiZr cells was measured for calibration and data normalization. For all measurements a sample changer at 50°C, regulated by using a water bath, was used.

GudrunN software [66] was used for data correction, background subtraction and normalization. Calculation of the high Q scattering intensity from the atomic compositions of the samples using GudrunN indicate less than 0.25 wt % water was present in the samples during measurements. The processed data was analyzed and fitted using the Empirical Potential Structure Refinement (EPSR) software[67]. The fitting procedure and parameters used for EPSR are given in the Supporting Information (SI table.1). DES components with their assigned atom specifications can be seen in Fig.1.

3. Results and discussion

3.1. EPSR fitting and molecular centers solvent structure

Using known properties of the DES such as density, molecular structure and suitable interaction parameters (see SI table 1), models of the DES systems were constructed within EPSR. These models were then refined against the experimental neutron diffraction data until they closely represented the experimental structure factor, running over 10000 iterations for each DES. Examples of the structure factor F(Q) data and fit for the different contrasts of ChCl:LTA can be seen in Fig.2. Data and fits of the different DES and contrasts (see SI Fig.1) show overall good agreement, with bigger divergences in the region of $q \leq 2\,\text{Å}^{-1}$, where it is more difficult to correct for inelastic scattering from ^{1}H nuclei, as no components besides D_2O could be obtained in a perdeuterated form. This is not expected to significantly influence the structure modelling results. None of the samples show significant small angle scattering indicative of particle formation or longer range solvent structuring into distinctive domains. This is similar to what has been observed for other DES [68, 44, 63].

In order to analyse and compare the structures of the different DES systems, the EPSR calculated radial distribution functions (RDFs) can be utilised. Molecular centers RDFs, using the C1T atom for the LTA, the C1D atom for the DTA, the N atom for the choline molecules, the O1 atom for water and the Cl atom as the central atoms approximating the geometrical center of the molecule, were calculated between components, and are shown in Fig.3. The position of the first peaks (r_{max}) and aggregation numbers up until the first minimums (N_{coord}) are shown in Fig.4. No long range ordering can be seen in the RDFs, with interactions being limited to one or two coordination shells. The length scales found for these interactions are within expectation, and are similar to what has been found for related DES such as 1:1 choline chloride : malic acid (ChCl:Ma)[44] and 1:1 choline chloride : oxalic acid (ChCl:Ox)[63] (Fig.4). Numerical values of r_{max} and N_{coord} of all six systems are listed in SI table 2.

The RDF distributions and peak positions show significant similarities between ChCl:LTA and ChCl:DLTA. Similar to other DES, interactions with Cl are strong and distinctive. For Ch - Cl r_{max} is at a distance of 4.4 Å in ChCl:LTA and at 4.3 Å in ChCl:DLTA, with N_{coord} of 4.01±1.45 and 3.60±1.21 respectively. The r_{max} are very similar to those found in 1:1 ChCl:Ma (4.2 Å) and 1:1 ChCl:Ox (4.5 Å), while the coordination numbers of the 2:1 ChCl:TA mixtures are slightly above those in ChCl:Ma (3.22±1.19) and ChCl:Ox (3.25± 1.07). A slightly higher N_{coord} can be expected at higher concentrations of choline chloride in the mixtures, similar to what Turner et al. found when comparing 1:1 and 1:2 choline chloride:glycerol. The pRDF in both ChCl:LTA and ChCl:DLTA shows a side peak at around 5.0 Å, which can be associated with binding to the choline hydroxyl group and the weaker binding to the choline trimethylammonium region respectively, similar to what has been found in both ChCl:Ma and ChCl:Ox before. A weak second coordination shell around 9.4 Å and 9.3 Å for ChCl:LTA and ChCl:DLTA can be seen.

The r_{max} of Ch - Ch in ChCl:LTA and ChCl:DLTA are also identical, and similar to what can be found in other systems, with a weak second coordination shell around 11.8 Å in both mixtures. The N_{coord} is a bit higher then what can be found in ChCl:Ma and ChCl:Ox, indicating stronger self association in these systems.

For the interactions of the acids with Cl and Ch little difference can be seen between ChCl:LTA and ChCl:DLTA in terms of r_{max} (TA - Ch at 6.1 to 6.3 Å , TA - Cl at 3.5 Å). In comparison to ChCl:Ma and ChCl:Ox the Acid - Ch distances are a bit longer (5.9 Å in ChCl:Ma, 5.7 Å in ChCl:Ox), which could be attributed to the slightly bulkier size (TA>MA>OA) of the molecules. The Acid - Cl distances are shorter in comparison to ChCl:Ma and ChCl:Ox (4.3 Å and 3.7 Å), which could be due to the increase in the number of hydrogen bonding OH-groups. In all systems the pRDF of the Acid - Cl interaction shows a relatively sharp peak. The N_{coord} of Cl - Acid in ChCl:DLTA is split between the D- and the L-form (1.06±1.17 for LTA, 1.10±1.25 for DTA) at around half of the amount of the single enantiomer in ChCl:LTA (2.12±0.75) for each. This shows that there is no preference for either form, which is expected, as non-chiral molecules such as Ch are not sensitive to differences in chirality. The overall coordination lies between those of ChCl:Ma (1.11±0.82) and ChCl:Ox (4.72±2.55), but within a standard deviation. For Ch - Acid the N_{coord} is 9.05±1.85 in ChCl:LTA, and the sum of 3.97±2.41 (LTA) and 3.97±2.51 (DTA) in ChCl:DLTA. It is again split between the different enantiomers, with a slightly lower number of Ch - Acid in ChCl:DLTA, which could be due to steric effects leading to less efficient packing. For this interaction the split is very visible when looking at the distribution of coordination numbers (see SI Fig.2), with hardly any probability at 10 or above in the racemic mixture but more then 30% probability in ChCl:LTA. The N_{coord} lies between that of ChCl:Ma (6.78±1.93) and ChCl:Ox (11.91±0.75), which could be due to a combination of an increased number of sites available for bonding and steric hindrance.

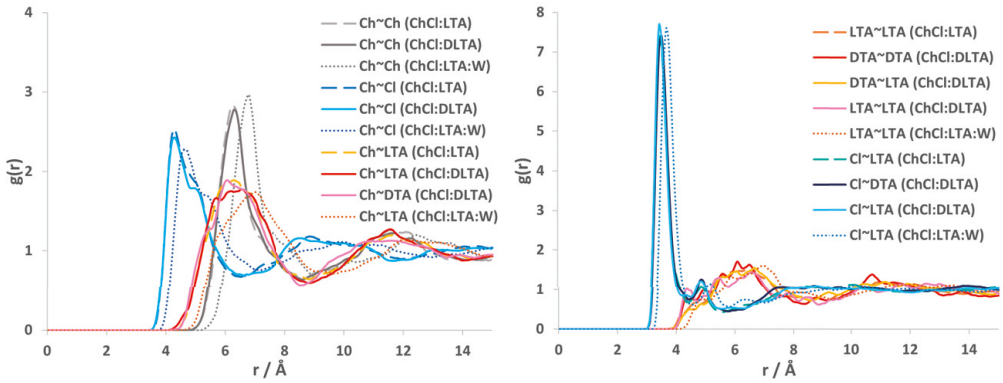

Figure 3: Molecular centers pRDFs for 2:1 ChCl:LTA (dashed lines), 2:1 ChCl:DLTA (solid lines) and 2:1:2 ChCl:LTA:W (dotted lines).

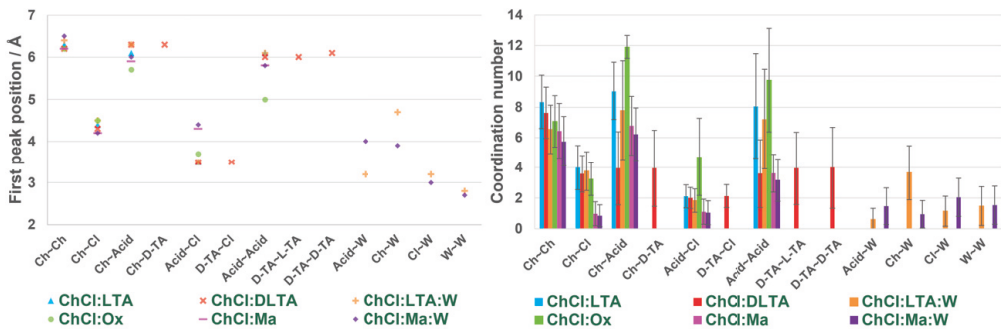

Figure 4: Position of the first peaks r_{max} and coordination number up until the first minimums N_{coord} of the molecular centers pRDFs of the DES components in ChCl:LTA, ChCl:DLTA and ChCl:LTA:W, as well as in ChCl:Ox[63] and ChCl:Ma[44] for comparison. "Acid" stands for L-tartaric acid, oxalic acid or malic acid depending on the DES. The error on the peak position is approximately 0.1 Å. The errors on the coordination number are calculated to one standard deviation.

Finally, looking at the Acid - Acid interactions, r_{max} are similar in ChCl:LTA and ChCl:DLTA (6.0 to 6.1 Å). N_{coord} again shows a split from 8.06±3.42 in ChCl:LTA to 3.62±2.24 for LTA - LTA, 4.01±2.67 for DTA - DTA and 3.96±2.38 for LTA - DTA, with a very apparent shift in the distribution of coordination numbers (see SI Fig.2). In comparison to ChCl:Ma (5.8 Å) and ChCl:Ox (5.0 Å) r_{max} is bigger, which can be explained as an effect of molecular size. Its N_{coord} lies significantly above that in ChCl:Ma (3.64±1.25) and below ChCl:Ox (9.75±3.38), which again could be an effect of size in combination with available hydrogen bonding groups.

Solid LTA and racemic DLTA show differences in crystal structures (spacegroups $P2_1$ [69] and P1 [70] respectively), as the most favourable interactions between chiral molecules are different depending on the chirality of the other molecule. In this case no significant effect of this difference can be seen in these liquids by looking at just the molecular RDFs and coordination numbers. As will be discussed below, there are differences in the atomic interactions and 3 dimensional arrangement. But this effect is weak enough to have little influence on the overall molecular network, as the stronger Acid - Chloride and Acid - Choline interactions buffer the effects due to chirality. Overall, the Acid - Acid interactions remain relatively weak and dispersed in the liquid DES at these temperatures. This shows that in this case interactions between non-chiral components and TA, and non-chiral components with each other have a stronger effect on the overall liquid structure.

3.2. Specific solvent structure

Through analysis of the interatomic pRDFs (Fig.5, Fig.6, numerical values of r_{max} and N_{coord} can be found in SI Table 3) and spatial density functions (SDF) (Fig.7), predominant interactions and molecular positions relative to each other can be shown. Cluster analysis (SI Fig. 10-12) shows system spanning percolation of the main interacting molecules (choline – chloride, tartaric acid – chloride, tartaric acid – tartaric acid). The formation of small clusters of up to 10 molecules, above the

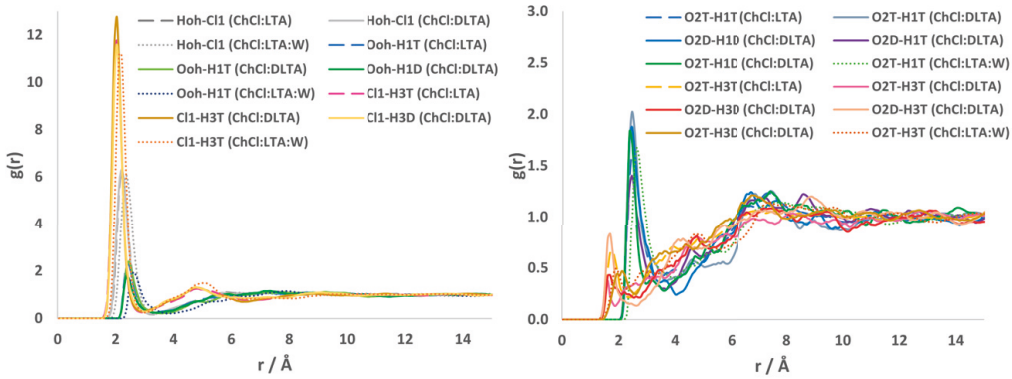

Figure 5: Representative inter-atomic pRDFs for 2:1 ChCl:LTA (dashed lines), 2:1 ChCl:DLTA (solid lines) and 2:1:2 ChCl:LTA:W (dotted lines). The atoms of the components are labeled as shown in Fig.3. Additional pRDFs can be found in the SI Fig.3.

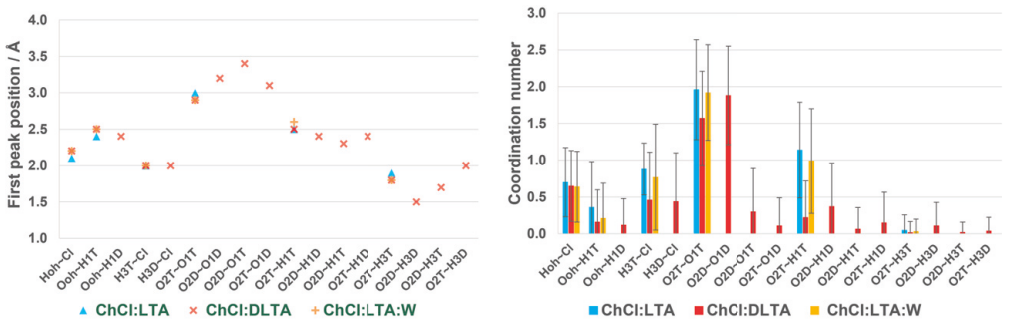

Figure 6: Position of the first peak r_{max} and coordination number N_{coord} of representative inter-atomic pRDFs of the DES components in ChCl:LTA, ChCl:DLTA and ChCl:LTA:W (Fig.6). The error on the peak position is approximately 0.1 Å. The errors on the coordination number are calculated to one standard deviation. The atoms of the components are labeled as shown in Fig.3. Values of additional distinct pRDFs are listed in the SI Tab.3.

percolation threshold of $N=S^{-2.2}$ [71] denoting a random distribution, could be seen for other significant interactions (tartaric acid – chloride, water – chloride, water – water). Analysing the frequency of links between molecules for all intermolecular bonds with a pRDF peak around 2.0Å and a first minimum up to around 2.5Å, the clustering interactions can be compared to their hydrogen bonding behavior. Through this analysis, no chains of a length of more than 3 could be observed (SI Fig.13-15), indicating the lack of a distinctly connected long range hydrogen bonding network of molecules of the same type or between two types in this system. For choline chloride with acetic acid (1:2) and formic acid (1:2) [72]. DES similar system spanning percolation with only short hydrogen bonded chains has been found, unlike in systems e.g. based on glycerol [65]. These analyses indicate that a variety of interactions are present and prominent in the tartaric acid based systems.

In both ChCl:LTA and ChCl:DLTA the chloride anions show similar strong interactions with the choline cations, prominently with the OH and the trimethylammonium region. These interactions are at a shorter distance with a similar to slightly higher coordination number then in ChCl:Ma and ChCl:Ox, which could be effect of the higher relative content of ChCl in the DES. Similar to what has been shown for other ChCl containing DES these two fairly distinct Cl populations are sandwiched between the choline and the HBD, here the LTA and DTA, as a dominant structure directing interaction (Fig.7, bottom row).

A strong but less distinctly localized interaction occurs between Cl and tartaric acid, with strong interactions between the Cl and all hydrogen atoms, but especially the terminal H3T and H3D. These distances are similar to what has been found in ChCl:Ma and ChCl:Ox, but unlike in ChCl:Ma the terminal OH-group shows a slightly stronger interaction with Cl then the central OH-group, in interatomic distance and coordination.

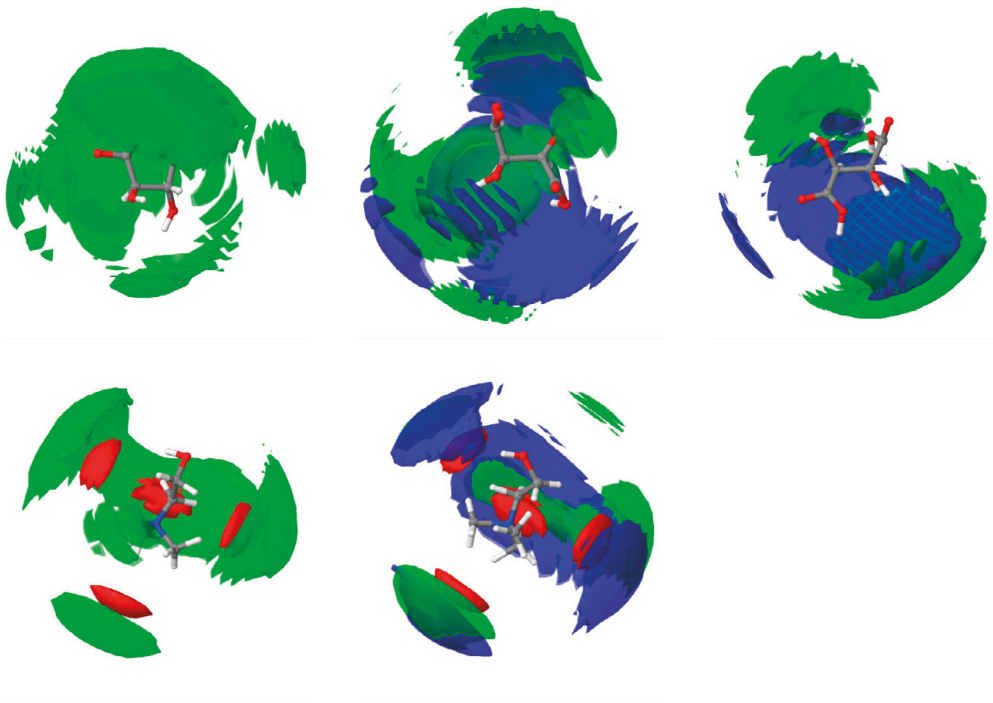

Figure 7: Spatial density function (SDF) of the 20% probability surface showing the solvation of the molecule types around each other in 3D. The top row shows distributions centering the tartaric acid (left: LTA in ChCl:LTA; middle: LTA in ChCl:DLTA; right: DTA in ChCl:DLTA) and the bottom row centering the choline (left: in ChCl:LTA; middle: in ChCl:DLTA). Central molecules are aligned along a central bond, but displayed molecule conformations differ due to rotational freedom of groups. The red isosurfaces correspond to chloride anions, the yellow to choline cations, the green to L-tartaric acid molecules, the dark blue to D-tartaric acid molecules and the light blue to water molecules. Additional SDFs can be found in SI Fig.4.

In comparison, the interactions between choline and tartaric acid are weaker, with the shortest interaction indicative of hydrogen bonding showing clear peaks being between being Ooh and H3T/H3D as well as a clear interaction with H1T, but both having very low N_{coord} (0.065±0.25 and 0.36±0.62 in ChCl:LTA) in both DES. Interactions with higher coordination numbers occur over a wider range and longer distance, with both N - C1T and N - H1T around 6.4 Å with a N_{coord} of 8.83±3.26 and 8.87±3.27 (ChCl:LTA) respectively. This shows that while the two molecules are in close vicinity of each other, their hydrogen bonding is not a dominant interaction. They are more likely to arrange themselves in relation to Cl, as can be seen in the SDFs. This is similar to what occurs in ChCl:Ox and ChCl:Ma as well.

While the molecular centers pRDFs for the tartaric acid - tartaric acid interactions do not show significant differences between the single enantiomer ChCl:LTA and the racemic ChCl:DLTA, differences can be seen in the atomic pRDFs, different atomic N_{coord} and SDFs (Fig.5, table6, Fig.7). While the peak positions r_{max} remain similar between the two systems and tartaric acids, a split can again be seen for the N_{coord} of the racemic mixture. For the atoms located towards the molecular centers (C1T and C1D) this split is even, similar to tartaric acid interactions with non chiral molecules (C1T-C1T in ChCl:LTA: 8.06±3.42 vs. C1T-C1T: 3.62±2.24, C1D-C1D: 4.01±2.67 and C1T-C1D: 3.96±2.38 in ChCl:DLTA). Looking at the shorter range distributions indicative of direct interactions, the split in N_{coord} is significantly shifted towards interactions of enantiomers with themselves (O2T-O1T in ChCl:LTA: 1.96±0.68 vs. O2T-O1T: 1.57±0.64, O2D-O1D: 1.88±0.67, O2T-O1D: 0.11±0.38 and O2D-O1T: 0.30±0.59 in ChCl:DLTA). This is different to their behavior in crystalline form, where DL-tartaric acid has a stronger bond than L-tartaric acid. But the main structure determining interaction in crystalline tartaric acid is the O2T-H3T, in addition to the other hydrogen bonds, so it can be expected that relative to the pure crystal the tartaric acid self interaction is majorly disrupted by the presence of stronger hydrogen bonding partners such as Cl and choline in the liquid

mixture. Under the structuring influence of these interactions, the positioning of tartaric acids relative to each other is changed and sterically hindered, in this case leading to a stark reduction in significant interactions between DTA and LTA. This can also be seen in the reduction of peak intensity in the pRDFs. The SDFs also show differences the location of the spatial density for the same enantiomer and between the different enantiomers. Analysing all pRDFs between the molecules, no significant shift towards other interactions can be seen either. This suggests that interactions as a chiral solvent could significantly depend on how well the substrate is able to bind to the tartaric acid bonding sites, in competition with choline and chloride.
The overall interaction length scales and N_{coord} are similar to what can be found in ChCl:Ma, but are different from ChCl:Ox. Here the atoms close to the molecular centers have a shorter r_{max} (CA-CA in ChCl:Ox = 4.5 Å vs. C1T-C1T in ChCl:LTA = 6.1 Å), which makes sense as oxalic acid is a smaller molecule. This size difference might then contribute to a higher N_{coord} for the other atom-atom interactions, allowing for different positioning and an overall closer distances of any atom pair, and especially of the hydrogen bonding carboxylic acid groups, when the two molecules are close.
Finally for the choline - choline interactions, no significant differences between ChCl:LTA and ChCl:DLTA can be seen. In comparison to ChCl:Ma and ChCl:Ox the tartaric acid based DES has similar r_{max}, with the exception of Ooh-Hoh, which shows clear hydrogen bonding at a peak position at 1.8 Å, which is not present in the ChCl:Ma and ChCl:Ox systems. This, combined with the low coordination number of this interaction (0.14±0.36 in ChCl:LTA, 0.085±0.28 in ChCl:DLTA), could be an effect of the higher relative amount of choline in the system making this weak interaction more likely.

3.3. Effect of water

Dry 2:1 ChCl:LTA and hydrated 2:1:2 ChCl:LTA:W show an overall similar structure, with the addition of water inducing slight shifts in r_{max} and a general decrease in coordination number (Fig.3, Fig.4, Fig.5, SI: table 2 and 3; Fig.2, 3, 4 and 6). As seen with other hydrated DES[64, 44] the overall structure seems relatively robust, and no phase separation or formation of water domains can be seen at this concentration. The most significant changes can be seen in the interactions of choline with itself and with LTA. They both experience a shift of about 0.1 to 0.2 Å to larger distances and a decrease in coordination number of 1-2. Accordingly, choline shows the highest coordination with water at 3.68±1.78, at an r_{max} of 4.7 Å. Water self clustering is present, but not the dominant interaction with a coordination of 1.48±1.27, indicative of the formation of dimers and trimers. While water shows clear interactions with TA and Cl in the pRDFs (r_{max} of 3.5 Å and 3.2 Å), its coordination to these is moderately low with 0.6±0.74 water around TA and 1.15±0.98 water around Cl. This also leads only a weak influence on TA - TA and TA - Cl interactions, which do not show significant shifts in r_{max} and deceases in N_{coord} of less then 1.
Comparing the atomic pRDFs leads to similar trends as the molecular pRDFs. The water oxygen interacts with TA in a similar way to Cl, primarily over the H3T. Water also interacts with choline in a similar way, interacting slightly more with the trimethyl ammonium group then with the OH end. The SDFs show that water is overall much more disperse then Cl in interacting with TA or choline. Analysing the chains and clusters with water, only short chains of up to three molecules and small clusters of up to around 10 molecules around the percolation threshold for Cl - W and W - W interactions and clusters of up to 5 molecules for N - W and C1T - W interactions can be seen (SI Fig.12, 15). This is similar to what can be found for the other molecule interactions in the system and indicates a variety of interactions, with no long range water percolation.
In comparison to the effect of water in a 1:1:2 choline chloride : malic acid : water (ChCl:Ma:W) system, reported previously by Hammond et al.[44], a similar degree of water interactions with itself can be seen, with slightly reduced interactions of water with Cl and the acid, and a higher coordination of water around choline (see SI table 2). The differences in Ch - water coordination are especially prominent (3.68±1.78 in the ChCl:LTA:W and 0.94±0.90 in ChCl:Ma:W). This could partially be an effect of the difference in acid to CC molar ratio between the two systems, with more choline leading to a higher likelihood for interaction in the TA based system. That the effect can not be seen with the Cl could be due to the relatively stronger coordination of Cl to the acid (1.84±0.77 in ChCl:LTA:W vs. 1.04±0.78 in ChCl:Ma:W), and the relatively large standard deviation relative to the value for the interaction.

4. Conclusions

Here we have shown the structure of 2:1 choline chloride : tartaric acid, for both the single enantiomer (L-tartaric acid) and the racemic (DL-tartaric acid) containing DES, as well as the hydrated single enantiomer system (2:1:2 choline chloride : L-tartaric acid : water) through neutron scattering experiments with EPSR modelling. From this we have shown that the overall structure of the single enantiomer and the racemic tartaric acid containing mixtures is almost identical, with differences in interaction only between the tartaric acid molecules themselves. While the molecular centers pRDFs show similar distances and the interactions have similar coordination numbers, analysis of the atomic interactions and spatial density function show differences between LTA or DTA with themselves, and between the different enantiomers. SDFs show differences in preferred positioning between the different forms, while the coordination numbers indicate interactions occur mostly between the same enantiomers, with very low coordination numbers for close range interactions between L- and DTA. Here the DES shows a significant difference to the solid, crystalline LTA or DLTA, where interactions in DLTA are stronger. This can be explained by the fact that in the DES tartaric acid is sterically restricted by strong interactions with choline and especially chloride. It is strongly located towards a position where it can be located on one side of the chloride, while choline interacts with the other side of the chloride. These stronger structure directing interactions could lead to a decrease in the conformations that are more favourable in ChCl:DLTA. But as the TA - TA interactions are

overall relatively weak and disperse, this has no significant influence on the overall liquid structure. In terms of use as a chiral solvent the relatively strong interaction between the TA - Cl and TA - Ch could also cause a reduction of interaction with other substrate molecules.
Similar to what has been found in other DES[64, 44] the main structure of the DES remains intact upon the addition of 2 mole of water. Only a slight decrease in overall coordination numbers can be seen, especially in choline - choline and choline - tartaric acid interactions.
One of the main structure driving interactions in our DES is the HBD - chloride - HBA arrangement, which is similar to other carboxylic acid and choline chloride comprising DES like 1:1 oxalic acid : choline chloride and 1:1 malic acid : choline chloride [44, 63]. A clear effect of molecule size can be observed, with other molecules located at shorter intermolecular distances around the smaller carboxylic acids. Steric effects can also lead to higher coordination numbers for the smaller acids as this allows for closer packing, but here this effect overlaps with the effect of difference in molar ratio and available hydrogen bonding sites, where the presence of more of one species can lead to a higher probability of its presence and interaction with it.

Declaration of Competing Interest

There are no conflicts of interest to declare.

Data availability

Raw neutron data is available at DOI: 10.5286/ISIS.E.RB1920738.

Acknowledgements

The authors thank the UK Science and Technology Facilities Council (STFC) and Lund University for co-funding the a PhD studentship, as well as the University of Bath and the Centre for Sustainable and Circular Technologies for their support. We also thank the ISIS Pulsed Neutron and Muon Source for their support and the allocation of experimental beam time on NIMROD under RB1920738 (data can be downloaded from DOI: 10.5286/ISIS.E.RB1920738).

References

[1] A. P. Abbott, Deep eutectic solvents and their application in electrochemistry, Current Opinion in Green and Sustainable Chemistry 36 (2022). doi:10.1016/j.cogsc.2022.100649.
[2] L. I. N. Tome, V. Baiao, W. da Silva, C. M. A. Brett, Deep eutectic solvents for the production and application of new materials, Applied Materials Today 10 (2018) 30–50. doi:10.1016/j.apmt.2017.11.005.
[3] S. E. Hooshmand, R. Afshari, D. J. Ramon, R. S. Varma, Deep eutectic solvents: cutting-edge applications in cross-coupling reactions, Green Chemistry 22 (12) (2020) 3668–3692. doi:10.1039/d0gc01494j.
[4] F. F. Mulks, B. Pinho, A. W. J. Platten, K. J. Edler, E. Hevia, M. R. Andalibi, A. J. Exposito, L. Torrente-Murciano, Continuous, stable, and safe organometallic reactions in flow at room temperature assisted by deep eutectic solvents, Chem 8 (12) (2022) 3382–3394. doi:10.1016/j.chempr.2022.11.004.
[5] O. S. Hammond, K. J. Edler, D. T. Bowron, L. Torrente-Murciano, Deep eutectic-solvothermal synthesis of nanostructured ceria, Nature Communications 8 (2017). doi:10.1038/ncomms14150.
[6] O. S. Hammond, S. Eslava, A. J. Smith, J. F. Zhang, K. J. Edler, Microwave-assisted deep eutectic-solvothermal preparation of iron oxide nanoparticles for photoelectrochemical solar water splitting, Journal of Materials Chemistry A 5 (31) (2017) 16189–16199. doi:10.1039/c7ta02078c.
[7] D. K. Yu, Z. M. Xue, T. C. Mu, Deep eutectic solvents as a green toolbox for synthesis, Cell Reports Physical Science 3 (4) (2022). doi:10.1016/j.xcrp.2022.100809.
[8] M. Ruesgas-Ramon, M. C. Figueroa-Espinoza, E. Durand, Application of deep eutectic solvents (des) for phenolic compounds extraction: Overview, challenges, and opportunities, Journal of Agricultural and Food Chemistry 65 (18) (2017) 3591–3601. doi:10.1021/acs.jafc.7b01054.
[9] S. C. Cunha, J. O. Fernandes, Extraction techniques with deep eutectic solvents, Trac-Trends in Analytical Chemistry 105 (2018) 225–239. doi:10.1016/j.trac.2018.05.001.
[10] C. Padwal, H. D. Pham, S. Jadhav, T. T. Do, J. Nerkar, L. T. M. Hoang, A. K. Nanjundan, S. G. Mundree, D. P. Dubal, Deep eutectic solvents: Green approach for cathode recycling of li-ion batteries, Advanced Energy and Sustainability Research 3 (1) (2022). doi:10.1002/aesr.202100133.
[11] S. N. Pedro, M. G. Freire, C. S. R. Freire, A. J. D. Silvestre, Deep eutectic solvents comprising active pharmaceutical ingredients in the development of drug delivery systems, Expert Opinion on Drug Delivery 16 (5) (2019) 497–506. doi:10.1080/17425247.2019.1604680.
[12] A. Hayyan, F. S. Mjalli, I. M. AlNashef, T. Al-Wahaibi, Y. M. Al-Wahaibi, M. A. Hashim, Fruit sugar-based deep eutectic solvents and their physical properties, Thermochimica Acta 541 (2012) 70–75. doi:10.1016/j.tca.2012.04.030.
[13] A. P. Abbott, G. Capper, D. L. Davies, H. L. Munro, R. K. Rasheed, V. Tambyrajah, Preparation of novel, moisture-stable, lewis-acidic ionic liquids containing quaternary ammonium salts with functional side chains, Chemical Communications (2001) 2010–2011doi:10.1039/b106357j.
[14] A. P. Abbott, D. Boothby, G. Capper, D. L. Davies, R. K. Rasheed, Deep eutectic solvents formed between choline chloride and carboxylic acids: Versatile alternatives to ionic liquids, Journal of the American Chemical Society 126 (29) (2004) 9142–9147. doi:10.1021/ja048266j.
[15] Y. Liang, W. J. Duan, X. X. An, Y. Y. Qiao, Y. Y. Tian, H. F. Zhou, Novel betaine-amino acid based natural deep eutectic solvents for enhancing the enzymatic hydrolysis of corncob, Bioresource Technology 310 (2020). doi:10.1016/j.biortech.2020.123389.
[16] W. T. Bi, M. L. Tian, K. H. Row, Evaluation of alcohol-based deep eutectic solvent in extraction and determination of flavonoids with response surface methodology optimization, Journal of Chromatography A 1285 (2013) 22–30. doi:10.1016/j.chroma.2013.02.041.
[17] C. Florindo, L. Romero, I. Rintoul, L. C. Branco, I. M. Marrucho, From phase change materials to green solvents: Hydrophobic low viscous fatty acid based deep eutectic solvents, Acs Sustainable Chemistry Engineering 6 (3) (2018) 3888–3895. doi:10.1021/acssuschemeng.7b04235.
[18] K. J. Xu, P. L. Xu, Y. Z. Wang, Aqueous biphasic systems formed by hydrophilic and hydrophobic deep eutectic solvents for the partitioning of dyes, Talanta 213 (2020). doi:10.1016/j.talanta.2020.120839.
[19] H. Cruz, N. Jordao, A. L. Pinto, M. Dionisio, L. A. Neves, L. C. Branco, Alkaline iodide-based deep eutectic solvents for electrochemical applications, Acs Sustainable Chemistry Engineering 8 (29) (2020) 10653–10663. doi:10.1021/acssuschemeng.9b06733.
[20] V. Agieienko, R. Buchner, A comprehensive study of density, viscosity, and electrical conductivity of (choline chloride plus glycerol) deep eutectic solvent and its mixtures with dimethyl sulfoxide, Journal of Chemical and Engineering Data 66 (1) (2021) 780–792. doi:10.1021/acs.jced.0c00869.
[21] Y. Chen, L. Fu, Y. T. Duan, Y. Bai, X. Wang, X. C. Sun, C. Liu,

B. Y. Zhang, Z. M. Di, Effect of organic solvents on the conductivity of polyethylene glycol-based deep eutectic solvents, Journal of Molecular Liquids 346 (2022). doi:10.1016/j.molliq.2021.117038.

[22] C. R. Wright, L. VandenElzen, T. A. Hopkins, Deep eutectic solvents for induced circularly polarized luminescence, Journal of Physical Chemistry B 122 (37) (2018) 8730–8737. doi:10.1021/acs.jpcb.8b06148.

[23] T. Palomba, G. Ciancaleoni, T. Del Giacco, R. Germani, F. Ianni, M. Tiecco, Deep eutectic solvents formed by chiral components as chiral reaction media and studies of their structural properties, Journal of Molecular Liquids 262 (2018) 285–294. doi:10.1016/j.molliq.2018.04.096.

[24] D. Jung, J. B. Jung, S. Kang, K. Li, I. Hwang, J. H. Jeong, H. S. Kim, J. Lee, Toxico-metabolomics study of a deep eutectic solvent comprising choline chloride and urea suggests in vivo toxicity involving oxidative stress and ammonia stress, Green Chemistry 23 (3) (2021) 1300–1311. doi:10.1039/d0gc03927f.

[25] M. P. Garralaga, L. Lomba, A. Leal-Duaso, S. Gracia-Barberan, E. Pires, B. Giner, Ecotoxicological study of bio-based deep eutectic solvents formed by glycerol derivatives in two aquatic biomodels, Green Chemistry 24 (13) (2022) 5228–5241. doi:10.1039/d2gc01293f.

[26] I. J. Ferreira, A. Paiva, M. Diniz, A. R. Duarte, Uncovering biodegradability and biocompatibility of betaine-based deep eutectic systems, Environmental Science and Pollution Research (2023). doi:10.1007/s11356-022-25000-6.

[27] N. R. Rodriguez, L. Machiels, K. Binnemans, p-toluenesulfonic acid-based deep-eutectic solvents for solubilizing metal oxides, Acs Sustainable Chemistry Engineering 7 (4) (2019) 3940–3948. doi:10.1021/acssuschemeng.8b05072.

[28] H. Palmelund, M. P. Andersson, C. J. Asgreen, B. J. Boyd, J. Rantanen, K. Lobmann, Tailor-made solvents for pharmaceutical use? experimental and computational approach for determining solubility in deep eutectic solvents (des), International Journal of Pharmaceutics-X 1 (2019). doi:10.1016/j.ijpx.2019.100034.

[29] P. V. D. Pontes, I. A. Shiwaku, G. J. Maximo, E. A. C. Batista, Choline chloride-based deep eutectic solvents as potential solvent for extraction of phenolic compounds from olive leaves: Extraction optimization and solvent characterization, Food Chemistry 352 (2021). doi:10.1016/j.foodchem.2021.129346.

[30] A. Sanchez-Fernandez, K. J. Edler, T. Arnold, R. K. Heenan, L. Porcar, N. J. Terrill, A. E. Terry, A. J. Jackson, Micelle structure in a deep eutectic solvent: a small-angle scattering study, Physical Chemistry Chemical Physics 18 (20) (2016) 14063–14073. doi:10.1039/c6cp01757f.

[31] S. J. Bryant, R. Atkin, G. G. Warr, Spontaneous vesicle formation in a deep eutectic solvent, Soft Matter 12 (6) (2016) 1645–1648. doi:10.1039/c5sm02660a.

[32] R. S. Atri, A. Sanchez-Fernandez, O. S. Hammond, I. Manasi, J. Doutch, J. P. Tellam, K. J. Edler, Morphology modulation of ionic surfactant micelles in ternary deep eutectic solvents, Journal of Physical Chemistry B 124 (28) (2020) 6004–6014. doi:10.1021/acs.jpcb.0c03876.

[33] I. Manasi, M. R. Andalibi, R. S. Atri, J. Hooton, S. M. King, K. J. Edler, Self-assembly of ionic and non-ionic surfactants in type iv cerium nitrate and urea based deep eutectic solvent, Journal of Chemical Physics 155 (8) (2021). doi:10.1063/5.0059238.

[34] Y. H. Choi, J. van Spronsen, Y. T. Dai, M. Verberne, F. Hollmann, I. Arends, G. J. Witkamp, R. Verpoorte, Are natural deep eutectic solvents the missing link in understanding cellular metabolism and physiology?, Plant Physiology 156 (4) (2011) 1701–1705. doi:10.1104/pp.111.178426.

[35] D. Seebach, H. A. Oei, Mechanism of electrochemical pinacolization. the first asymmetric synthesis in a chiral medium, Angewandte Chemie International Edition in English 14 (9) (1975) 634–636. doi:https://doi.org/10.1002/anie.197506342.

[36] C. Baudequin, D. Bregeon, J. Levillain, F. Guillen, J. C. Plaquevent, A. C. Gaumont, Chiral ionic liquids, a renewal for the chemistry of chiral solvents? design, synthesis and applications for chiral recognition and asymmetric synthesis, Tetrahedron-Asymmetry 16 (24) (2005) 3921–3945. doi:10.1016/j.tetasy.2005.10.026.

[37] K. Bica, P. Gaertner, Applications of chiral ionic liquids, European Journal of Organic Chemistry 2008 (19) (2008) 3235–3250. doi:10.1002/ejoc.200701107.

[38] T. A. Hopkins, L. VandenElzen, B. P. Nelson, V. Vaid, J. Brickley, P. Ariza, G. Whitacre, I. Patel, O. Gooch, M. Bechman, C. Jordan, Chiral solvent discovery: Exploring chiral eutectic mixtures and deep eutectic solvents, Industrial Engineering Chemistry Research (2023). doi:10.1021/acs.iecr.2c03702.

[39] M. Tiecco, D. A. Alonso, D. R. Niguez, G. Ciancaleoni, G. Guillena, D. J. Ramon, A. A. Bonillo, R. Germani, Assessment of the organocatalytic activity of chiral l-proline-based deep eutectic solvents based on their structural features, Journal of Molecular Liquids 313 (2020). doi:10.1016/j.molliq.2020.113573.

[40] S. P. Ma, F. F. Li, L. L. Liu, L. P. Liao, L. Chang, Z. J. Tan, Deep-eutectic solvents simultaneously used as the phase-forming components and chiral selectors for enantioselective liquid-liquid extraction of tryptophan enantiomers, Journal of Molecular Liquids 319 (2020). doi:10.1016/j.molliq.2020.114106.

[41] A. Li, S. Xue, Y. Xu, S. H. Ding, D. Wen, Q. Zhang, A feasibility study on the use of hydrophobic eutectic solvents as pseudo-stationary phases in capillary electrophoresis for chiral separations, Analytica Chimica Acta 1239 (2023). doi:10.1016/j.aca.2022.340693.

[42] S. Arnaboldi, A. Mezzetta, S. Grecchi, M. Longhi, E. Emanuele, S. Rizzo, F. Arduini, L. Micheli, L. Guazzelli, P. R. Mussini, Natural-based chiral task-specific deep eutectic solvents: A novel, effective tool for enantiodiscrimination in electroanalysis, Electrochimica Acta 380 (2021). doi:10.1016/j.electacta.2021.138189.

[43] L. VandenElzen, T. A. Hopkins, Monosaccharide-based deep eutectic solvents for developing circularly polarized luminescent materials, Acs Sustainable Chemistry Engineering 7 (19) (2019) 16690–16697. doi:10.1021/acssuschemeng.9b04100.

[44] O. S. Hammond, D. T. Bowron, A. J. Jackson, T. Arnold, A. Sanchez-Fernandez, N. Tsapatsaris, V. Garcia Sakai, K. J. Edler, Resilience of malic acid natural deep eutectic solvent nanostructure to solidification and hydration, The Journal of Physical Chemistry B 121 (31) (2017) 7473–7483. arXiv:https://doi.org/10.1021/acs.jpcb.7b05454, doi:10.1021/acs.jpcb.7b05454.

[45] M. A. Ali, M. S. Rahman, R. Roy, P. Gambill, D. E. Raynie, M. A. Halim, Structure elucidation of menthol-based deep eutectic solvent using experimental and computational techniques, Journal of Physical Chemistry A 125 (12) (2021) 2402–2412. doi:10.1021/acs.jpca.0c10735.

[46] P. L., Transformation of tartaric acid into racemic acid. the discovery of inactive tartaric acid. a new method for the separation of racemic acid into right and left tartaric acids, Comptes Rendus Hebdomadaires des Seances de l'Academie des Sciences 37 (1853) 162–166. doi:10.1098/rspa.1923.0010.

[47] W. T. Astbury, W. H. Bragg, The crystalline structure and properties of tartaric acid, Proceedings of the Royal Society of London. Series A, Containing Papers of a Mathematical and Physical Character 102 (718) (1923) 506–528. doi:10.1098/rspa.1923.0010.

[48] K. I. Batarseh, Anomaly and correlation of killing in the therapeutic properties of silver (1) chelation with glutamic and tartaric acids, Journal of Antimicrobial Chemotherapy 54 (2) (2004) 546–548. doi:10.1093/jac/dkh349.

[49] G. Boisier, N. Pebere, C. Druez, M. Villatte, S. Suel, Fesem and eis study of sealed aa2024 t3 anodized in sulfuric acid electrolytes: Influence of tartaric acid, Journal of the Electrochemical Society 155 (11) (2008) C521–C529. doi:10.1149/1.2969277.

[50] Z. H. Wan, Y. Q. Sun, D. C. W. Tsang, Z. B. Xu, E. Khan, S. H. Liu, X. D. Cao, Sustainable impact of tartaric acid as electron shuttle on hierarchical iron-incorporated biochar, Chemical Engineering Journal 395 (2020). doi:10.1016/j.cej.2020.125138.

[51] M. O. Lorenzo, S. Haq, T. Bertrams, P. Murray, R. Raval, C. J. Baddeley, Creating chiral surfaces for enantioselective heterogeneous catalysis: R,r-tartaric acid on cu(110), Journal of Physical Chemistry B 103 (48) (1999) 10661–10669. doi:10.1021/jp992188i.

[52] Y. Luan, K. S. Barbato, P. N. Moquist, T. Kodama, S. E. Schaus, Enantioselective synthesis of 1,2-dihydronaphthalene-1-carbaldehydes by addition of boronates to isochromene acetals catalyzed by tartaric acid, Journal of the American Chemical Society 137 (9) (2015) 3233–3236. doi:10.1021/jacs.5b00757.

[53] P. Wang, F. P. Ma, Z. H. Zhang, L-(+)-tartaric acid and choline chloride based deep eutectic solvent: An efficient and reusable medium for synthesis of n-substituted pyrroles via clauson-kaas reaction, Journal of Molecular Liquids 198 (2014) 259–262. doi:10.1016/j.molliq.2014.07.

015.

[54] I. M. Aroso, A. Paiva, R. L. Reis, A. R. C. Duarte, Natural deep eutectic solvents from choline chloride and betaine - physicochemical properties, Journal of Molecular Liquids 241 (2017) 654–661. doi:10.1016/j.molliq.2017.06.051.

[55] A. Butor Skulcova, V. Majová, A. Haz, F. Kreps, A. Russ, M. Jablonsky, Long-term isothermal stability of deep eutectic solvents based on choline chloride with malonic or lactic or tartaric acid, International Journal of Scientific and Engineering Research 8 (2017) 2249–2252.

[56] S. Koutsoukos, T. Tsiaka, A. Tzani, P. Zoumpoulakis, A. Detsi, Choline chloride and tartaric acid, a natural deep eutectic solvent for the efficient extraction of phenolic and carotenoid compounds, Journal of Cleaner Production 241 (2019). doi:10.1016/j.jclepro.2019.118384.

[57] Z. Naseem, R. A. Shehzad, A. Ihsan, J. Iqbal, M. Zahid, A. Pervaiz, G. Sarwari, Theoretical investigation of supramolecular hydrogen-bonded choline chloride-based deep eutectic solvents using density functional theory, Chemical Physics Letters 769 (2021). doi:10.1016/j.cplett.2021.138427.

[58] U. Saeed, A. L. Khan, M. A. Gilani, M. R. Bilad, A. U. Khan, Supported liquid membranes comprising of choline chloride based deep eutectic solvents for co2 capture: Influence of organic acids as hydrogen bond donor, Journal of Molecular Liquids 335 (2021). doi:10.1016/j.molliq.2021.116155.

[59] N. Satyanarayana, K. Sathish, S. Nagaraju, R. Pawar, M. Faizan, M. Arumugavel, T. Shirisha, D. Kashinath, Metal-free, one-pot synthesis of 2-styrylquinolines via friedlander annulation and sp(3) c-h activation using 1,3-dimethylurea and l-tartaric acid (3:1) as a deep eutectic solvent, New Journal of Chemistry 46 (4) (2022) 1637–1642. doi:10.1039/d1nj00132a.

[60] I. A. Rather, R. Ali, An efficient and versatile deep eutectic solvent-mediated green method for the synthesis of functionalized coumarins, Acs Omega 7 (12) (2022) 10649–10659. doi:10.1021/acsomega.2c00293.

[61] C. T. Li, Z. P. Cai, Y. D. Ma, Y. N. Cao, K. Huang, L. L. Jiang, Densities and viscosities of, and solubilities of acidic gases (so2 and h2s) in natural deep eutectic solvents, Journal of Chemical Thermodynamics 167 (2022). doi:10.1016/j.jct.2021.106713.

[62] N. M. Pereira, P. M. V. Fernandes, C. M. Pereira, A. F. Silvaz, Electrodeposition of zinc from choline chloride-ethylene glycol deep eutectic solvent: Effect of the tartrate ion, Journal of the Electrochemical Society 159 (9) (2012) D501–D506. doi:10.1149/2.004209jes.

[63] M. Gilmore, L. M. Moura, A. H. Turner, M. Swadzba-Kwasny, S. K. Callear, J. A. McCune, O. A. Scherman, J. D. Holbrey, A comparison of choline: urea and choline: oxalic acid deep eutectic solvents at 338 k, Journal of Chemical Physics 148 (19) (2018). doi:10.1063/1.5010246.

[64] O. S. Hammond, D. T. Bowron, K. J. Edler, The effect of water upon deep eutectic solvent nanostructure: An unusual transition from ionic mixture to aqueous solution, Angewandte Chemie-International Edition 56 (33) (2017) 9782–9785. doi:10.1002/anie.201702486.

[65] A. H. Turner, J. D. Holbrey, Investigation of glycerol hydrogen-bonding networks in choline chloride/glycerol eutectic-forming liquids using neutron diffraction, Physical Chemistry Chemical Physics 21 (39) (2019) 21782–21789. doi:10.1039/c9cp04343h.

[66] A. Soper, Science, T. F. C. G. Britain), GudrunN and GudrunX: Programs for Correcting Raw Neutron and X-ray Diffraction Data to Differential Scattering Cross Section, Technical report (Science and Technology Facilities Council (Great Britain))), Science & Technology Facilities Council, 2011.

[67] A. K. Soper, Partial structure factors from disordered materials diffraction data: An approach using empirical potential structure refinement, Phys. Rev. B 72 (2005) 104204. doi:10.1103/PhysRevB.72.104204.

[68] O. S. Hammond, D. T. Bowron, K. J. Edler, Liquid structure of the choline chloride-urea deep eutectic solvent (reline) from neutron diffraction and atomistic modelling, Green Chem. 18 (2016) 2736–2744. doi:10.1039/C5GC02914G.

[69] F. Stern, C. A. Beevers, The crystal structure of tartaric acid, Acta Crystallographica 3 (5) (1950) 341–346. doi:10.1107/S0365110X50000975.

[70] P. E. Luner, A. D. Patel, D. C. Swenson, (±)-Tartaric acid, Acta Crystallographica Section C 58 (6) (2002) o333–o335. doi:10.1107/S0108270102006650.

[71] J. J. Towey, A. K. Soper, L. Dougan, Molecular insight into the hydrogen bonding and micro-segregation of a cryoprotectant molecule, Journal of Physical Chemistry B 116 (47) (2012) 13898–13904. doi:10.1021/jp3093034.
URL <GotoISI>://WOS:000311650300010

[72] K. K. Chai, Y. Q. Zhou, X. M. Lu, T. Yamaguchi, K. Ohara, H. Y. Liu, F. Y. Zhu, Structure of choline chloride-carboxylic acid deep eutectic solvents by wide-angle x-ray scattering and dft calculations, Physical Chemistry Chemical Physics 25 (15) (2023) 10481–10494. doi:10.1039/d3cp00570d.
URL <GotoISI>://WOS:000958800600001

Supplementary:

The influence of chirality on the structure of a tartaric acid-choline chloride deep eutectic solvent

Elly K. Bathke[a], Daniel Bowron[b], Iva Manasi[c], Karen J. Edler[a]

[a]Center for Analysis and Synthesis, Department of Chemistry, Lund University, Getingevägen 60, Lund, 22241, Scania, Sweden

[b]ISIS Neutron and Muon Source, Science and Technology Facilities Council, Rutherford Appleton Laboratory, Didcot, OX11 0QX, Oxfordshire, United Kingdom

[c]Department of Chemistry, University of Bath, Claverton Down, Bath, BA2 7AY, Somerset, United Kingdom

E-mail:

elly_kim.bathke@chem.lu.se

karen.edler@chem.lu.se

EPSR methodology

EPSR26 was used to build the model and fit the data. The initial molecules to be used in EPSR were generated using Jmol software. The distinct atoms were then re-labeled (Fig.1 in main text), the dihedral angles were removed and substituted by rotations (full rotational freedom was implemented). Lennard-Jones potentials and charges were taken from literature [1], which were based on the OPLS All-Atom force field potential [2], and modified where needed based Jmol parameters and on the OPLS All-Atom force field potential. They are listed in table 1.

For ESPR modelling, a box was build comprising of 400 choline cations, 400 chloride anions and 200 tartaric acid molecules, split into 100 DTA and 100 LTA in case of the racemic DES, or 300 choline cations, 300 chloride anions, 150 L-tartaric acid molecules and 300 water molecules. A box was setup with an atomic density of 0.098$Å^{-3}$ and randomized. The box was expanded through the sizefactor, increasing it to 20 ensure no molecular overlap occurred, and reduced step-wise back to 1 with each iteration of EPSR. The system was run until equilibration and then fit against the neutron scattering data. Once a good fit was reached the system equilibrated for more than 10000 iterations, before accumulating partials and coordination numbers for over 3000 iterations.

Table 1: Lennard Jones parameters and charges used within EPSR for modelling of neutron scattering data.

Atom type	ε (kJ mol^{-3})	σ (Å)	q (e)
N	0.700	3.200	1.000
Ooh	0.650	3.100	-0.683
Hcm	0.200	2.580	0.060
Hoh	0.000	0.000	0.418
Hcn	0.200	2.580	0.060
Hco	0.200	2.580	0.060
Cn	0.800	3.700	-0.120
Cm	0.800	3.700	-0.180
Coh	0.800	3.700	0.145
Cl1	0.566	4.191	-1.000
C1T	0.276	3.500	0.205
C2T	0.439	3.750	0.520
O1T	0.711	3.120	-0.683
O2T	0.879	2.960	-0.440
O3T	0.711	3.000	-0.530
H1T	0.126	2.500	0.450
H2T	0.000	0.000	0.418
H3T	0.000	0.000	0.450
O1	0.634	3.151	-0.834
H1	0.000	0.000	-0.417

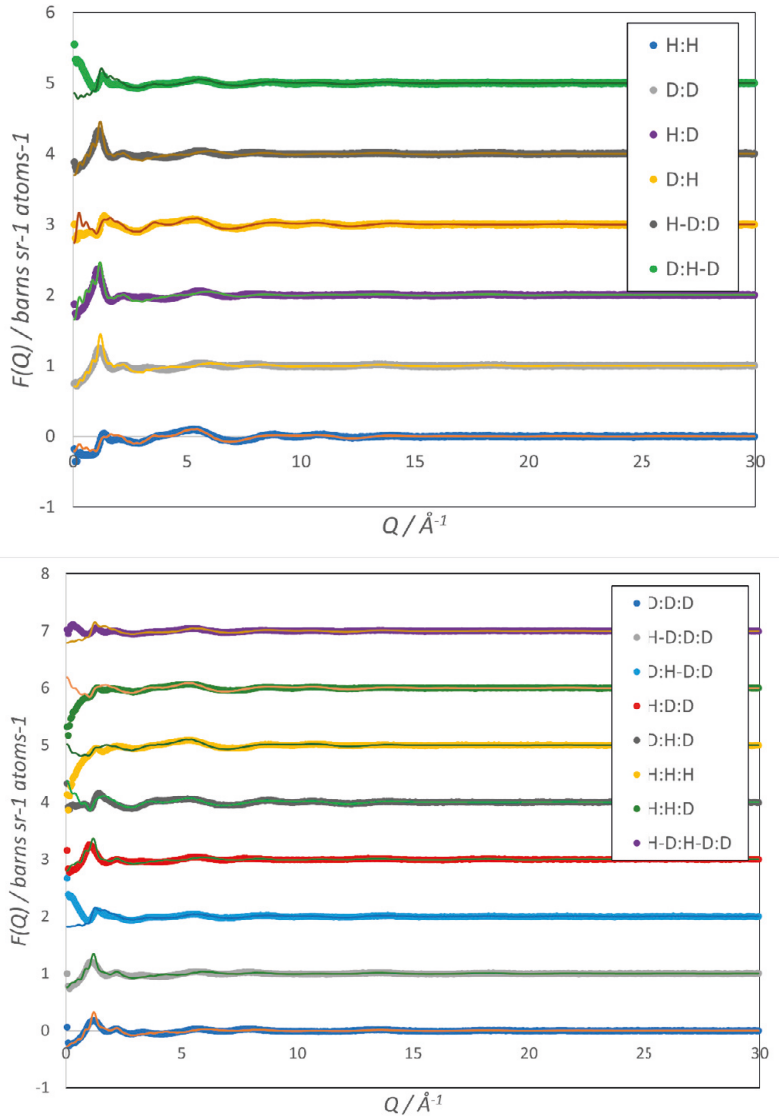

Fig. 1: Structure factors F(Q) over Q of the six measured isotropic contrasts of 2:1 ChCl:DLTA and 2:1:2 ChCl:LTA:W from neutron scattering data (dots) and their EPSR fits (solid lines). The different contrasts are offset from each other for better readability.

Molecular interactions

Table 2: Position of the first peak r_{max} and coordination number N_{coord} of the molecular centers RDFs of the DES components in ChCl:LTA, ChCl:DLTA and ChCl:LTA:W, as well as in ChCl:Ma, ChCl:Ma:W [1] and ChCl:Ox [3] for comparison. "Acid" stands for L-tartaric acid, oxalic acid or malic acid depending on the DES. The error on the peak position is approximately 0.1Å. The errors on the coordination number are calculated to one standard deviation and represent the spread in this moving system.

	r_{max} / Å						N_{coord}					
Pair	**ChCl: LTA**	**ChCl: DLTA**	**ChCl: LTA: W**	**ChCl: Ox[3]**	**ChCl: Ma[1]**	**ChCl: Ma: W[1]**	**ChCl:LTA**	**ChCl:DLTA**	**ChCl:LTA: W**	**ChCl:Ox[3]**	**ChCl:Ma[1]**	**ChCl:Ma: W[1]**
Ch - Ch	6.3	6.2	6.4	6.2	6.2	6.5	8.34±1.74	7.63±1.68	6.54±1.59	7.07±1.69	6.44±1.80	5.75±1.63
Ch - Cl	4.4	4.3	4.5	4.5	4.2	4.2	4.01±1.46	3.60±1.21	3.78±1.28	3.25±1.07	0.98±0.78	0.85±0.72
Ch - Acid	6.1	6.3	6.3	5.7	5.9	6	9.05±1.87	3.97±2.41	7.78±3.23	11.91±0.75	6.78±1.93	6.22±1.72
Ch - DTA		6.3						3.97±2.51				
Acid - Cl	3.5	3.5	3.5	3.7	4.3	4.4	2.12±0.75	2.01±0.69	1.84±0.77	4.72±2.55	1.11±0.82	1.04±0.78
DTA - Cl		3.5						2.14±0.75				
Acid - Acid	6.1	6	6.1	5	5.8	5.8	8.06±3.42	3.62±2.24	7.19±3.26	9.75±3.38	3.64±1.25	3.19±1.40
DTA - LTA		6						3.96±2.38				
DTA - DTA		6.1						4.01±2.67				
Acid - W			3.2			4			0.60±0.74			1.47±1.2
Ch - W			4.7			3.9			3.68±1.78			0.94±0.90
Cl - W			3.2			3			1.15±0.98			2.05±1.25
W - W			2.8			2.7			1.48±1.27			1.54±1.24

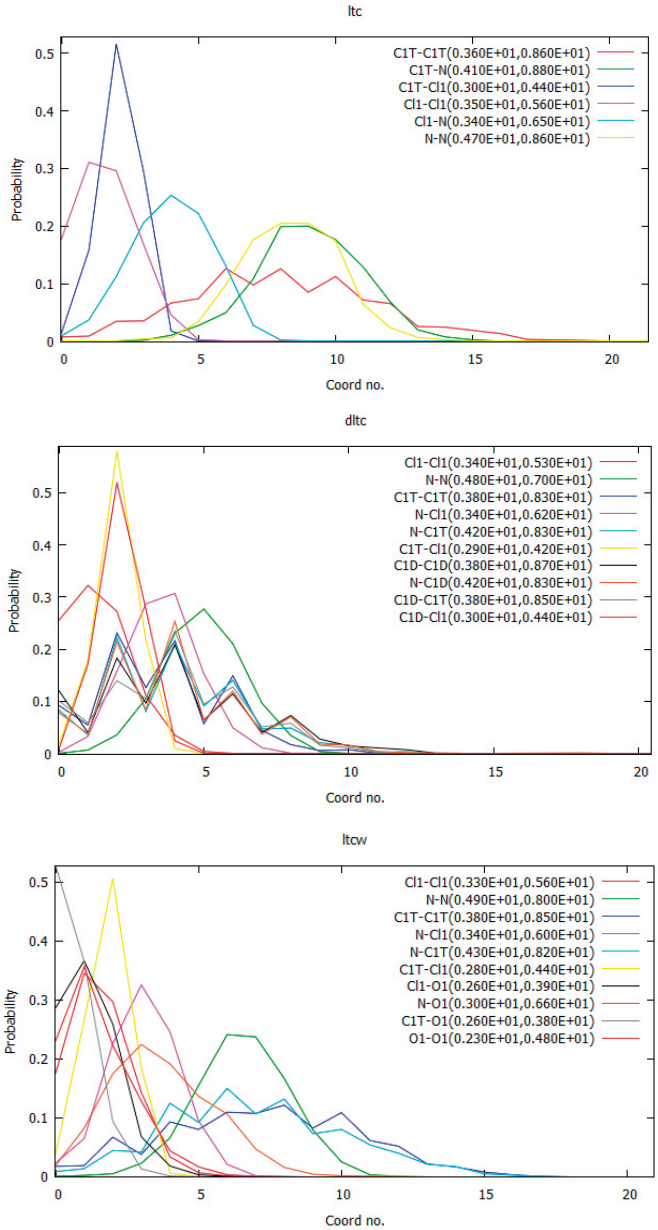

Fig. 2: Coordination number probability distribution of first shell of molecule interactions in ChCl:LTA (top), ChCl:DLTA (middle) and ChCl:LTA:W (bottom). The coordination numbers are integral numbers, connecting lines are included as a visual guide. Numbers in brackets (in Å) correspond to the minima before and after the first peak in the corresponding pRDF, representing the distance range of the first shell.

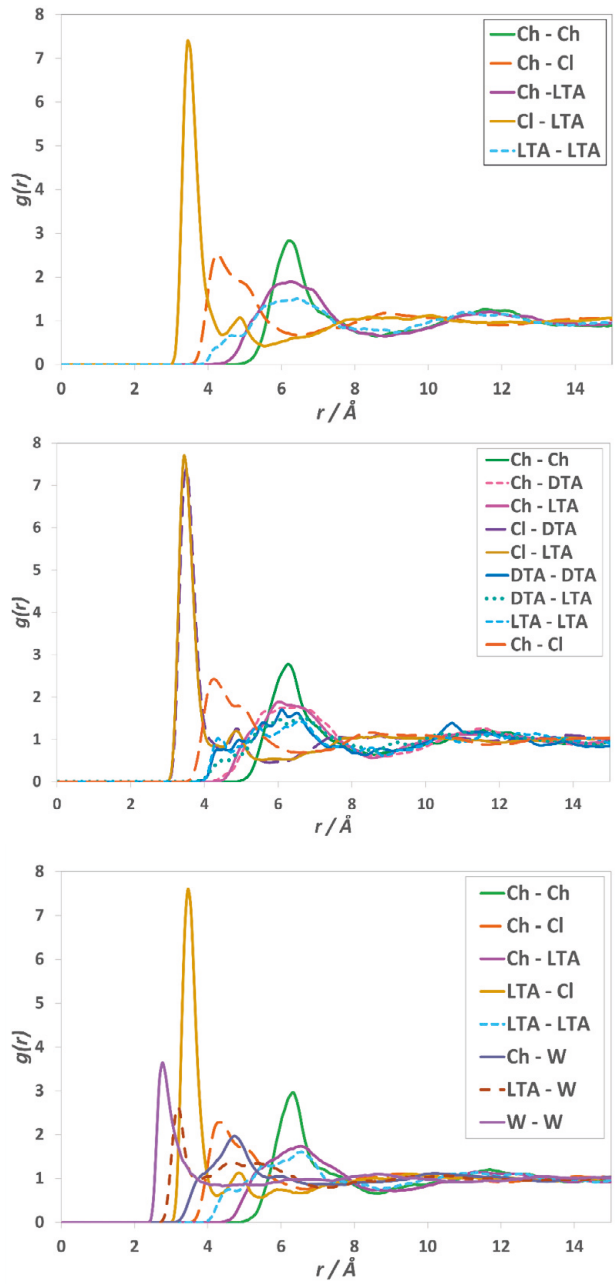

Fig. 3: Molecular centers pRDFs for 2:1 ChCl:LTA (top), 2:1 ChCl:DLTA (middle) and 2:1:2 ChCl:LTA:W (bottom).

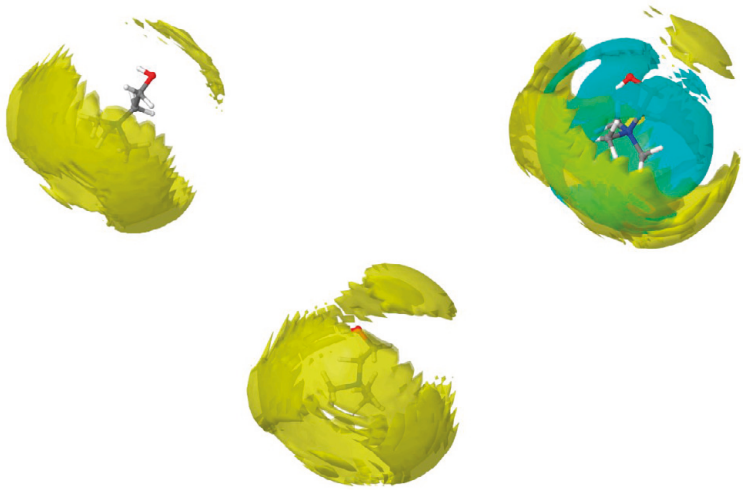

Fig. 4 a): Spatial density function (SDF) of the 20% probability surface showing the solvation of the molecule types around each other in 3D. Distribution centered around choline (top left: in ChCl:LTA, top right: in ChCl:LTA:W, bottom: in ChCl:DLTA), the yellow isosurfaces correspond to choline cations and the light blue to water molecules.

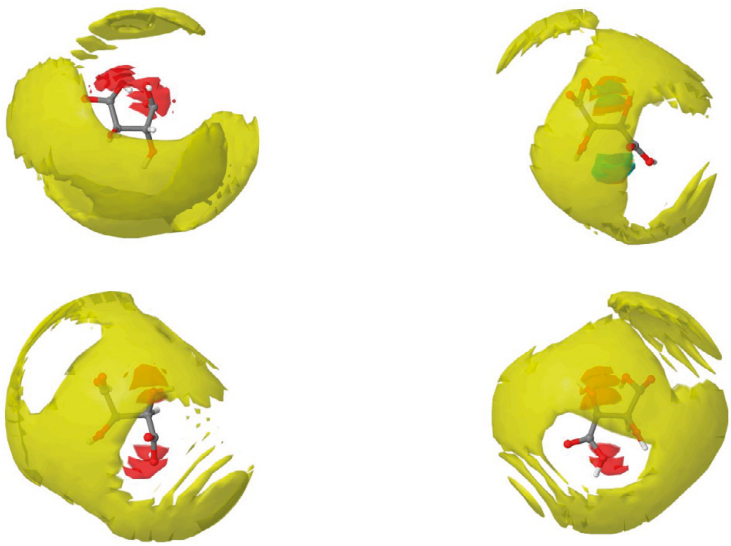

Fig. 4 b): Spatial density function (SDF) of the 20% probability surface showing the solvation of the molecule types around each other in 3D. Distribution centered around tartaric acid (top left: LTA in ChCl:LTA, top right: LTA in ChCl:LTA:W, bottom left: LTA in ChCl:DLTA, bottom right: DTA in ChCl:DLTA), the yellow isosurfaces correspond to choline cations, the red to chloride anions and the light blue to water molecules.

Fig. 4 c): Spatial density function (SDF) of the 20% probability surface showing the solvation of the molecule types around each other in 3D. Distribution centered around choline ChCl:LTA:W, the green isosurfaces correspond to L-tartaric acid molecules and the red to chloride anions.

Atomic interactions

Table 3: Position of the first peak r_{max} and coordination number N_{coord} up until the first minimum of representative inter-atomic pRDFs of the DES components in ChCl:LTA, ChCl:DLTA and ChCl:LTA:W. The error on the peak position is approximately ±0.1Å. The errors on the coordination number are calculated to one standard deviation.

	r_{max} / Å			N_{coord}		
	ChCl:LTA	**ChCl:DLTA**	**ChCl:LTA:W**	**ChCl:LTA**	**ChCl:DLTA**	**ChCl:LTA:W**
Choline - Choline						
N - N	6.3	6.2	6.4	8.34±.74	7.63±1.68	6.54±1.59
N - Cm	5.2	5.1	5.2	6.40±2.37	6.75±2.36	5.81±2.39
N - Cn	6.9	6.8	6.9	7.43±1.73	7.60±1.75	6.36±1.63
N - Hcm	4.5	4.6	4.5	10.17±3.67	9.94±03.54	10.17±4.12
Ooh - Hoh	3.5	1.8	1.8	0.14±0.36	0.085±0.28	0.09±0.29
Cm - Ooh	3.5	3.6	3.5	1.36±0.92	1.40±0.92	1.29±0.89
Choline - Cl						
N - Cl	4.4	4.3	4.5	4.01±1.46	3.60±1.21	3.78±1.28
Cm - Cl	3.9	3.9	4.0	1.76±0.96	1.69±0.94	1.62± 0.95
Coh - Cl	4.0	3.9	4.0	1.49±0.89	1.47±0.85	1.33±0.84
Ooh - Cl	3.1	1.2	3.2	0.79±0.56	0.69±0.51	0.72±0.56
Hoh - Cl	2.1	2.2	2.2	0.70±0.47	0.65±0.48	0.64±0.48
Choline - LTA						
N - C1T	6.4	6.3	6.3	8.83±3.26	3.97±2.41	7.78±3.23
N - C2T	5.0	5.3	5.0	3.34±1.75	1.54±1.22	2.52±1.57
N - O2T	4.5	4.3	4.5	2.22±0.99	1.14±1.08	2.07±1.50
N - H1T	6.4	6.4	6.6	8.87±3.27	4.53±2.60	8.92±3.48
Ooh - H1T	2.4	2.5	2.5	0.36±0.62	0.16±0.44	0.21±0.48
Ooh - H3T	1.7	1.6	1.6	0.065±0.25	0.018±0.13	0.047±0.21
Cm - O2T	3.5	3.4	3.6	1.04±1.00	0.52±0.71	0.69±0.81
Choline - DTA						
N - C1D		6.3			3.97± 2.51	
N - C2D		5.3			1.54±1.22	
N - O2D		4.5			1.07±1.03	
N - H1D		6.4			4.27±2.57	
Ooh - H1D		2.4			0.12±0.36	
Ooh - H3D		1.8			0.03±0.17	
Cm - O2D		3.5			0.50±0.71	
LTA - Cl						
C1T - Cl	3.5	3.5	3.5	2.21±0.77	2.01±0.69	1.84±0.77
C2T - Cl	3.7	3.7	3.7	1.39±0.69	0.72±0.79	1.15±0.65
H1T - Cl	2.7	2.8	2.8	1.86±0.77	0.98±1.13	1.7±1.25
H2T - Cl	2.1	2.0	2.2	0.79±0.44	0.40±0.59	0.63±0.66
H3T - Cl	2.0	2.0	2.0	0.88±0.35	0.46±0.65	0.77±0.72
O3T - Cl	3.0	3.0	3.0	0.92±0.39	0.49±0.68	0.88±0.78
O1T - Cl	3.1	3.1	3.0	0.84±0.52	0.43±0.61	0.6±0.65
DTA - Cl						

C1D - Cl		3.5			1.08±1.22	
C2D - Cl		3.7			0.68±0.81	
H1D - Cl		2.8			0.91±1.07	
H2D - Cl		2.1			0.41±0.63	
H3D - Cl		2.0			0.44±0.66	
O3D - Cl		3.0			0.51±0.72	
O1D - Cl		3.1			0.47±0.67	
LTA - LTA						
C1T -C1T	6.1	6.0	6.1	8.06±3.42	3.62±2.24	7.19±3.26
O2T - C1T	3.2	3.3	3.3	2.11±0.73	1.57±0.69	1.61±0.78
O2T - H1T	2.5	2.5	2.6	1.14±0.65	0.22±0.5	0.99±0.71
O2T - H3T	1.9	1.8	1.8	0.048±0.21	0.018±0.15	0.03±0.17
O2T - O1T	3.0	2.9	2.9	1.96±0.68	1.57±0.64	1.92±0.65
O1T - O1T	2.9	2.9	2.8	1.24±0.50	0.88±0.54	1.13±0.54
DTA - DTA						
C1D - C1D		6.1			4.01±2.67	
O2D - C1D		3.2			1.09±0.47	
O2D - H1D		2.4			0.37±0.59	
O2D - H3D		1.5			0.11±0.32	
O2D - O1D		3.2			1.88±0.67	
O1D - O1D		2.9			0.45±0.55	
LTA - DTA						
C1D - C1T		6.0			3.96±2.38	
O2D - C1T		3.2			0.11±0.38	
O2T - C1D		3.4			0.15±0.42	
O2D - H1T		2.3			0.066±0.29	
O2T - H1D		2.4			0.15±0.42	
O2D - H3T		1.7			0.02+0.14	
O2T - H3D		2.0			0.036±0.19	
O2T - O1D		3.1			0.11±0.38	
O2D - O1T		3.4			0.30±0.59	
O1D - O1T		2.8			0.18±0.411	
Choline - Water						
N - O1			4.7			3.68±1.78
N - H1			4.6			7.01±3.36
Hcm - O1			2.8			0.55±0.70
Hoh - O1			1.7			0.12±0.33
Ooh - H1			1.9			0.14±0.37
LTA - Water						
C1T - O1			3.2			0.6±0.74
C2T - O1			3.5			1.63±1.21
H1T - O1			2.4			0.51±0.63
H2T - O1			1.7			0.14±0.34
H3T - O1			1.6			0.14±0.35
O3T - H1			3.2			1.55±1.61

Cl - Water						
Cl1 - O1			3.1			1.51±1.13
Cl1 - H1			2.2			1.00±1.96
Water - Water						
O1 - O1			2.8			1.37±1.16
H1 - O1			1.8			0.16±0.385
H1 - H1			2.4			1.82±1.09

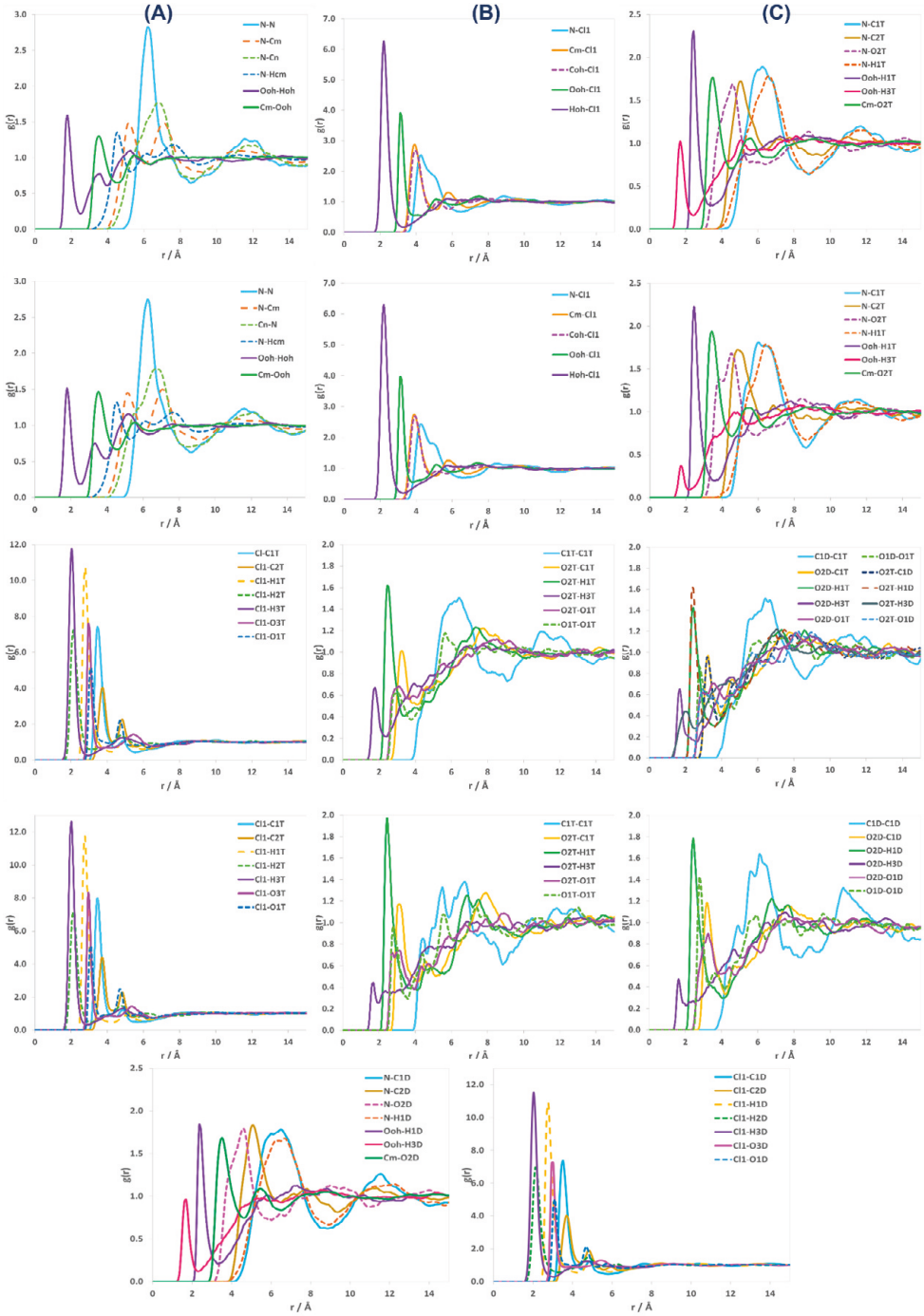

Fig. 5: Representative inter-atomic pRDFs for ChCl:LTA (row 1, 3 A+B) and ChCl:DLTA (row 2, 3 C, 4, last row).

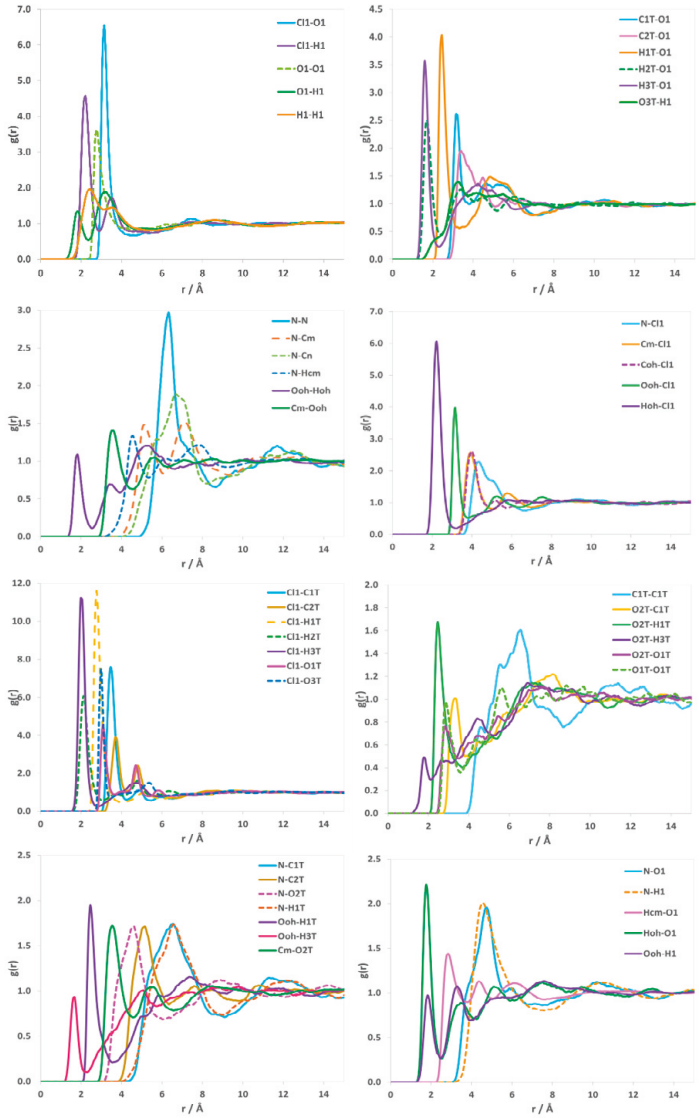

Fig. 6: Additional atom-atom pRDFs for ChCl:LTA:W.

Ester formation within the DES

For a range of DES comprised of choline chloride and carboxylic acids it has been shown that their components can undergo chemical reactions upon prolonged heating, to differing degrees depending on composition, temperature and length of heating [4]. The most prominent reaction is an ester formation between the OH-group of the choline and the OH-group of the acid. Here, ^{1}H-NMR in D_2O was performed to determine the degree of ester formation within the DES formed for neutron experimentation (Fig.7-9). Not all contrasts were measured due to sample recovery issues after neutron data collection. Most samples exhibited 3-5% of ester formation relative to the amount of choline, with 1 DL-TA : 2 ChCl (H:H) showing a higher degree of ester formation due to prolonged heating (16 hours). EPSR models considering the presence of ester (5%) were build and fit to the neutron data, but showed little significant differences to models in the absence of ester. The influence of the presence of ester was therefore determined to be negligible, and results shown in this paper do not consider ester formation.

Table 4: Degree of ester formation in the different DES and contrasts as a percentage of ChCl.

Sample	Ester [% of ChCl]
1 L-TA : 2 ChCl (H:H)	5.1
1 L-TA : 2 ChCl (D:H)	5.8
1 L-TA : 2 ChCl (D:H/D)	6.3
1 DL-TA : 2 ChCl (H:H)	12.2
1 DL-TA : 2 ChCl (D:H/D)	4.0
1 DL-TA : 2 ChCl (D:H)	5.6
1 L-TA : 2 ChCl : 2 W (H:H:H)	5.9
1 L-TA : 2 ChCl : 2 W (D:H/D:D)	4.7
1 L-TA : 2 ChCl : 2 W (D:H:D)	3.4

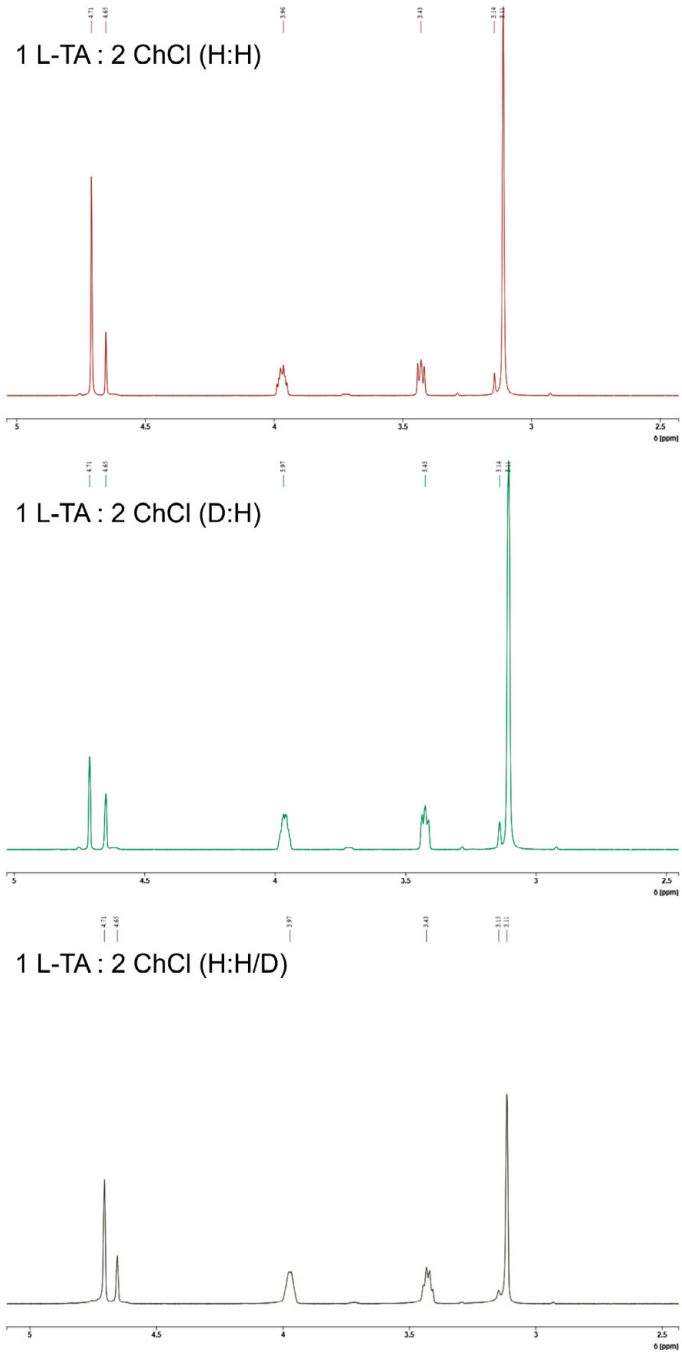

Figure 7: ^{1}H-NMR of ChCl:LTA at different contrasts measured in D_2O.

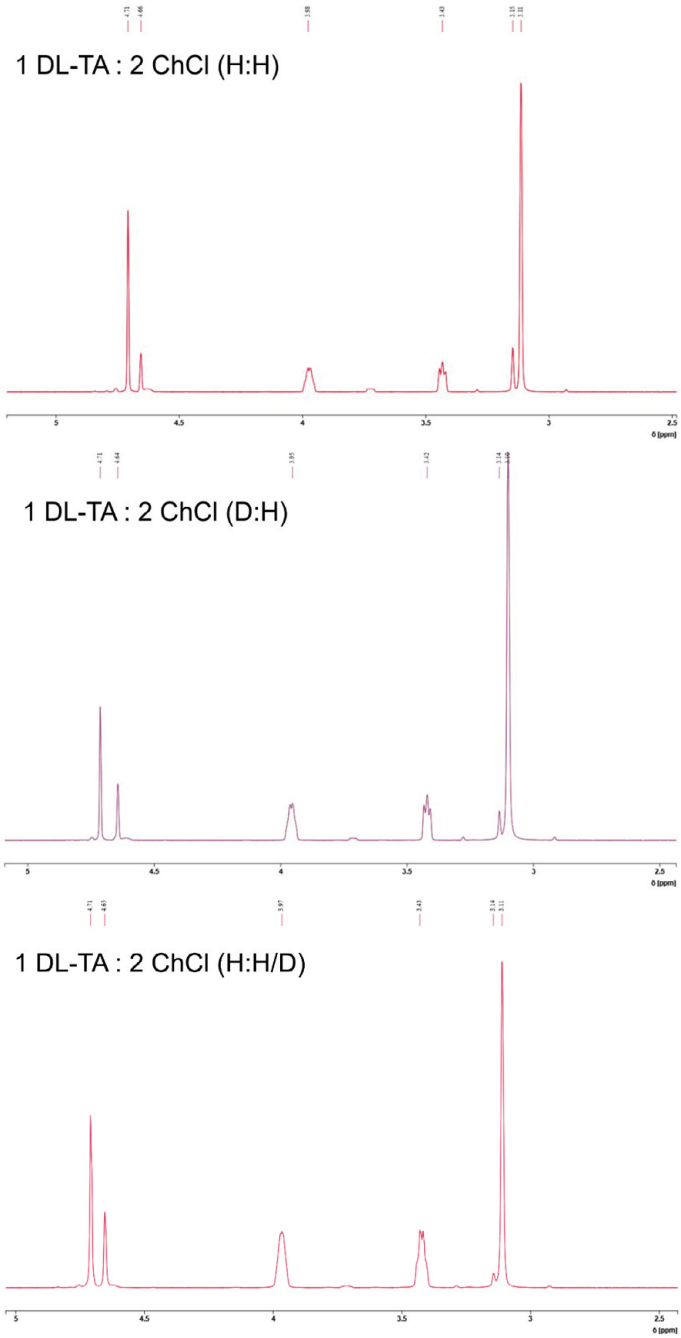

Figure 8: ^{1}H-NMR of ChCl:DLTA at different contrasts measured in D_2O.

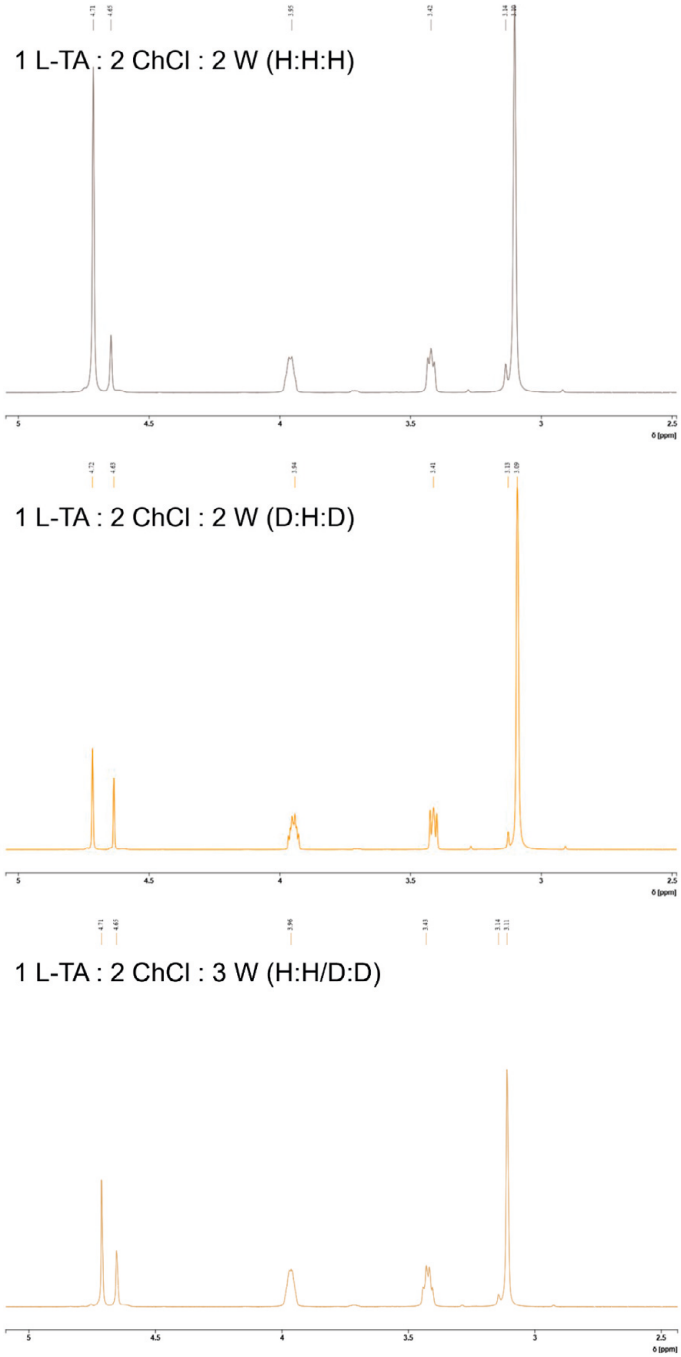

Figure 9: ^{1}H-NMR of ChCl:LTA:W at different contrasts measured in D_2O.

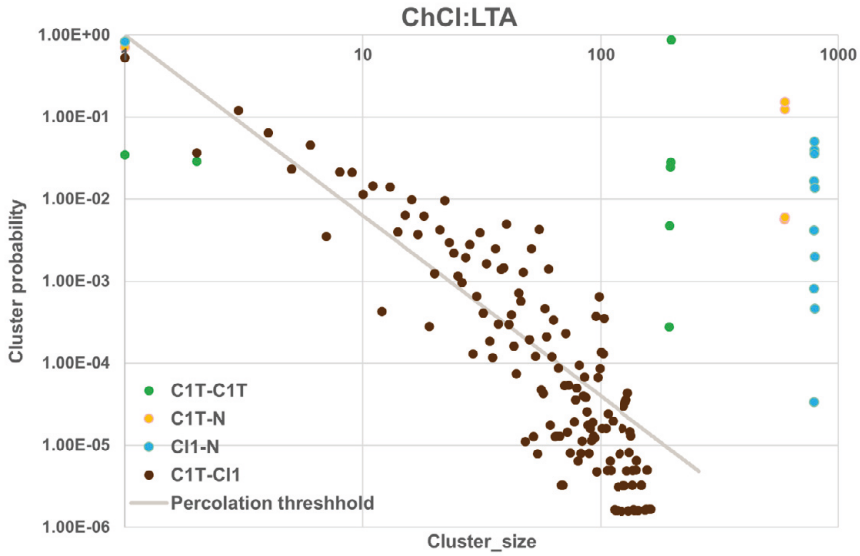

Figure 10: Cluster distribution and percolation[5] threshold for ChCl:LTA.

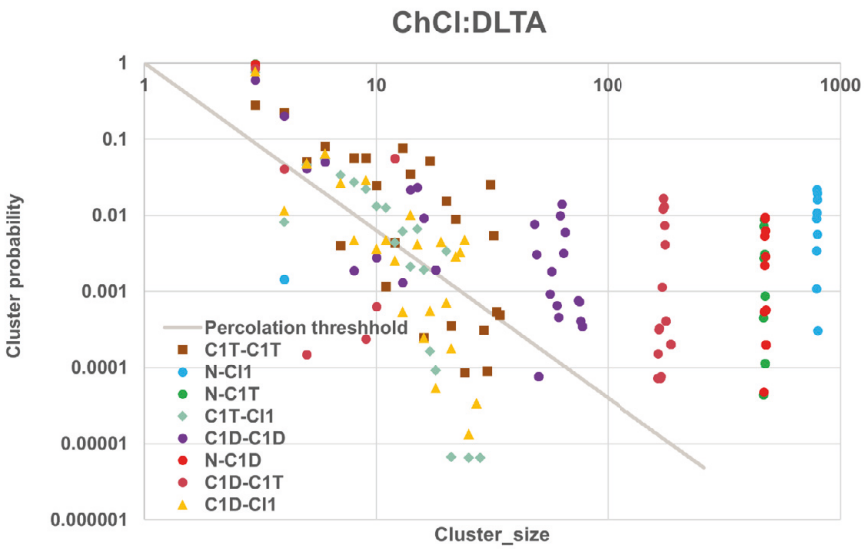

Figure 11: Cluster distribution and percolation[5] threshold for ChCl:DLTA.

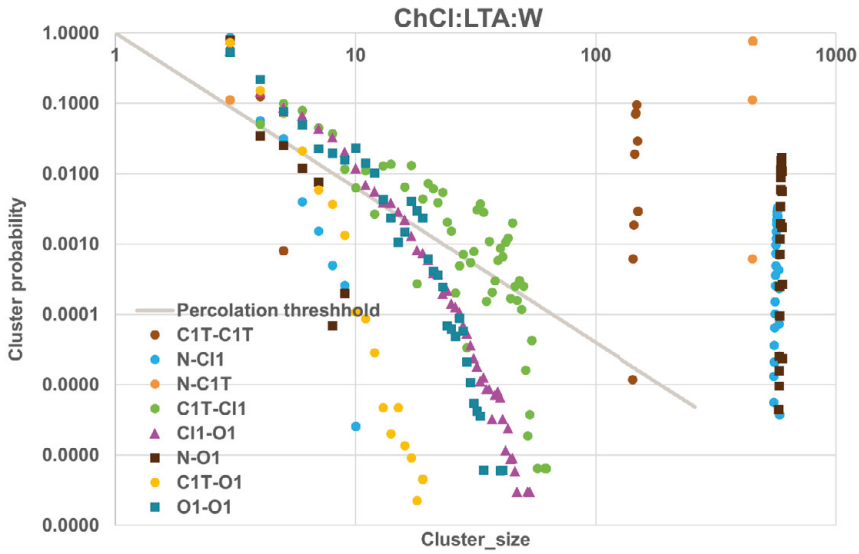

Figure 12: Cluster distribution and percolation[5] threshold for ChCl:LTA:W.

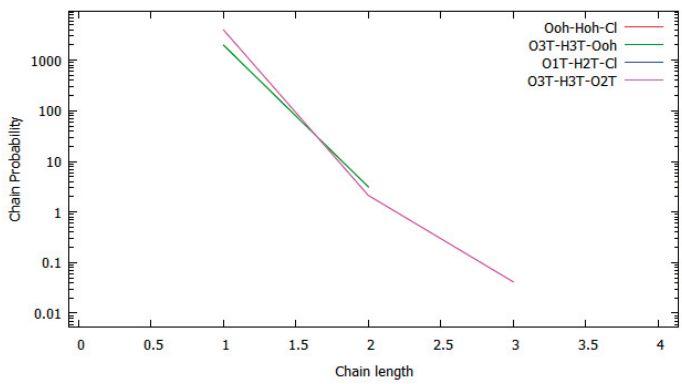

Figure 13: Hydrogen bonding chain distribution for ChCl:LTA**.**

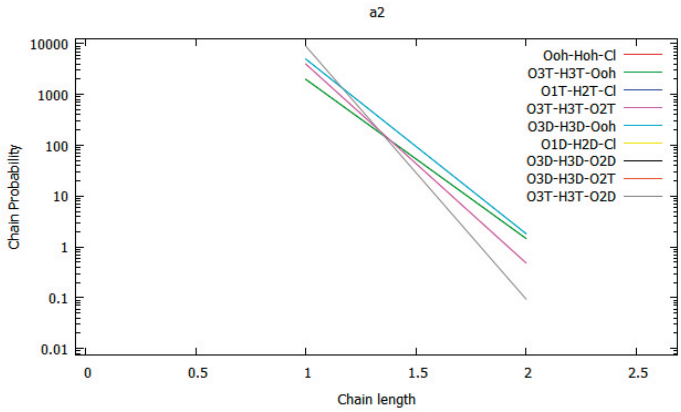

Figure 14: Hydrogen bonding chain distribution for ChCl:DLTA.

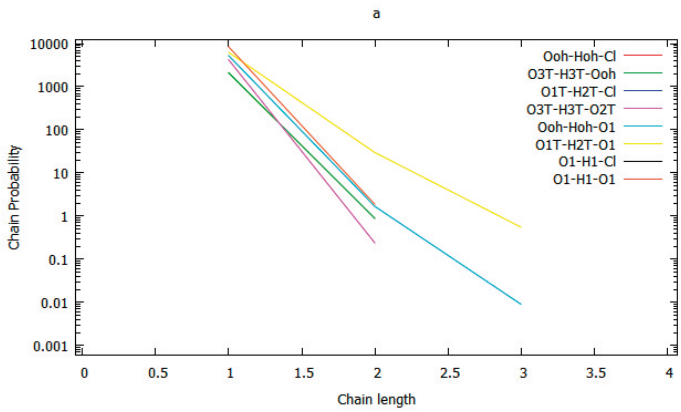

Figure 15: Hydrogen bonding chain distribution for ChCl:LTA:W.

References

[1] O. S. Hammond, D. T. Bowron, A. J. Jackson, T. Arnold, A. Sanchez- Fernandez, N. Tsapatsaris, V. Garcia Sakai, K. J. Edler, Resilience of malic acid natural deep eutectic solvent nanostructure to solidification and hydration, The Journal of Physical Chemistry B 121 (31) (2017) 7473–7483. doi: 10.1021/acs.jpcb.7b05454

[2] W. L. Jorgensen, D. S. Maxwell, J. TiradoRives, Development and testing of the opls all-atom force field on conformational energetics and properties of organic liquids, Journal of the American Chemical Society 118 (45) (1996) 11225–11236. doi: 10.1021/ja9621760

[3] M. Gilmore, L. M. Moura, A. H. Turner, M. Swadzba-Kwasny, S. K. Callear, J. A. McCune, O. A. Scherman, J. D. Holbrey, A comparison of choline: urea and choline: oxalic acid deep eutectic solvents at 338 k, Journal of Chemical Physics 148 (19) (2018). doi: 10.1063/1.5010246.

[4] N. R. Rodriguez, A. van den Bruinhorst, L. Kollau, M. C. Kroon, K. Binxnemans, Degradation of deep-eutectic solvents based on choline chloride and carboxylic acids, Acs Sustainable Chemistry Engineering 7 (13) (2019) 11521–11528. doi: 10.1021/acssuschemeng.9b01378.

[5] J.J. Towey, A.K. Soper et al., Molecular Insight Into the Hydrogen Bonding and Micro-Segregation of a Cryoprotectant Molecule, J. Phys. Chem. B 116, 47 (2012) 13898–13904